# MECHANISMS OF TETRODOTOXIN PRODUCTION AND RESISTANCE IN THE POISONOUS ROUGH-SKINNED NEWT (*TARICHA GRANULOSA*)

By

Patric M. Vaelli

A DISSERTATION

Submitted to
Michigan State University
in partial fulfillment of the requirements
for the degree of

Integrative Biology—Doctor of Philosophy
Ecology, Evolutionary Biology and Behavior—Dual Major

2019

## ABSTRACT

## MECHANISMS OF TETRODOTOXIN PRODUCTION AND RESISTANCE IN THE POISONOUS ROUGH-SKINNED NEWT (*TARICHA GRANULOSA*)

By

Patric M. Vaelli

Rough-skinned newts (*Taricha granulosa*) are poisonous salamanders that possess high concentrations of tetrodotoxin (TTX), a potent neurotoxin that blocks voltage-gated sodium channel ($Na_v$) conductance in neurons and muscle cells. TTX is present in all species of the genus Taricha, but some populations of *T. granulosa* (hereafter "newts") possess extreme quantities not seen in any other TTX-bearing species, including puffer fishes, blue-ringed octopuses, and many diverse marine invertebrates. Geographic variation in TTX toxicity across different newt populations is thought to be driven by ecological interactions with predators. Despite the central role of TTX in the physiology and evolution of newts, the mechanisms of TTX production and neurophysiological resistance are unknown. Because of the polyphyletic distribution of TTX toxicity among animals, we explored the hypothesis that TTX is produced by symbiotic skin bacteria in newts. We conducted 16S rRNA gene-based sequencing surveys to characterize skin-associated bacterial communities of newts from toxic and non-toxic populations. From here, we employed ecologically-guided cultivation strategies to target skin-associated symbionts and produce pure cultures. We screened cultures for TTX production using a customized HILIC-MS/MS method and confirmed TTX production in multiple isolated bacterial strains. Furthermore, we investigated the molecular adaptations underlying apparent TTX resistance in the $Na_v$s of newts. We cloned and sequenced the TTX binding site, the S5-S6 pore loop regions, of all six $Na_v$ genes present in this species

and compared sequences from toxic and non-toxic populations, as well as from other vertebrates. As a result, we identified several mutations present in the S5-S6 pore loops of all six genes, indicating a remarkable parallel evolution of TTX resistance across the $Na_v$ gene family. To determine whether these mutations impact TTX resistance, we used site-directed mutagenesis to insert three newt mutations identified in neural subtype $Na_v1.6$ into the TTX-sensitive mouse ortholog and examined their effects on TTX binding by heterologous expression and electrophysiological recording in Xenopus laevis oocytes. We found that each individual mutation increased TTX resistance to varying degrees, but the triple mutant was extremely resistant to TTX concentrations exceeding 100 μM. Taken together, our results indicate that TTX is derived from the skin microbiome in the extremely toxic rough-skinned newt and that multiple adaptations in newt $Na_v$s were required for the nervous system to adapt to TTX toxicity. Overall, this research contributes to a growing understanding that symbiotic microbes can affect the physiology of animal hosts and their nervous systems, and that evolution by natural selection may target genetic variation across both host and symbiont genomes, collectively termed the ‘hologenome’.

*For my family, friends, ancestors, and descendants.*

## ACKNOWLEDGEMENTS

Scientific research is a hugely collaborative process, and I owe many thanks to the wonderfully talented and inspirational people in my life who have guided me through my time at Michigan State. First and foremost, I want to thank my graduate advisor, Dr. Heather Eisthen, for providing the freedom and support to embrace my curiosity and explore new ideas in her lab. I want to thank Dr. Kevin Theis for his guidance in experimental and computational microbiology, and for continuing to serve as a mentor after departing MSU. I would also like to thank the other members of my graduate committee, Drs. Ke Dong, Ashlee Rowe, and Jason Gallant, for their generosity in sharing their expertise, their time, and resources in their labs. I was fortunate to have a committee of top experts in their respective fields, and their guidance has significantly impacted my development as a scientist. Thank you.

I have also worked with many wonderful people at MSU over the years, including but not limited to Drs. Barry Williams, A. Daniel Jones, Scott Smith, Chen Zhang, Carol Flegler, James Kremer, Abhijna Parigi, and Eli Strauss. Other people who have helped me with data analysis include Mauricio Losilla, Connie Rojas, and Dr. Cory Kohn. Outside of MSU, I had the privilege of working with Drs. James Foster and Janet Williams on microbiome analyses, and Dr. Michael Markham on electrophysiological analysis of voltage-gated sodium channels in oocytes. Dr. Lauren O'Connell helped to generate the *Taricha granulosa* transcriptome used in Chapter 2. In Summer 2016, I enrolled in the Neural Systems & Behavior course at the Marine Biological Laboratory in Woods Hole, and it was the greatest summer of my life. I met wonderfully talented

scientists from all around the world and worked alongside them on a variety of neurophysiological preparations, including leeches, fruit flies, and crab stomatogastric ganglia. My time at Woods Hole cemented my desire to pursue an academic career, and I'm thankful for everyone who shared that summer with me, especially Dr. Jan Ache, Dr. David Schultz, Jóse Duhart, Yerko Fuentealba, and Nagaraj Mahajan.

I am eternally grateful to the BEACON Center for the Study of Evolution in Action for embracing my research ideas and providing financial support to generate much of the data included in this thesis. BEACON also provided a unique intellectual environment for interdisciplinary research connecting computational science with animal behavior and evolution, and I am thankful to have been a part of that community over the years.

Last, I want to thank my family, who embraced and fostered my curiosity in the natural world from an early age, and my friends, the Jamokes, for the many amazing times at MSU. From pick-up soccer to BBQs and parties, we had a great time together, and that companionship kept me going through challenging times. I especially want to remember our friend Shengpan Lin, who was killed in a traffic accident. Shengpan was an endlessly kind, thoughtful, and loving individual, and we'll never forget him. Finally, I want to thank my partner, Hillary Woodworth, for her love and support as we continue to navigate our post-graduate lives together at Harvard University.

This work was supported by grants from the National Science Foundation (GRFP DGE-1424871 to PMV, and IOS-1354089 and IOS-1655392 to HLE), and from the BEACON Center for the Study of Evolution in Action (NSF Cooperative Agreement DBI-0939454).

## TABLE OF CONTENTS

## LIST OF TABLES

## LIST OF FIGURES

## KEY OF ABBREVIATIONS

| | |
|---|---|
| AIS | Axon Initial Segment |
| ANOVA | Analysis of Variance |
| BLAST | Basic Local Alignment Search Tool |
| BUSCO | Benchmarking Universal Single-Copy Orthologs |
| cDNA | Complementary DNA |
| CNS | Central Nervous System |
| cRNA | Capped RNA |
| D | Domain |
| dATP | Deoxyadenosine Triphosphate |
| DMSO | Dimethyl Sulfoxide |
| DNA | Deoxyribonucleic Acid |
| dsDNA | Double-stranded DNA |
| dUTP | Deoxyuridine Triphosphate |
| EDTA | Ethylenediaminetetraacetic acid |
| EST | Expressed Sequence Tag |
| GABA | Gamma Aminobutyric Acid |
| HBSS | Hank's Buffered Salt Solution |
| HEPES | 4-(2-Hydroxyethyl)-1-Piperazineethanesulfonic Acid |
| HILIC | Hydrophilic Interaction Liquid Chromatography |
| $IC_{50}$ | Half Maximal Inhibitory Concentration |
| $I_{max}$ | Peak Current |

| | |
|---|---|
| $I_{TTX}$ | Peak Current in Presence of TTX |
| LB | Lysogeny Broth |
| LC-MS/MS | Liquid Chromatography Tandem Mass Spectrometry |
| LEfSe | Linear Discriminant Analysis Effect Size |
| MCX | Mixed Cation Exchange |
| mRNA | Messenger RNA |
| MS-222 | Tricaine Methanesulfonate |
| $Na^+$ | Sodium Ion |
| Nav | Voltage-gated Sodium Channel Protein |
| NCBI | National Center for Biotechnology Information |
| OTU | Operational Taxonomic Unit |
| P-loop | Pore Loop |
| PB | Phosphate Buffer |
| PBS | Phosphate Buffered Saline |
| PCR | Polymerase Chain Reaction |
| R2A | Reasoner's 2 Agar |
| R2B | Reasoner's 2 Broth |
| RAxML | Randomized Axelerated Maximum Likelihood |
| RDP | Ribosomal Database Project |
| RE | Restriction Enzyme |
| RNA | Ribonucleic Acid |
| RO | Reverse Osmosis |
| rRNA | Ribosomal RNA |

| | |
|---|---|
| S | Segment |
| SCN | Voltage-gated Sodium Channel Gene |
| SDM | Site-Directed Mutagenesis |
| SDS | Sodium Dodecyl Sulphate |
| SEM | Scanning Electron Microscopy |
| SOC | Super Optimal Broth |
| SPE | Solid Phase Extraction |
| STX | Saxitoxin |
| TQ-D | Triple Quadrupole Mass Spectrometer |
| TTX | Tetrodotoxin |

## INTRODUCTION

One of the central goals of evolutionary biology is to understand how the biotic and abiotic environments of an organism shape the origin and elaboration of adaptive traits. Many plants, animals, and fungi possess morphological, physiological, or behavioral traits that impact their survival and fitness relative to conspecifics, and if these traits are heritable, they can become fixed in the population, leading to an adaptive evolutionary event (1, 2). This view of adaptive evolution in multicellular organisms has its roots in the modern synthesis of the early 1900's, in which pioneering biologists such as Sewall Wright, Ronald Fisher, Theodosius Dobzhansky, and many others fused the earlier discoveries of the founders of genetics and evolutionary biology, Gregor Mendel and Charles Darwin, respectively, to generate the mathematical and statistical frameworks underlying modern evolutionary theory (3). The modern synthesis took a nucleocentric perspective towards evolution, focusing primarily on heritable traits that are encoded by the genome (4). In recent years, however, the discovery of widespread symbiotic interactions between multicellular and microbial organisms has challenged this view (5).

Multicellularity emerged in eukaryotes nearly two billion years after the origin of microbial life, and the vast majority of eukaryotes maintain commensal or symbiotic interactions with microorganisms including eubacteria, archea, fungi, protists, and viruses (6). The impacts of symbiotic microbes (i.e. the microbiome) on host physiology, development, behavior, and evolution is currently a major topic across several subdisciplines in biology (7-9). The contributions of the microbiome to host phenotypes that are undergoing selection are often difficult to disentangle from other genetic and

environmental factors impacting host fitness, and the roles of the microbiome are further complicated by the lack of clear vertical transmission mechanisms that would underlie heritability, and thus adaptive evolution (6).

The origin and evolution of tetrodotoxin (TTX) toxicity in animals offers an excellent model for overcoming this limitation. TTX is a potent neurotoxin that inhibits neural and muscular signaling through selective binding of voltage-gated sodium ($Na_v$) channels, causing paralysis and death if consumed (10). TTX is thus an excellent chemical defense, as it targets a highly-conserved protein present in the nervous systems of nearly all animals. TTX toxicity has evolved across a diverse range of animal taxa including pufferfishes, newts, frogs, octopus, crabs, starfish, flatworms, and others; this observation led researchers to investigate whether this chemical toxin evolved independently in each of these groups, or whether these animals acquire TTX exogenously (11). Beginning in the mid 1980's, researchers began to identify TTX-producing bacteria living in symbiotic interactions with a variety of animal hosts (reviewed in 12). The majority of toxic marine animals studied to date appear to derive their TTX primarily from symbiosis with TTX-producing bacteria (11, 13). The microbial origin of TTX in host animals thus provides a tractable model system for studying host-microbe symbiosis, as the microbial contribution to the host phenotype, TTX toxicity, is quantifiable, and relative fitness values can be determined for evolutionary analyses. Furthermore, the pharmacological target of TTX, $Na_v$ channels, is known, facilitating genetic approaches to understanding the molecular basis of TTX resistance across different species.

One of the most interesting animals with regard to TTX toxicity is the rough-skinned newt (*Taricha granulosa*). This species is endemic to the Pacific Northwest of North America, and newts produce some of the highest levels of TTX detected for any animal (14). Individual newts can possess up to 14 mg of TTX, which is enough to kill several adult humans (human $LD_{50}$ = 10.2 μg/kg). The extreme toxicity of this species is thought to arise from a coevolutionary interaction with predatory garter snakes that have evolved TTX-resistant $Na_v$ channels (15, 16), thereby driving selection for higher levels of toxicity in newts. The ecological and evolutionary ramifications of TTX toxicity in newts has been well-documented across their geographic range (17, 18), but the evolutionary origin of TTX toxicity in this species is unknown. Previous attempts to determine whether TTX is produced by newts or by symbiotic microbes have yielded inconclusive results. Newts maintain TTX toxicity through long term captivity, and they are able to slowly regenerate toxin levels after being forced to secrete their TTX by electric shock (19, 20). A previous PCR-based study failed to amplify 16S rRNA sequences from newt tissues, which was reported as evidence that newts lack a microbiome and must therefore produce TTX themselves (21). This result was largely overinterpreted in the literature, and many studies since have attempted to determine whether newts have independently evolved the ability to produce TTX (22-24).

In Chapter 1, I re-evaluated whether TTX toxicity in rough-skinned newts could be derived from their microbiome using a combination of cultivation-based approaches and high-throughput sequencing. I cultured and isolated symbiotic bacteria from the skin of toxic newts to screen for TTX production in vitro, and identified four bacteria symbionts that produced TTX: *Pseudomonas, Aeromonas, Shewanella*, and

*Sphingopyxis*. I then collected swab samples from two populations of wild adult newts that differ dramatically in their TTX toxicity and compared their microbiomes by 16S rRNA sequencing and ecologically-based analyses. I found that toxic and non-toxic newts differ dramatically in the composition and relative abundances of different bacteria (e.g. OTUs) in their skin, and that *Pseudomonas* are significantly more abundant in toxic newts than non-toxic newts. These results demonstrate that TTX is indeed derived from the microbiome in newts, and that the differential abundance of TTX-producing bacteria in the microbiomes of toxic and non-toxic newts may contribute to the phenotypic variation observed across different newt populations. Importantly, this result indicates that symbiotic TTX-producing bacteria are directly involved in the coevolutionary response to selection pressure by TTX-resistant predator garter snakes (15, 17). My results further provide a foundation for future studies to explore the microbial basis of phenotypic variation in TTX toxicity among newts, evolutionary responses to selective pressures from TTX-resistant predators, and the mechanisms of heritability in this microbially-derived phenotype.

TTX toxicity provides animals with a potent chemical defense against predation by targeting $Na_v$ channels in the nervous system of potential predators. But how are toxic animals able to avoid self-toxicity? What are the mechanisms underlying apparent auto-resistance in poisonous newts? Further, given the repeated independent origins of TTX toxicity across different animals, are the molecular mechanisms underlying TTX resistance unique for each animal, or does resistance emerge convergently by a similar set of selective pressures and functional constraints?

To determine the molecular basis of TTX resistance in newts, I used transcriptomics and degenerate PCR to clone and sequence the six $Na_v$ channel genes (SCN genes) from newts. I examined the highly conserved pore-loop (P-loop) region, the TTX binding site in $Na_v$ channels, for mutations that may reduce TTX sensitivity. I found that newts possess mutations in the P-loops of all six channels, and in one case, a substitution occurs in parallel across the same locus in four separate genes. To examine the functional effects of these mutations on TTX binding, I focused on the Nav1.6 channel subtype, which is widely expressed in both the central and peripheral nervous systems of tetrapods (25). I used site-directed mutagenesis to insert newt-specific mutations into a TTX-sensitive mouse channel ortholog and expressed this channel heterologously in Xenopus laevis oocytes for electrophysiological recording. I found that each of the three mutations examined reduced TTX sensitivity in the mouse channel, and one mutation in the domain I P-loop (Y371A) provided a substantial, 120-fold increase in TTX resistance. However, when expressed together in the same channel, these three mutations interact additively to increase TTX resistance 3,500-fold, much more than the sum of the individual mutations. Interestingly, the two mutations that confer mild TTX resistance are present in Mexican axolotls (Ambystoma mexicanum), suggesting that these mutations arose early in the salamander lineage and may have served as preadaptations that facilitated the initiation of extreme TTX resistance in newts.

Overall, my dissertation research unites disparate biological subdisciplines to evaluate the organismal and evolutionary biology of TTX toxicity in highly poisonous salamanders. The evolution of TTX toxicity in newts could serve as a model system for

exploring host-microbe symbiosis and coevolution. Moreover, I determined that individual mutations in newt $Na_v$ channels can impact toxin binding non-linearly, and that the initial evolution of TTX resistance may have been facilitated by ancestral mutations in the common ancestor of newts and ambystomid salamanders. I propose that rough-skinned newts should serve as model system for future studies exploring the origins, maintenance, and coevolution of host-microbe symbioses.

## REFERENCES

## REFERENCES


1. Smith JM (1978) Optimization theory in evolution. Annual Review of Ecology and Systematics 9(1):31–56.

2. Smith JM (2004) Natural selection and the concept of a protein space. Nature 225(5232):563–564.

3. Hartl JK, Hartl DL (2006) A Primer of Ecological Genetics.

4. Theis KR, et al. (2016) Getting the hologenome concept right: An eco-evolutionary framework for hosts and their microbiomes. mSystems 1(2):1–6.

5. Opstal EJV, Bordenstein SR (2015) Rethinking heritability of the microbiome. Science 349(6253):1172–1173.

6. Rosenberg E, Zilber-Rosenberg I (2014) The Hologenome Concept: Human, Animal and Plant Microbiota (Springer Science & Business Media).

7. Archie EA, Theis KR (2011) Animal behaviour meets microbial ecology. Animal Behaviour 82(3):425–436.

8. McFall-Ngai M, et al. (2013) Animals in a bacterial world, a new imperative for the life sciences. 110(9):3229–3236.

9. Shropshire JD, Bordenstein SR (2016) Speciation by symbiosis: the microbiome and behavior. mBio 7(2):e01785–15–15–11.

10. Narahashi T (2008) Tetrodotoxin—A brief history—. Proceedings of the Japan Academy Series B, Physical and biological sciences 84(5):147.

11. Chau R, Kalaitzis JA, Neilan BA (2011) On the origins and biosynthesis of tetrodotoxin. Aquat Toxicol 104(1-2):61–72.

12. Yu VC-H, Yu PH-F, Ho K-C, Lee FW-F (2011) Isolation and identification of a new tetrodotoxin-producing bacterial species, Raoultella terrigena, from Hong Kong marine puffer fish Takifugu niphobles. Marine Drugs 9(12):2384–2396.

13. Williams BL (2010) Behavioral and chemical ecology of marine organisms with respect to tetrodotoxin. Marine Drugs 8(3):381–398.

14. Hanifin CT (2010) The chemical and evolutionary ecology of tetrodotoxin (TTX) toxicity in terrestrial vertebrates. Marine Drugs 8(3):577–593.

15. Brodie ED, Ridenhour BJ, Brodie ED (2002) The evolutionary response of predators to dangerous prey: hotspots and coldspots in the geographic mosaic of coevolution between garter snakes and newts. Evolution 56(10):2067–2082.

16. Geffeney SL, Fujimoto E, Brodie ED, Ruben PC (2005) Evolutionary diversification of TTX-resistant sodium channels in a predator-prey interaction. Nature 434(7034):759–763.

17. Hanifin CT, Yotsu-Yamashita M, Yasumoto T, Brodie ED III, Brodie ED Jr. (1999) Toxicity of dangerous prey: variation of tetrodotoxin levels within and among populations of the newt *Taricha granulosa*. J Chem Ecol 25(9):2161–2175.

18. Hanifin CT, Brodie ED (2008) Phenotypic mismatches reveal escape from arms-race coevolution. PLoS Biol 6(3):e60.

19. Hanifin CT, Brodie ED (2002) Tetrodotoxin levels of the rough-skinned newt, *Taricha granulosa*, increase in long-term captivity. Toxicon 40(8):1149–1153.

20. Cardall BL, Brodie ED Jr., Brodie ED III, Hanifin CT (2004) Secretion and regeneration of tetrodotoxin in the rough-skinned newt (*Taricha granulosa*). Toxicon 44(8):933–938.

21. Lehman EM, Brodie ED Jr., Brodie ED III (2004) No evidence for an endosymbiotic bacterial origin of tetrodotoxin in the newt *Taricha granulosa*. Toxicon 44(3):243–249.

22. Gall BG, et al. (2011) Tetrodotoxin levels in larval and metamorphosed newts (*Taricha granulosa*) and palatability to predatory dragonflies. Toxicon 57(7-8):978–983.

23. Gall BG, Stokes AN, French SS, Brodie ED III, Brodie ED Jr. (2012) Female newts (*Taricha granulosa*) produce tetrodotoxin laden eggs after long term captivity. Toxicon 60(6):1057–1062.

24. Gall BG, et al. (2014) Tetrodotoxin concentrations within a clutch and across embryonic development in eggs of the rough-skinned newts (*Taricha granulosa*). Toxicon 90(C):249–254.

25. Zakon HH, Jost MC, Lu Y (2011) Expansion of voltage-dependent Na+ channel gene family in early tetrapods coincided with the emergence of terrestriality and increased brain complexity. Molecular Biology and Evolution 28(4):1415–1424.

# CHAPTER 1: Symbiotic Bacteria Produce Tetrodotoxin in Poisonous Rough-skinned Newts

**Authors:** Patric M. Vaelli, Kevin R. Theis, Janet E. Williams, James A. Foster, and Heather L. Eisthen.

This chapter is a modified version of a manuscript under review.

## ABSTRACT

Rough-skinned newts (*Taricha granulosa*) are poisonous salamanders that possess tetrodotoxin (TTX), an extremely potent neurotoxin that selectively blocks voltage-gated sodium channels in the nervous system. Consequently, TTX serves as an excellent chemical defense against predation; however, some garter snake (*Thamnophis sirtalis*) populations in Western North America have evolved resistance to TTX, initiating coevolutionary “arms races” in which natural selection favors increasing levels of toxicity and resistance in newts and snakes, respectively. While the molecular and eco-evolutionary interactions between newts and snakes have been well-described, the biosynthetic origin of TTX in newts and other TTX-producing amphibians is unknown. Here, we demonstrate that symbiotic bacteria isolated from the skin of toxic newts produce TTX in laboratory culture. We isolated skin symbionts from toxic newts and screened for TTX production by hydrophilic interaction liquid chromatography tandem mass spectrometry (HILIC-MS/MS). Overall, we detected TTX in cultures from four bacterial genera: *Aeromonas, Pseudomonas, Shewanella*, and *Sphingopyxis*. We then used 16S rRNA sequencing to characterize and compare the skin microbiota of populations of toxic newts and newts that lack TTX. We found that skin-associated

bacterial communities were distinct in composition and structure, and that *Pseudomonas* spp. were enriched among toxic newts, suggesting a potential microbiome-level mechanism for increased toxicity in newt hosts. Overall, our results indicate that the newt skin microbiome contributes to TTX production in newts, raising important questions concerning the target of selection in the well-characterized coevolutionary arms race between newts and predatory garter snakes.

## INTRODUCTION

Tetrodotoxin (TTX, $C_{11}H_{17}N_3O_8$) is a potent small molecule neurotoxin present in a wide diversity of marine and terrestrial animals, as well as some algae and dinoflagellates (1, 2). TTX is the primary neurotoxin found in poisonous pufferfishes, from which the toxin was first isolated and described (3). Since the elucidation of its molecular structure (4-6), TTX has been discovered in several additional animal species from a variety of habitats, including xanthid crabs (7), horseshoe crabs (8), starfishes (9), flatworms (10), ribbon worms (11), arrow worms (12), several marine snails (13-15), and blue-ringed octopuses (16). In addition to pufferfishes, among vertebrates, TTX has been found in goby fishes (17), *Atelopus* toads (18, 19), frogs (20, 21), and several species of newt (22, 23). The broad phylogenetic distribution of TTX-containing animals, along with TTX's unusual molecular structure and potent neurotoxicity, has motivated several studies regarding the biosynthetic and evolutionary origin(s) of TTX (reviewed in (1, 24-26).

TTX selectively binds the alpha subunit of voltage-gated sodium ($Na_v$) channels expressed in neurons, muscles, and other excitable tissues, preventing membrane

depolarization and the generation of action potentials that underlie a significant portion of neural signaling and muscular function (27-29). Consequently, ingestion of TTX can result in numbness, muscular paralysis, ataxia, hypotension, cardiac arrhythmia, and respiratory failure (30), thereby rendering TTX an effective, near universal chemical defense against animal predators. The high affinity and specificity for $Na_v$ channels has also made TTX an important molecular tool in neuroscience research: it is routinely used to block $Na^+$ conductance in experimental preparations, allowing researchers to examine the role of $Na^+$ in cellular transduction pathways and the activity of other ion channels (31, 32). TTX also has potential for use in medical applications as a non-opioid analgesic or anesthetic (33, 34).

Curiously, the biosynthetic and evolutionary origins of TTX remain unknown. Its broad phylogenetic distribution across animals could result from repeated convergent evolution, horizontal gene transfer, and/or environmental acquisition from exogenous sources, such as bioaccumulation through diet or exposure to TTX-producing microorganisms (e.g. algae, dinoflagellates, or bacteria). Investigations into the biosynthetic origin of TTX are hindered by the inability to identify genetic loci associated with TTX production (but see 35) and are further complicated by the lack of resemblance between TTX and molecular intermediates from characterized biogenic pathways (36). However, a substantial body of evidence suggests that TTX in marine ecosystems is produced primarily by bacteria and subsequently accumulates in animals through the diet or symbiosis with TTX-producing bacteria. To date, TTX-producing bacteria from 23 genera have been isolated from toxic marine animal hosts (2, 37, 38). These bacterial symbionts are typically isolated from the toxic tissues of host animals,

such as the skin, ovaries, and liver of pufferfishes (39). Furthermore, free-living TTX-producing bacteria have also been isolated from marine and freshwater samples (40, 41). However, the primary source of TTX in terrestrial and freshwater animals is unknown.

TTX toxicity in animals can have substantial impacts on eco-evolutionary interactions among species, and no animal better demonstrates this than the rough-skinned newt (*Taricha granulosa*; hereafter, “newts”). TTX concentrations in certain populations of newts are higher than levels detected in any other organism, and in some cases individual newts are sufficiently toxic to kill several adult humans (26). Classic ecological studies have established that variation in newt toxicity is driven in part by the evolution of TTX-resistant $Na_v$ channels in populations of predatory garter snakes (*Thamnophis sirtalis* spp.) that prey on newts (42-44). Interestingly, toxicity and toxin resistance in newts and snakes, respectively, are strongly correlated geographically, suggesting that these two phenotypes are coevolving (45). Resistance has evolved independently in different garter snake populations across the geographical range of newts (46), and TTX resistance has itself evolved in parallel across the $Na_v$ channel gene family in snakes (47). Garter snakes that ingest toxic newts are then able to store TTX within their own tissues for chemical defense against predation (48).

Despite the central role of TTX in the well-documented coevolutionary interactions between newts and snakes, the biosynthetic and evolutionary origin of TTX in rough-skinned newts and all other TTX-laden amphibians are unknown (25, 26). Previous studies have sought to identify the origin of TTX in newts, but to date the available evidence is indirect. While some other animals accumulate TTX dietarily, TTX

levels in newt skin increase over long-term captivity and are partially regenerated after the toxin is secreted in response to a mild electric shock, regardless of diet (49, 50). Furthermore, newts that were fed radiolabeled TTX precursors did not ultimately produce labeled TTX (51). More recently, the presence of TTX-producing endosymbiotic bacteria among newts was examined by PCR amplification of the bacterial 16S rRNA gene from total DNA isolated from surface sterilized newt skin; the authors were unable to detect bacterial DNA, leading them to conclude that TTX in newt skin could not be produced by bacteria (52). This experiment has often been cited as demonstrating that amphibians do not derive TTX from symbiotic bacteria (50, 53-56).

Thus, the origin of TTX in newts and other amphibians remains unresolved. In this study, we re-evaluated whether TTX could be produced by symbiotic (i.e. resident) bacteria in newts. Because the TTX biosynthetic pathway has not been described, genetic screens or metagenomic sequencing approaches cannot be applied to determine whether newt host or resident skin microbes possess the genes necessary for TTX production (1, 36). Instead, we isolated symbiotic bacteria in pure culture and examined individual bacterial isolates for TTX production following the general approach applied in isolating TTX-producing bacteria from other animal hosts (38, 57). While bacterial cultivation can be difficult, we employed a variety of strategies including the use of long incubation times, low incubation temperatures, and nutrient-limited, selective, or enriched (e.g. blood) media to inhibit rapid growth and promote biodiversity in lab culture (58, 59).

Through these efforts, we cultured ~500 bacterial strains representing >60 genera from the skin of toxic newts. We screened bacterial strains and their cultivation

media using hydrophilic interaction liquid chromatography tandem mass spectrometry (HILIC-MS/MS) and established TTX production by several bacterial monocultures. 16S rRNA gene analysis revealed these isolates were from the genera *Aeromonas*, *Pseudomonas*, *Shewanella*, and *Sphingopyxis*. Using electron microscopy, we detected symbiotic bacteria residing near the apex and within the pore of toxin-sequestering granular glands in the dorsal skin of newts, indicating that bacteria and TTX are co-localized in the skin. Finally, we characterized the skin-associated bacterial communities from two populations of newts that possess either high or undetectable quantities of TTX and found that both the composition and relative abundances of different bacterial operational taxonomic units (OTUs) were distinct between the two populations, and that *Pseudomonas* OTUs were more abundant in the microbiota of toxic newts, indicating a possible hologenomic mechanism for elevated whole animal toxicity (60). Our results indicate that TTX toxicity in *T. granulosa* arises in part from a symbiotic relationship with TTX-producing bacteria.

## RESULTS

### Newt toxicity varies geographically.

We measured TTX concentrations in rough-skinned newts from a population in Oregon, USA (January Pond; 44°36'13.8"N 123°38'12.1"W), which have previously been shown to be highly toxic (45, 61). For subsequent microbiome-level comparisons, we also investigated a reportedly non-toxic population in Idaho, USA with little to no TTX (Virgil Phillips Farm Park; 46°48'49.9"N 117°00'57.2"W) (**Figure 1.1A**). Our results confirmed that newts from Oregon possessed TTX with mean concentrations of 126.5 ±

42.1 ng $mL^{-1}$ per mg skin (mean ± SEM, n = 5) and individual concentrations varying from 27.3 to 261.6 ng $mL^{-1}$ per mg of dorsal skin. TTX was undetectable in any newt from Idaho (n = 17) with a limit of detection of 0.1 ng/ml (**Figure 1.1B**).

**Skin bacteria from toxic newts produce TTX in lab culture.**

We investigated skin-associated bacteria for TTX production, as the skin is the most toxic organ in newts and TTX-producing strains have been repeatedly isolated from toxic tissues in the aquatic host animals listed above. TTX levels in the gut are just above detection thresholds and are lower than skin by 1-2 orders of magnitude (62, 63),

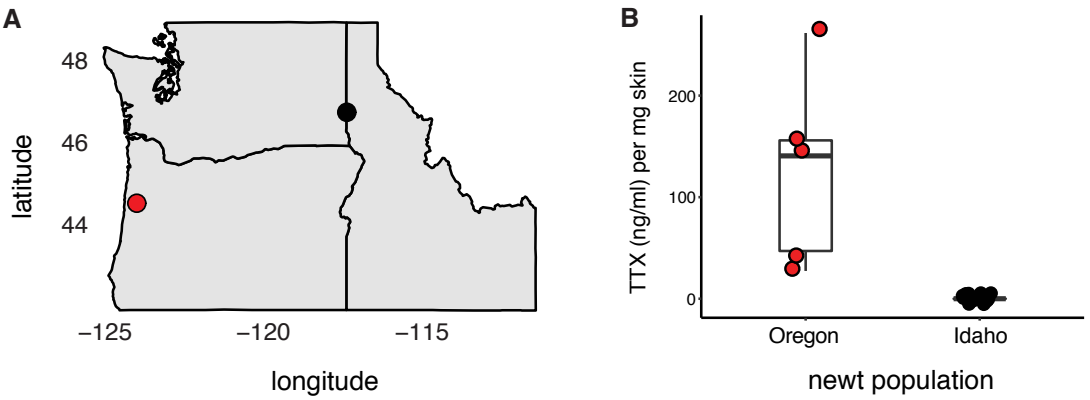


**Figure 1.1: Geographic variation in newt toxicity. (A)** We focused on two populations of newts previously shown to possess either high quantities of TTX (red dots; January Pond, OR, USA, 44°36'13.8"N 123°38'12.1"W) or negligible quantities (black dots; Virgil Phillips Farm Park, Idaho, USA, 46°48'49.9"N 117°00'57.2"W). **(B)** HILIC-MS/MS quantification of TTX purified from 2 mm diameter newt skin biopsies from both populations. All newts from January Pond (n=5) possessed TTX, but TTX was not detected in the skin of any newt from Virgil Phillips Farm Park (n=17); limit of detection = 0.1 ng/ml.

and no TTX transport mechanisms are known to exist that could result in differential toxicity among newt tissues. We therefore focused on cutaneous bacterial communities as a potential source of TTX in this species.

Bacterial strains were cultured from newt skin and screened for TTX production by hydrophilic interaction liquid chromatography tandem mass spectrometry (HILIC-MS/MS) (**Figure 1.2**). We maintained toxic wild-caught newts from Oregon in the lab and repeatedly collected skin swab samples to generate multi-species bacterial cultures. Individual colonies were streaked for purity and isolated strains were then

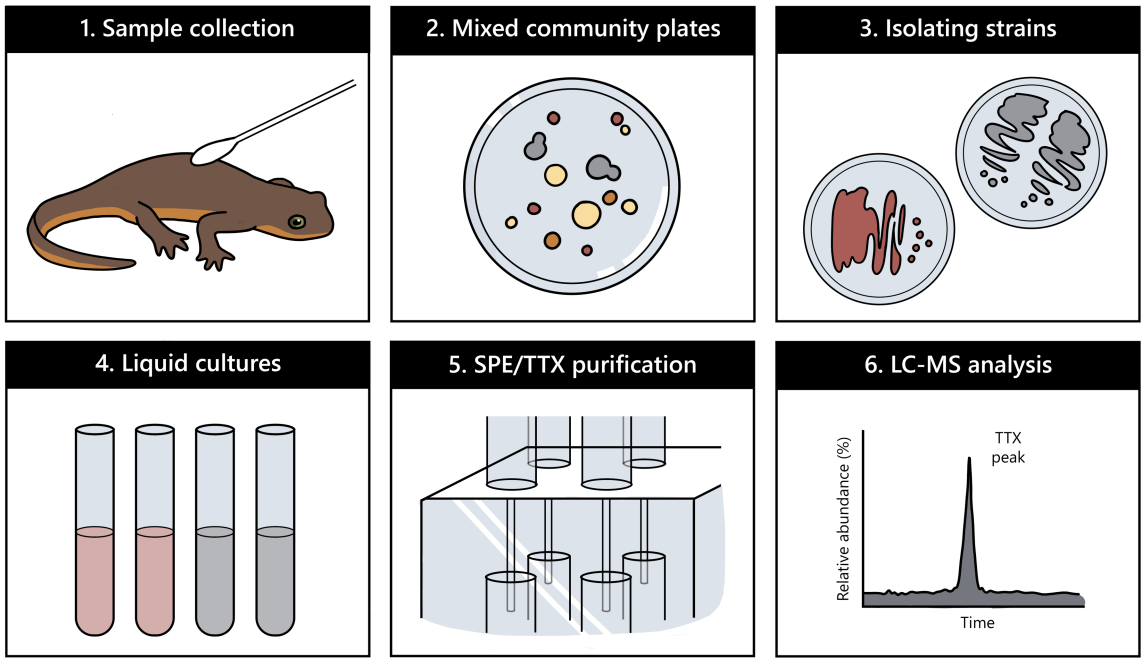


**Figure 1.2: Overview of the TTX screening approach.** Bacterial samples were collected from the skin of toxic newts and plated on agar media. Individual colonies were picked and streaked on new plates to establish pure cultures, which were subsequently used for 16S rRNA gene sequencing-based taxonomic identification and frozen for preservation. Following taxonomic identification, individual strains were inoculated in liquid culture media and grown for 2 weeks. Culture supernatant was purified for TTX by solid-phase extraction (SPE), and extracts were screened against TTX analytical standards by hydrophilic chromatography tandem mass spectrometry (HILIC-MS/MS).

identified by 16S rRNA gene sequencing and analysis. Bacterial sequences were assigned genus-level classifications using the Ribosomal Database Project Classifier tool with an 80% confidence threshold (64). Newt symbionts were stored in cryoprotectant at -80 °C for our culture collection prior to HILIC-MS/MS analysis.

Overall, we isolated approximately 500 strains from newt skin and obtained high-quality 16S rRNA gene sequences for taxonomic identification of 354 strains (**Table A1.1**). The sequenced strains comprised 65 genera, the majority of which were Proteobacteria (57.6%) and Bacteroidetes (28.2%), but Actinobacteria (8.5%) and Firmicutes (5.6%) were also present. The most commonly isolated strains were Gammaproteobacteria such as *Pseudomonas*, *Aeromonas*, and *Shewanella*. Bacteroidetes, including *Flavobacterium* and *Chryseobacterium*, and Alphaproteobacteria, including *Rhizobium*, *Sphingomonas*, and *Sphingopyxis*, were also common. Maximum-likelihood phylogenetic analysis based on an alignment of newt bacterial 16S rRNA gene sequences to the SILVA ribosomal RNA gene database (65) reconstructed topologies similar to currently hypothesized relationships among major bacterial phyla (**Figure A1.1**).

Selected bacterial isolates were then cultured in dilute nutrient broth (10% R2B) at 20°C for 2 weeks. At the end of cultivation, 1 mL of supernatant from each sample was purified for TTX by solid-phase extraction (SPE) and analyzed by HILIC-MS/MS in positive electrospray ionization mode (**Materials and Methods**). TTX was identified by an observed retention time identical to authentic TTX standards and multiple reaction monitoring of both primary (320.1 > 162.1 m/z) and secondary (320.1 > 302.1 m/z) precursor-to-product ion transitions. Cultivation media supplemented with TTX (100 ng

$mL^{-1}$) or without TTX were run as controls in all experiments to monitor SPE efficiency and to screen for potential contamination, respectively.

Using this approach, we detected TTX in cultures from 11 bacterial strains. Representative chromatograms for standards, bacterial media controls, and TTX positive bacterial samples are shown in **Figure 1.3**. HILIC-MS/MS confirmed the presence of ions at 162.1 and 302.1 m/z, which correspond to the two most abundant product ions formed by TTX fragmentation. The observed retention time for TTX was ~ 3 mins, and calibration curves from 0.5 to 25 ng $mL^{-1}$ were linear (e.g., Y = 6950X + 2620, $R^2$ = 0.9972, **Figure A1.2**). TTX was detected in all positive controls, confirming the efficacy of SPE purification. Negative controls showed background matrix signal with a broad peak from 2.4 – 3.2 mins, but these peaks were clearly distinguishable from TTX standards and TTX positive samples. Furthermore, unlike TTX positive samples, the secondary fragmentation (320.1 > 302.1 m/z) was never observed at the correct retention time in negative controls.

Taxonomic identification based on 16S rRNA gene sequence data indicated that the TTX positive strains were derived from four bacterial genera: *Aeromonas*, *Pseudomonas*, *Shewanella*, and *Sphingopyxis* (**Table 1.1**). The first three genera are members of the Gammaproteobacteria, and each genus contains TTX-producing strains that have been previously identified in other toxic animals (38). Sphingopyxis is within Alphaproteobacteria and no TTX-producing strains have yet been identified in this genus; however, this class contains two TTX-producing strains from the genera *Caulobacter* and *Roseobacter* (38). Overall, we identified seven isolates of *Pseudomonas* spp. that produced TTX. A pairwise comparison of 16S rRNA gene

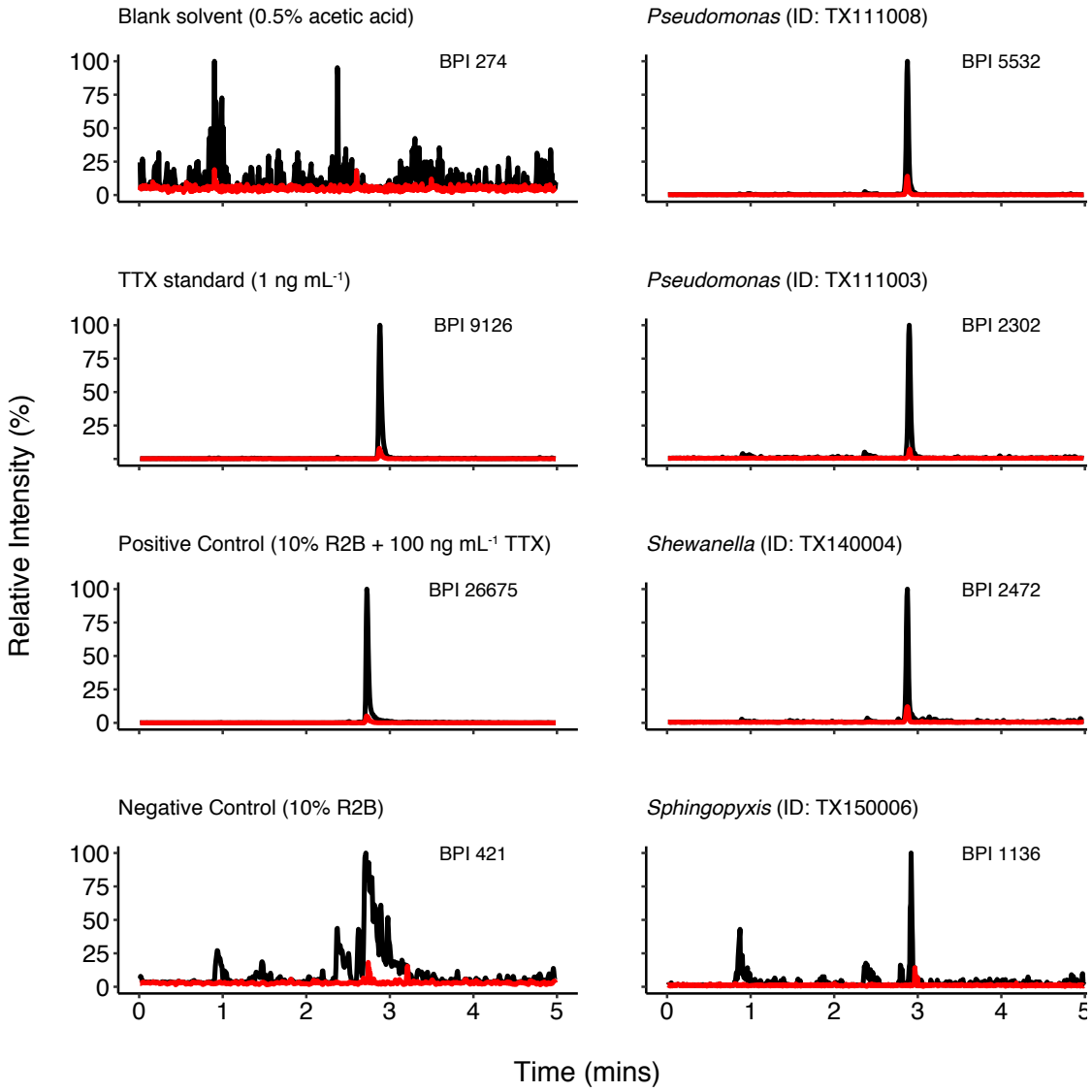


**Figure 1.3: Representative chromatograms demonstrating the presence of TTX in bacterial cultures.** The left column shows data from standards and controls, including sample solvent (0.5% acetic acid), a pure TTX standard dissolved in the sample solvent at 1 ng/ml, a positive control with 100 ng/ml TTX added to 10% R2A medium prior to SPE, and a negative control of 10% R2A without TTX. The chromatograms in the right column are from four strains found to produce TTX in this study. Black and red lines indicate primary (320.1 > 162.1 *m/z*) and secondary (3201.1 > 302.1 *m/z*) precursor-to-product ion transitions for TTX, respectively. The observed retention time was approximately ~ 3 mins. All chromatograms are plotted as abundance relative to the base peak intensity (BPI) for the run, and BPI for each chromatogram is included as a measure of TTX signal strength.

TX180010 shared > 99% nucleotide identity across homologous bases, and TX135003 and TX135004 also shared > 99% sequence identity, and yet these two groups appeared to be distinct from each other (maximum similarity is 96.05%). 16S rRNA gene sequences for the remaining two isolates, TX111008 and TX111009, were unique from each other and the other two groups (**Table A1.2 and Figure 1.3**). Thus, the seven isolates of TTX-producing *Pseudomonas* spp. appear to represent four distinct strains. Furthermore, 16S rRNA gene sequences for the two TTX-producing Shewanella spp. strains were 94.16% identical, sharing only 725 of 782 nucleotide identities; these sequences may represent two distinct strains. Thus, we found multiple unique strains of TTX-producing bacteria inhabiting the skin of toxic newts.

**Table 1.1: Summary of TTX-producing bacteria identified in this study.** Bacteria strains were isolated from toxic newts and screened for TTX production by HILIC-MS/MS. Strains were identified by 16S rRNA gene sequencing and classification by the Ribosomal Database Project Classifier tool at a 0.8 similarity cut-off. GenBank accession numbers of top BLAST hits (>99% similarity) are also shown below. *Pseudomonas* spp. were the most commonly identified TTX producers in this study, but strains from three additional genera were also found to produce TTX.

| Genus | Strain ID | Isolation media | Pigmentation | Top BLAST Hit |
|---|---|---|---|---|
| *Aeromonas* | TX196002 | Blood agar | Yellow | KC202260.1\| A. allosaccharophila strain S5-1 |
| *Pseudomonas* | TX111003 | Blood agar | White | KJ726609.1\| P. migulate |
| - | TX111008 | Blood agar | Gray | KM114925.1\| A. beijerinckii |
| - | TX111009 | Blood agar | Pink | KC108718.1\| P. aeruginosa |
| - | TX135003 | R2A | White | KX279667.1\| Pseudomonas sp. OT42 |
| - | TX135004 | R2A | White | AB633201.1\| Pseudomonas sp. HKF-3 |
| - | TX174011 | R2A | Yellow | MF948930.1\| Pseudomonas sp. strain PrPr088 |
| - | TX180010 | Blood agar | White | LC339940.1\| P. pseudoalcaligenes Hiro-2 |
| *Shewanella* | TX140004 | R2A | White | JQ511863.1\| Shewanella sp. HJ-53 |
| - | TX180013 | Blood agar | Pink | MG428720.1\| S. xiamenensis strain F_12 |
| *Sphingopyxis* | TX150006 | R2A | Yellow | HQ113210.1\| Sphingomonas sp. CL-9.15a |

**Bacteria inhabit the skin and dorsal glands of Rough-skinned newts**.

We used scanning electron microscopy (SEM) to visualize symbiotic microbiota from the dorsal epithelia of a toxic adult newt from Oregon (**Figure 1.4**). In amphibians, granular glands are the primary storage sites of toxic or noxious chemicals, including tetrodotoxin in newts and alkaloid toxins in poison dart frogs (66-69). Rough-skinned newts have especially enlarged granular glands in their dorsal skin, and previous work

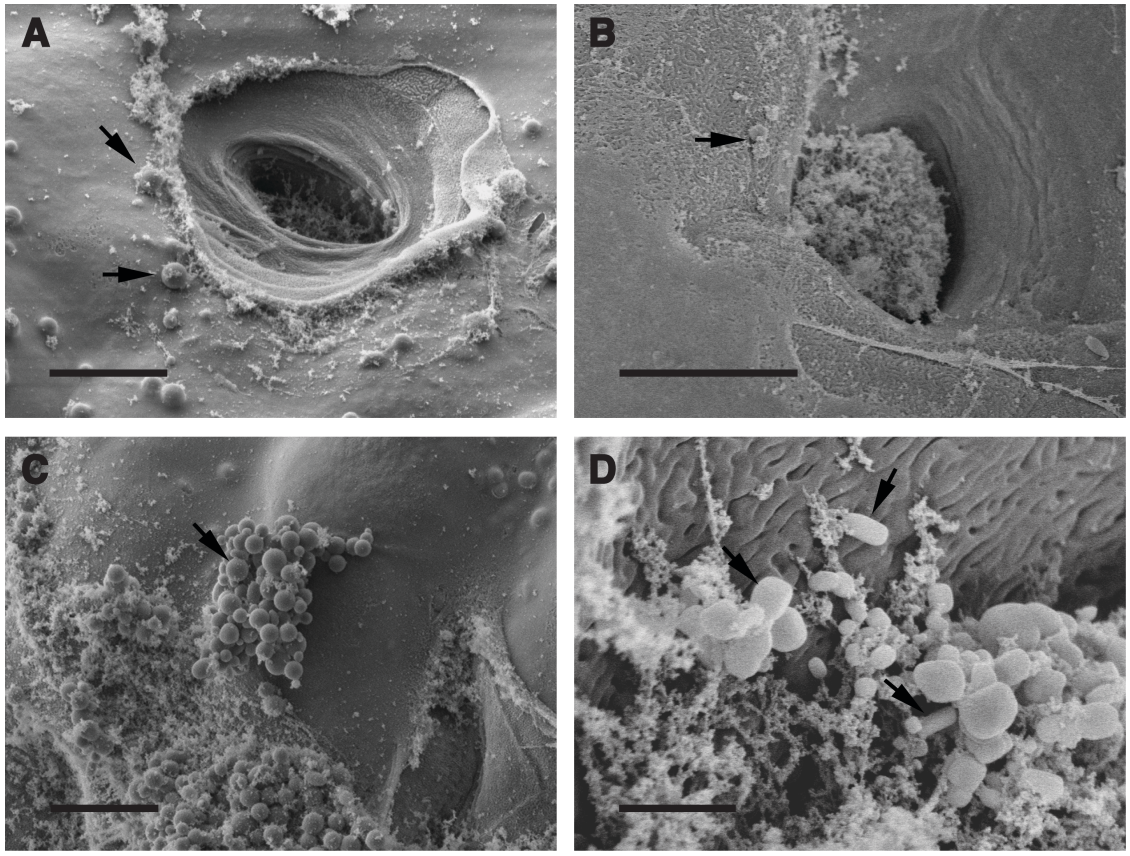


**Figure 1.4: Scanning electron micrographs reveal communities of morphologically distinct bacteria inhabiting the skin of a male rough-skinned newt.** Black arrows indicate bacteria present on the skin near glandular openings **(A, B)**, present on the skin **(C),** and in the glandular ducts **(D)**. Scale bars for near field objects = 10 μm (A - C), 1 μm (D).

has shown that granular gland density is strongly predictive of individual variation in whole animal toxicity (70).

SEMs from the pores and surrounding area near the apex of dorsal granular glands revealed the presence of resident bacteria (**Figure 1.4A** and **B**). At higher magnification within the ducts of these glands, we observed mixed bacterial communities including rod- and coccus-shaped bacteria (**Figure 1.4C** and **D**). The physical association between resident skin bacteria and toxic granular glands may provide a mechanism of TTX sequestration in amphibians, as TTX-producing bacteria have been isolated directly from toxic organs in other animals such as pufferfishes.

**Characterization and comparison of the skin microbiota from toxic and non-toxic newts.**

We then applied culture-independent 16S ribosomal RNA gene sequencing to characterize the skin-associated microbiota of newts from a toxic and a non-toxic population (**Figure 1.1**). Bacterial samples were collected in the field from wild-caught adult male newts in Oregon (n=10) and Idaho (n=17) at four body sites: dorsal skin, ventral skin, cloaca, and submandibular (i.e. chin) glands. Bacterial DNA was extracted and the V4 hypervariable region of the 16S rRNA gene was amplified and subjected to high-throughput Illumina sequencing (71). Prior to analysis, 16S amplicons were clustered into operational taxonomic units (OTUs) defined by 97% or greater homologous nucleotide identity and assigned taxonomic classifications using the Ribosomal Database Project (RDP) classifier tool (64). 16S amplicon data were then subsampled to 5,000 sequences for community-level comparisons. An average Good's

coverage estimate of 0.9454 ± 0.0067 (mean ± SEM) (72) and saturation of rarefaction curves (**Figure A1.4**) indicated that this subsampling depth was sufficient to capture the breadth of bacterial diversity within samples in this study.

In total, we identified 4,160 unique bacterial types (i.e. OTUs) across all newt samples: 614 OTUs were unique to toxic newts, 1,943 were unique to non-toxic newts, and 1,603 were shared between the two populations. The observed number of OTUs (mean ± SEM) in each sequenced community was 401 ± 70 OTUs for toxic newts, and 733 ± 82 OTUs for non-toxic newts. Among the 20 most relatively abundant OTUs, 12 were present only in one population while 8 were present in both populations (**Table A1.3 and Figure 1.5**). These highly abundant and conserved OTUs identified in both populations may represent core skin microbiota inhabiting newt hosts living hundreds of miles apart.

The composition (i.e. presence/absence of OTUs) and structure (i.e. relative abundances of OTUs) across bacterial communities also differed between the two populations. Principal coordinates analysis revealed a strong clustering pattern based on geographic location in both composition (Jaccard index) and structure (Bray-Curtis index) of OTUs (**Figure 1.5B** and **C**), but no clustering based on body site, even when analyzed separately within each population (**Figure A1.8**). Permutational multivariate analysis of variance (PERMANOVA) tests confirmed a significant effect of location in community composition (Jaccard index, $F = 18.12$, $P = 0.0001$) and structure (Bray-Curtis index, $F = 40.40$, $P = 0.0001$). We also observed that Idaho newts were more variable in their skin communities (**Figure A1.9**), and this observation was confirmed by a permutational test for multivariate dispersion (PERMDISP, P =

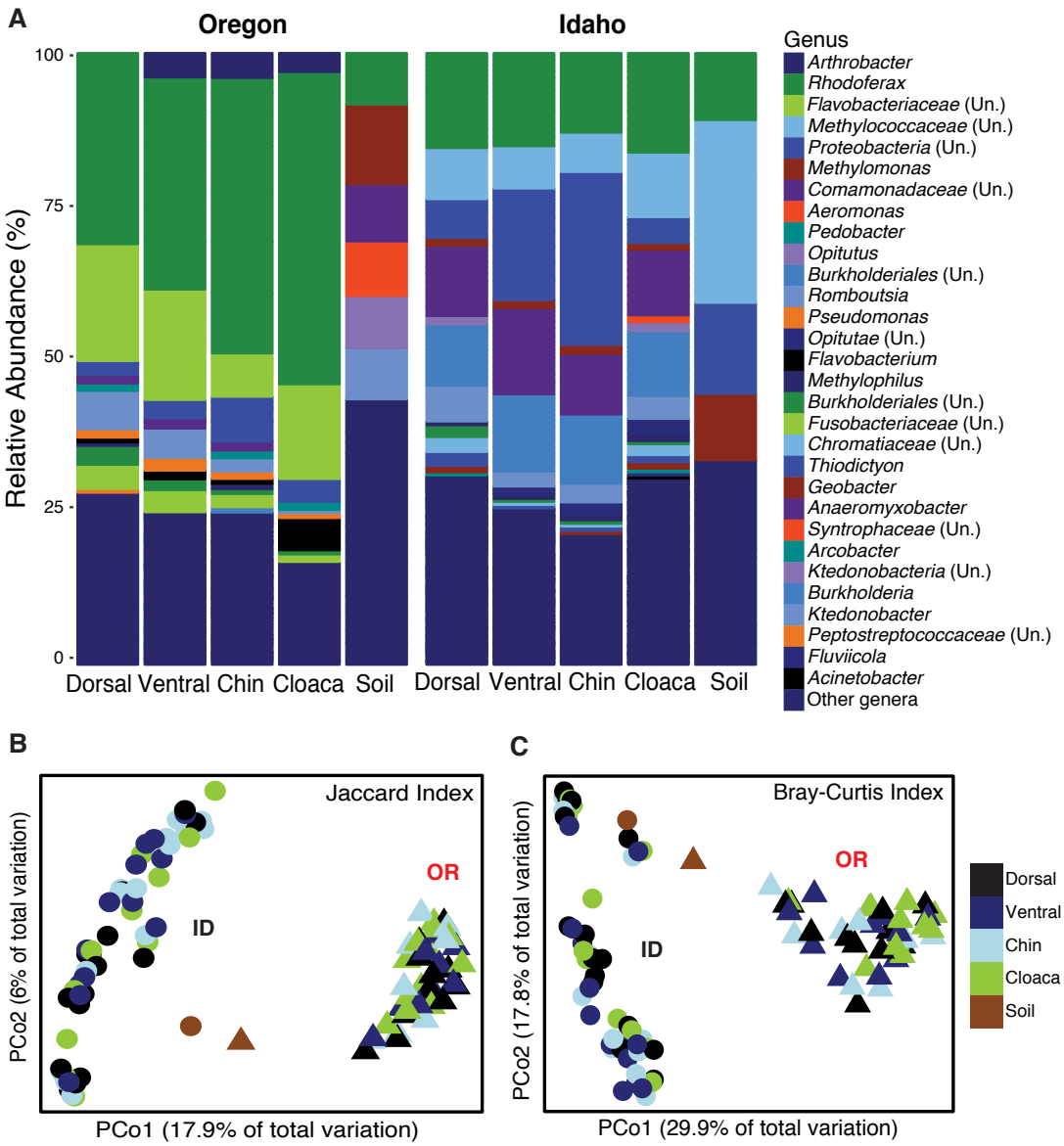


**Figure 1.5: Comparison of the skin microbiota from toxic and non-toxic newt populations. (A)** Mean relative abundance of bacterial OTUs found in newts from each population, as well as in soil samples from their habitat. All OTUs present at < 3% relative abundance were categorized as 'other genera'. The relative abundances of bacterial differed markedly between the two populations and between the newts and soil samples. Principle coordinates analysis of **(B)** OTU composition (Jaccard index) and **(C)** OTU abundance (Bray-Curtis index) of skin microbiota from Idaho (circles) and Oregon (triangles) newts reveal distinct clustering within the two populations. Non-parametric multivariate analysis of variance (PERMANOVA) tests confirm a significant effect of location on both the composition ($F$ = 18.12, $P$ = 0.0001) and structure ($F$ = 40.40, $P$ = 0.0001) of skin-associated bacterial communities. Soil samples from each site are shown in brown.

0.0053). Overall, these results demonstrate that newts are populated with diverse bacterial communities that are distinct between the Oregon and Idaho populations, and from soil samples collected from each site.

***Pseudomonas* OTUs are enriched in the microbiota of toxic newts**.

We next determined whether there was a differential abundance of OTUs assigned to the same genera as TTX-producing strains between the toxic Oregon and non-toxic Idaho newt populations. One source of geographic variation in whole animal TTX toxicity may be a differential abundance of TTX-producing bacteria in the microbiome. Indeed, Rosenberg and Zilber-Rosenberg have postulated that microbially-derived phenotypes may respond more rapidly to selection than phenotypes encoded by the host genome by simply altering the relative abundance of the specific microbes underlying that trait (73).

We searched for OTUs assigned to TTX positive genera (*Aeromonas*, *Pseudomonas*, *Shewanella*, and *Sphingopyxis*) among the top 1000 most abundant OTUs. We did not find evidence of differential abundance in Aeromonas, Shewanella, or Sphingopyxis between the two newt populations; OTU00027 Aeromonas spp. was highly abundant in newts from both populations, while Shewanella spp. and Sphingopyxis spp. were rare and did not show evidence of differential abundance between the populations. However, we found six *Pseudomonas* OTUs that were differentially abundant between the two populations: OTUs 00042, 00145, 00224, and 00485 were highly abundant in toxic newts, while OTU00600 was more abundant in non-toxic newts (**Figure 1.6A**). Note the difference in scale: OTU00042 is 5x more

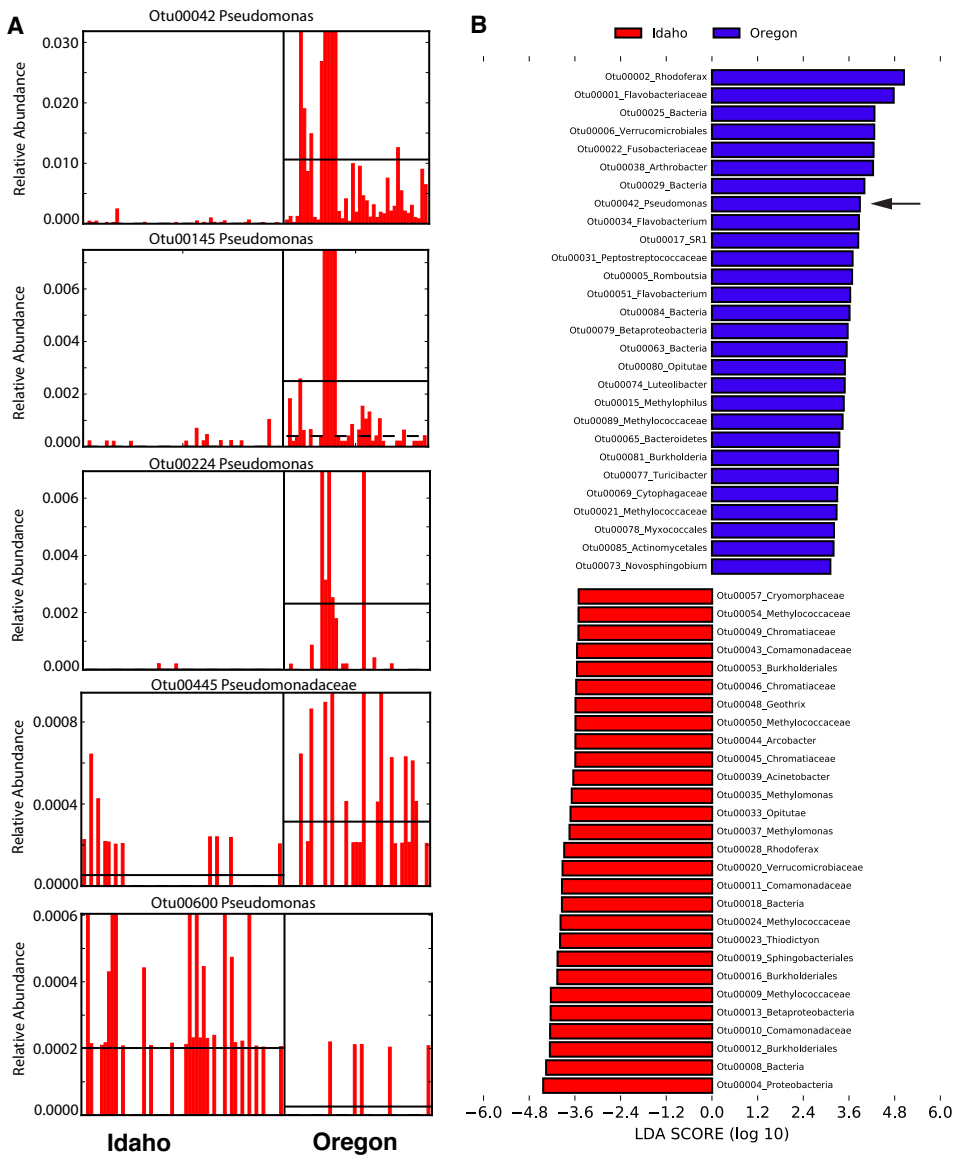


**Figure 1.6: Differential abundance of *Pseudomonas* spp. strains in toxic and non-toxic newts. (A)** Proportional relative abundances of five *Pseudomonas* spp. OTUs from each newt sampled from Idaho (left) and Oregon (right). Mean relative abundance of each OTU decreases from top to bottom, with the top plot (OTU00042) displaying the most abundant OTU. Black horizontal bars in each plot show the mean abundance across all samples within a population. **(B)** Linear discriminant analysis effect size (LEfSe) results for the top 50 most differentially abundant OTUs between the two newt populations. These OTUs are the major contributors to differences in beta diversity between the two populations. Among the most differentially expressed OTUs, we observed a statistically significant enrichment of OTU00042 *Pseudomonas* (black arrow) in toxic newts from Oregon. The differential presence of *Pseudomonas* spp. could partially underlie variation in TTX levels observed in newts.

abundant than OTUs 00145 and 00224 and 30x more abundant than OTUs 00485 and 00600. Thus, OTU00042 represents a *Pseudomonas* spp. that is highly and differentially abundant in toxic newts. To determine if these observed differences in *Pseudomonas* OTUs were significant drivers of beta diversity between toxic and non-toxic newt populations, we performed linear discriminant analysis effect size (LEfSe) (**Figure 1.6B**). We identified 50 OTUs whose relative abundances differed significantly between the two populations; most interestingly, *Pseudomonas* spp. OTU00042 was significantly more abundant in toxic Oregon newts than in nontoxic Idaho newts. These results show that *Pseudomonas* OTUs are differentially present in toxic vs. non-toxic newts, and that OTU00042 exerts a significant force in driving beta diversity between newt populations.

## DISCUSSION

The origin of TTX in newts and all other freshwater and terrestrial animals has long been a subject of debate (26). Many of the hypotheses regarding this subject have been difficult to test directly, and the experiments that have been performed have not allowed researchers to draw definitive conclusions. For example, Hanifin and colleagues found that TTX levels in wild caught toxic newts maintained in laboratory captivity and fed unnatural diets tend to increase over the course of a year (49). In that study, although the mean increase in TTX levels across all experimental animals was statistically significant, the data for individual newts were variable, with some newts decreasing in toxicity or maintaining TTX levels similar to those at the start of the experiment. A follow-up study showed that, overall, newts forced to secrete their toxin

by electric shock had regenerated their TTX levels after nine months, despite laboratory conditions that prevented access to the newts' typical diet and environmental microbiota (50). Again, the effect was measurable for mean values across the whole study, but only 2 of 31 newts in the study recovered their TTX levels to pre-secretion values and the remaining newts recovered an average 42% of their original TTX levels over the course of 9 months. This result was interpreted as supporting an endogenous origin for TTX in newts, although one might expect that, if endogenous, such a critical antipredator defense would be under strong homeostatic control. Further, the experiment does not rule out the possibility that TTX is produced by symbiotic bacteria. A final study attempted to amplify 16S rRNA genes from DNA extracted from newt tissues by PCR (52). Although microbial DNA was detected in the gut (a positive control), the authors were unable to amplify bacterial DNA from surface-sterilized skin tissue. This result has been widely cited as indicating that TTX in newts could not be produced by skin-associated microbes (1, 26, 45, 50, 53, 54, 74). The results we report here contradict this assertion.

Although TTX production by bacteria has been well documented for marine animals (1), this is the first time TTX-producing bacteria have been identified in association with any freshwater or terrestrial vertebrate. Newt species from diverse genera are known to possess TTX, including Notophthalmus, Triturus, Cynops, Paramesotriton, Pachytriton, and Laotriton (75-78). In addition, some species of toads in the genus Atelopus also possess TTX, as do frogs in the genera Colostethus and Polypedates (18, 19, 79-82). Indeed, until recently TTX in freshwater and terrestrial habitats had been found only among amphibians, leading some researchers to

speculate that TTX biosynthesis evolved convergently in amphibians (reviewed in (25, 26)). The recent discovery of TTX in two species of invasive freshwater flatworms confirms that another biosynthetic source of TTX exists in freshwater systems outside of amphibians (83), and our results suggest that TTX in diverse amphibians may ultimately be of bacterial origin.

Interestingly, we found that the composition of skin bacterial communities was more variable in non-toxic newts from Idaho than in toxic newts from Oregon. This difference may reflect a strong selective pressure on toxic newts to maintain a specific bacterial assemblage, perhaps to maximize colonization by TTX-producing symbionts or to provide a microbial ecosystem structure that is favorable for TTX biosynthesis. Amphibian skin is inhabited by a diverse array of microbes, and early studies suggested that amphibian hosts regulate their symbiotic communities through both adaptive immune responses and anti-microbial peptide expression (84-87). Indeed, McKenzie et al. demonstrated that host species identity is a stronger predictor of skin bacterial community composition than is the pond of origin in cohabiting tiger salamander and bullfrog larvae (88). Thus, we expect that *T. granulosa* should be able to regulate the composition of their skin microbiota and that the differences between the Oregon and Idaho newts are likely not due to environment alone; however, analysis of additional environmental samples and replicate populations are necessary.

One of the most interesting insights to arise from our discovery is the possibility that the skin microbiome is contributing to the predator-prey arms race between toxic newts and TTX-resistant garter snakes. Research carried out by the Brodies and their colleagues has shown that populations of garter snakes sympatric with TTX-laden

newts possess adaptive mutations in their $Na_V$ channels that prevent TTX from binding, allowing resistant snakes to prey on highly toxic newts (45, 53, 61, 89, 90). TTX resistance has evolved repeatedly across different populations of garter snakes as well as other species of snakes exposed to TTX-defended prey across the planet (46, 91). As snake populations accumulate adaptive mutations in their $Na_V$ channels, selection drives increasing levels of toxicity in newts (61). As newt populations become more toxic, selection favors increased resistance in snake populations, such that an asymmetric escalation of these two traits, or coevolutionary arms race, emerges between the two species (90). The means by which newts produce TTX has remained a central mystery throughout these studies.

If selection by predatory garter snakes favors increasing levels of toxicity in newt populations, our results suggest that selection is acting upon not only genetic variation in the host species, but also variation across the skin microbiome. Mutations in host traits critical in shaping the assembly and maturation of the skin microbiome, such as anti-microbial peptides, immune responses, production of nutrients favoring TTX-producing microbes, or production of TTX precursors may be critical for increased TTX toxicity across newt populations. However, selection could also act directly on TTX-producing skin symbionts either by increasing the amount of TTX synthesized per unit time or increasing the relative abundance of TTX-producing symbionts in the skin microbiome.

Newts and their resident microbiota are perhaps not well conceptualized as an animal-microbe dichotomy; it may be better to consider the effects of selection across the hologenome, the collective genetic variation present in both host and symbionts

(73). Indeed, many recent studies emphasize the critical importance of host-associated microbes in basic animal physiology, development, nutrition, nervous system function, and even behavior (92-97). In the coevolutionary arms race between toxic newts and resistant snakes, selection may act upon the phenotype that emerges from the collective interactions between the newt host and bacterial symbionts, termed the holobiont (73). One prediction of the hologenome theory is that adaptive evolution can occur rapidly by increasing the relative abundance of specific symbionts if the metabolites derived from that symbiont are critical for holobiont fitness (60). This potential evolutionary force would avoid a long and winding road through a complex adaptive landscape for the host, particularly for epistatic traits such as TTX biosynthesis, which is predicted to involve a dozen or more enzymes (1).

We have shown that rough-skinned newts possess TTX-producing symbiotic bacteria upon their skin. We demonstrate that newt bacterial symbionts can produce TTX in laboratory culture, and that population-level variation in the composition of the newt skin microbiome is correlated with variation in TTX toxicity across newt populations. Future studies exploring the relationship between newt host toxicity and the composition of newt skin microbiota could provide a mechanistic basis for the observed variation in newt toxicity across different populations, and possibly reveal interesting instances of parallel evolution occurring at the hologenomic level.

## MATERIALS AND METHODS

All procedures involving animals were approved by and conducted under the supervision of the Institutional Animal Care and Use Committee at Michigan State

University (approval no. 10/15-154-00), in accordance with guidelines established by the US Public Health Service.

**Laboratory Animals**

All laboratory procedures were performed using adult male rough-skinned newts (*Taricha granulosa*) collected in Oregon, USA (January Pond; 44°36'13.8"N 123°38'12.1"W). Newts were housed in glass aquaria containing Holtfreter's solution (60 mM NaCl, 0.67 mM KCl, 0.81 mM $MgSO_4$, and 0.68 mM $CaCl_2$; pH 7.2 – 7.6); floating platforms in each aquarium provided terrestrial refuges. Newts were maintained at 20 °C with a 14:10 light-dark cycle and fed blackworms (*Lumbriculus variegatus*) 2-3 times weekly.

**Bacterial cultivation**

To collect bacterial samples, newts were first rinsed in reverse osmosis (RO) $H_2O$ for 5 sec to remove transient bacteria and swabbed 10 times (down and back) each on the dorsal and ventral skin surfaces using a sterile cotton swab (Puritan Medical Products, Guilford, ME). The sample swab was then placed in 1 mL Hank's Buffered Salt Solution (HBSS; 0.137 M sodium chloride, 5.4 mM potassium chloride, 0.25 mM disodium phosphate, 0.56 M glucose, 0.44 mM monopotassium phosphate, 1.3 mM calcium chloride, 1.0 mM magnesium sulfate, 4.2 mM sodium bicarbonate) and diluted ten-fold over four serial dilutions: $10^{-1}$, $10^{-2}$, $10^{-3}$, and $10^{-4}$. 100 µL of each dilution was then plated on either R2A agar (0.5 g casein hydrolysate, 0.5 g dextrose, 0.5 g soluble starch, 0.5 g yeast extract, 0.3 g potassium phosphate, 0.3 g sodium

pyruvate, 0.25 g casein peptone, 0.25 g meat peptone, 0.024 g magnesium sulfate, 15 g agar, final volume 1 L); MacConkey agar (Sigma-Aldrich, St. Louis, MO); or blood agar (10 g peptone, 10 g meat extract, 5 g sodium chloride, 15 g agar, final volume 1 L) infused with defibrinated sheep's blood (10% v/v) (Fisher Scientific, Hampton, NH). Petri dishes containing these mixed community cultures were wrapped in Parafilm to prevent desiccation and incubated at room temperature (20 °C) for 1-2 weeks. The combination of nutrient-limited media, cool temperatures, and relatively long incubation periods has been shown to promote microbial diversity and the growth of previously uncultivated microbes (58, 59).

**Strain isolation**

Following cultivation of mixed communities, individual bacterial colonies were picked and streaked onto new plates to establish pure cultures. Plates were then wrapped in Parafilm and allowed to incubate at 20 °C until colonies appeared. Bacterial stocks were generated by collecting bacterial samples from each streaked plate and submerging in 0.5 mL HBSS with 10% dimethyl sulfoxide (DMSO) for cryoprotection. Samples were then stored at -80 °C.

**Taxonomic identification**

To identify bacterial isolates, we performed colony PCR using the 16S rRNA gene universal primers 8F (5'—AGAGTTTGATCCTGGCTCAG—3') and 1492R (5'—CGGTTACCTTGTTACGACTT—3'). Bacterial colonies were picked with sterile toothpicks and submerged directly into a PCR master mix (**Table A1.6**). PCR reactions

were performed using the following conditions: 3 min at 95 °C; 30 sec at 95 °C, 30 sec at 45 °C, 1.5 min at 72 °C repeated 30 times; and a final elongation for 5 min at 72 °C. PCR products were analyzed by gel electrophoresis and samples yielding products were cleaned using ExoSAP-IT (Affymetrix, Santa Clara, CA) following manufacturer's instructions. DNA samples were submitted to Michigan State University's Genomics Core (East Lansing, MI) for Sanger sequencing using 16S rRNA 8F universal primer (5'—AGAGTTTGATCCTGGCTCAG—3'). Sequences were screened for quality using 4Peaks (Nucleobytes, Amsterdam) and sequences with at least 400 bp of unambiguous base calls after quality trimming were assigned genus-level classifications using the Ribosomal Database Project (RDP) Classifier tool and an 80% confidence threshold (64).

**Phylogenetic analysis**

Evolutionary relationships among cultured bacteria were inferred by constructing maximum-likelihood phylogenetic trees. Multiple sequence alignments were generated by aligning 16S rRNA gene sequences with the SILVA ribosomal RNA reference database (65). Gaps and non-informative sites were trimmed to generate the final alignment. Trees were constructed using randomized axelerated maximum-likelihood (RAxML) with 1,000 bootstrap replicates (98) in Geneious v11.0.5 (99) and edited in FigTree v1.4.3 (https://github.com/rambaut/figtree/).

**TTX quantification in newt skin**

To estimate TTX concentrations in newt skin, we followed the non-lethal sampling technique described by Bucciarelli and coworkers (100). Animals were first anesthetized in pH-corrected 0.1% tricaine-S (MS-222) dissolved in Holtfreter's solution. Two skin biopsies were then collected from symmetrical sites on the dorsal skin surface, approximately 1 cm laterally from the vertebrae and 1 cm anterior to the hind limbs, using sterile, disposable 2 mm skin biopsy punches (Acu-Punch, Acuderm Inc., Fort Lauderdale, FL). The two skin biopsies from each individual then were combined in 300 µL 0.1 M acetic acid. Each sample was then placed into a boiling water bath for 5 min followed by an ice bath for an additional 5 min. Subsequent steps were carried out at room temperature. To minimize protein and macromolecular debris, samples were centrifuged at 13,000 x g for 20 min and the supernatant transferred to an Amicon Ultra 10,000 MWCO centrifugal filter (Sigma-Aldrich, St. Louis, MO) followed by a second centrifugation at 13,000 x g for 20 min. Finally, 100 µL 0.1 M acetic acid was added to the filter and a third centrifugation at 13,000 x g for 20 min was performed to wash any remaining TTX. The final sample volume was adjusted to 1 mL before proceeding to solid-phase extraction (below).

**TTX quantification in bacterial cultures**

To identify TTX-producing bacteria, isolated bacterial strains were revived from frozen stocks and inoculated in 5 ml of R2B broth (0.5 g casein hydrolysate, 0.25 g casein peptone, 0.25 g meat peptone, 0.5 g dextrose, 0.5 g soluble starch, 0.5 g yeast extract, 0.3 g potassium phosphate, 0.3 g sodium pyruvate, 0.024 g magnesium sulfate,

final volume 1 L) diluted to either 10% or 50% strength in RO $H_2O$. The use of dilute broth was intended to encourage the production of secondary metabolites (58, 59). Cultures were grown at room temperature 20 °C on a tissue culture rotator for 1 or 2 weeks. After cultivation, each culture was centrifuged at 13,000 x g for 5 min at room temperature, and 1 mL of supernatant was used in solid-phase extraction.

**Solid-phase extraction (SPE)**

TTX extractions were performed using a modified solid-phase extraction (SPE) protocol based on that described by Jen et al. (101, 102). Each skin or bacterial sample was loaded onto a mixed cation exchange cartridge (Oasis MCX cartridges, Waters, MA) previously regenerated with 1 mL of methanol and equilibrated with 1 mL RO $H_2O$. Samples were drawn through the cartridge over 30 sec using a Vac-Man laboratory vacuum manifold (Promega, Madison, WI) coupled with VacConnectors (Qiagen, Germantown, MD). Each cartridge was then washed with 1 mL acetonitrile, 1 mL methanol, and 1 mL distilled $H_2O$. TTX was eluted twice from the cartridge with 0.125 mL 0.2 M HCl in 20% methanol. Both eluates were combined and dried in a SpeedVac vacuum centrifuge (Savant SpeedVac SC110, Thermo Fisher Scientific, Waltham, MA), then resuspended in 0.2 mL 0.5% acetic acid in water. 50-µL aliquots of each sample were prepared for HILIC-MS/MS analysis.

**Hydrophilic interaction liquid chromatography tandem mass spectrometry (HILIC-MS/MS)**

TTX analyses were performed using a Waters TQ-D mass spectrometer coupled to a Waters ACQUITY UPLC system with a binary solvent manager. Chromatographic separations were performed on a Waters ACQUITY UPLC BEH amide column (2.1 × 100 mm; 1.7 µm particles; Waters Co., Milford, MA); column temperature was held at 40 °C. For liquid chromatography, we used 0.1% formic acid in water (mobile phase A) and acetonitrile (mobile phase B) with a flow rate of 0.4 mL/min. The injection volume was set to 10 µL. The linear gradient elution program was as follows (A/B): 0-1.0 min (5/95), 1.0-1.5 min (50/50), 1.5-2.0 min (55/45), 2.0-3.5 min (60/40), 3.5-4.0 min (65/35) before the gradient returned to the initial condition (5/95). TTX was analyzed in positive electrospray ionization mode using multiple reaction monitoring with a transition of 320.1 > 162.1 (cone voltage: 50 eV; collision energy: 40 eV) as the primary channel for quantification and 320.1 > 302.1 (cone voltage: 50 eV; collision energy: 40 eV) as the secondary channel for confirmation. The capillary voltage was 3.0 kV. Source and desolvation temperatures were 130 °C and 500 °C, respectively; cone gas and desolvation gas flows were 40 and 700 L/hr, respectively. Data were acquired using MassLynx 4.1 software (Waters Co.). Bacterial samples were compared with TTX analytical standards acquired from Sigma-Aldrich (St. Louis, MO). A calibration curve was included in each HILIC-MS/MS run with the following concentrations: 0.01, 0.05, 0.1, 0.5, 1, 2.5, 5, 10, 25, and 50 ng/ml. The presence of TTX in bacterial cultures was confirmed by a retention time identical to that of authentic TTX as well as the presence

of both primary and secondary ion transitions. All chromatograms were plotted in R v3.4.1.

**Scanning electron microscopy**

3x3 mm skin samples were dissected from the dorsal region of a euthanized newt. Each sample was fixed in 4% glutaraldehyde in 0.1 M sodium phosphate buffer (pH 7.4) overnight at 4 °C. Following fixation, samples were briefly rinsed in 0.1 M sodium phosphate buffer and dehydrated in an ethanol gradient (25, 50, 75, 95, 100, 100, 100%) for 10 min each. Any remaining liquid in the samples was removed by critical point drying in a Balzers Model 010 critical point dryer (Balzers Union Ltd., Balzers, Liechtenstein) using carbon dioxide as the transitional fluid. Each skin sample was then mounted on an aluminum stub using carbon suspension cement (SPI Supplies, West Chester, PA) and coated with platinum (8 nm thickness) using a Q150T turbo pumped sputter coater (Quorum Technologies, Laughton, East Sussex, England) purged with argon gas. Samples were examined and images obtained using a JEOL JSM-7500F cold field emission scanning electron microscope (JEOL Ltd, Tokyo, Japan).

**Field collection of microbiome samples**

Skin bacterial samples were collected from two populations of rough-skinned newts, one in Oregon (January Pond; 44°36'13.8"N 123°38'12.1"W) and one in Idaho (Virgil Phillips Farm Park, Idaho; 46°48'49.9"N 117°00'57.2"W). Microbial samples were collected from January Pond in Summer 2013 to allow initial characterization of

potentially culturable skin microbes; we then sampled the Idaho population in Fall 2016 to compare the cutaneous communities between the two populations. Animals were caught in ponds with dipnets and minnow traps baited with glow sticks, and each animal was handled with a fresh pair of nitrile gloves. Bacterial samples were collected from two skin sites (dorsal and ventral) and from the surfaces of two external glands (submandibular gland and cloaca) for a total of four samples per animal. Sterile cotton-tipped swabs were dipped into fresh aliquots of filter-sterilized wetting solution (0.15M NaCl and 0.1% Tween-20) and stroked across each body surface 20 times. Each swab was then placed into a sterile 1.5 mL conical tube and kept on dry ice until transported to the lab, where they were stored at -80 °C. Finally, in addition to swabs from newts we collected soil samples from pond sediment and pond water samples in sterile 50 mL conical tubes. Samples were collected under Oregon Department of Fish and Wildlife permit number 104-15 and Idaho Department of Fish and Game Wildlife Bureau permit number 150521.

**DNA extraction**

Total DNA from swab samples was extracted using a QIAamp DNA Mini Kit (Qiagen) as follows. First, 500 µl TE buffer (10 mM Tris-HCl, 50 mM EDTA, pH 8, 0.2 µm filter-sterilized) was added to each cotton swab sample and pulse vortexed for 15 sec. The buffer was then transferred to a sterile bead-beating tube containing 750 mg zirconia silica beads (0.1 mm, BioSpec, Bartlesville, OK) and each sample underwent bead-beating for 60 sec on a Thermo Savant FastPrep FP120 (Thermo Fisher, Waltham, MA) at setting 5. Samples were briefly centrifuged and the lysate transferred

to a new 2 mL tube. 25 µL proteinase K and 500 µL kit buffer AL were added to each sample, and samples were then pulse vortexed for 15 sec and incubated at 56 °C for 10 min on a heat block. Each lysate was then acidified by adding 100 µL sodium acetate (3M, pH 5.5), followed by 500 µL 100% ethanol. Samples were pulse vortexed for 15 sec and applied to QIAamp mini spin columns attached to a vacuum manifold via a sterile VacConnector (Qiagen) to a Luer valve. The entire lysate was pulled through the column by application of a vacuum and then each column was washed with 750 µL Buffer AW1 and Buffer AW2, respectively. Next, the spin column was transferred to a clean collection tube and centrifuged at 6,000 x g for 1 min in a bench-top microcentrifuge to dry the membrane. After drying, the spin column was placed into a clean 1.5 mL microcentrifuge tube, 50 µL nuclease-free $H_2O$ was applied to the membrane, and the column was incubated for 5 min at 20°C. Each tube was then centrifuged at 10,000 rpm for 1 min to elute the DNA. For soil and water samples, DNA extraction was performed using the MoBio DNeasy PowerSoil Kit (Qiagen) per manufacturer's instruction. For soil samples, 0.2 g of pond sediment was directly added to the PowerBead tubes provided by the kit; for pond water, we centrifuged 15 mL pond water at 10,000 x g for 10 min at 4 °C and resuspended the bacterial cell pellet in 500 µl TE buffer, which was then transferred to a bead beating tube. For negative controls, we performed DNA extractions and PCR reactions on cotton swab samples prepared in the field. We included PCR products from these negative controls with each batch of bacterial samples and included the resulting products in our 16S rRNA gene amplicon library preparation and sequencing.

**PCR amplification and barcoding**

Illumina paired-end reads overlap in the V4 region, allowing for poor quality base calls to be discarded in favor of higher quality sequence on the opposite strand (103). A dual-barcoded two-step PCR was therefore conducted to amplify the V4 hypervariable regions of the bacterial 16S rRNA gene. Our V4 primers were designed based on those provided by Kozich et al. (71) with the addition of adapter sequences for our dual-index barcodes, described below. Primer sequences are listed in **Table A1.7**. In a dedicated PCR hood, 2 µl DNA extract was added to a PCR mixture containing 0.05 µM primers (Integrated DNA Technologies, Coralville, IA), and Q5 Hot Start High Fidelity 2X Master Mix (New England Biolabs, Ipswich, MA) diluted with nuclease-free water to a 1X final concentration (25 µl final volume). PCR was conducted using a Veriti thermal cycler (Applied Biosystems, Foster City, CA) under the following conditions: 98°C for 30 sec; then 98°C for 10 sec, 51°C for 20 sec, and 72°C for 20 sec for 15 cycles. The machine was then paused and 2 µl primers (2 µM) with dual-index barcodes and Illumina sequencing adapters (University of Idaho IBEST Genomics Resources Core Facility) were added to each reaction, bringing the final reaction volume to 25 µl. Amplification resumed with 98°C for 30 sec; then 98°C for 10 sec, 60°C for 20 sec, and 72°C for 20 sec for 15 cycles; then a final extension step of 72°C for 2 min. Samples were held at 4°C in the thermocycler until being stored at -20°C. Quality of PCR amplicons was evaluated using a QIAxcel DNA screening cartridge (Qiagen) and DNA quantified using a Qubit fluorometer (Invitrogen, Carlsbad, CA) and the Qubit dsDNA High Sensitivity Assay (Thermo Fisher Scientific, Waltham, MA).

**Illumina library prep**

Volumes of each PCR product containing 50 ng DNA were pooled to create a composite sample for high-throughput sequencing and submitted to the University of Idaho IBEST genomics core. Amplicon pools were size-selected using AMPure beads (Beckman Coulter, Brea, CA). The cleaned amplicon pool was quantified using the KAPA Illumina library quantification kit (KAPA Biosciences, Roche, Basel, Switzerland) and StepOne Plus real-time PCR system (Applied Biosystems, Foster City, CA).

**Illumina sequencing**

Sequences were obtained using an Illumina MiSeq (San Diego, CA) v3 paired-end 300-bp protocol for 600 cycles. Raw DNA sequence reads were processed using the Python application dbcAmplicons (https://github.com/msettles/dbcAmplicons), which was designed to process Illumina double-barcoded amplicons generated in the manner described above. For sequence pre-processing, barcodes were allowed to have at most 1 mismatch (Hamming distance) and primers were allowed to have at most 4 mismatches (Levenshtein distance) as long as the final 4 bases of the primer perfectly matched the target sequence. Reads identified as lacking a corresponding barcode and primer sequence were discarded.

**Sequence processing**

V4 sequences were processed in mothur (v 1.39.5) following the MiSeq protocol (71). Paired sequence reads were joined into contigs, screened for quality and removal of chimeras, then aligned to the SILVA 16S ribosomal RNA database (65) and clustered

into operational taxonomic units (OTUs) based on 97% nucleotide identity. Taxonomic assignment of OTUs was then performed using the RDP classifier (64).

**Statistical analysis**

Prior to analysis, each 16S rRNA gene amplicon profile was subsampled to 5,000 sequences. Rarefaction and Good's coverage analyses were conducted using the rarefaction.single() and summary.single() commands in mothur, respectively. Relative abundances of bacterial OTUs were calculated and visualized using the Phyloseq package in R (v3.4.1) (104). All subsequent microbial ecology analyses were all conducted in R using the vegan package (v2.5-3) (105). Beta diversity matrices were produced using Jaccard and Bray-Curtis dissimilarity indices (106). Principal coordinates analyses (PCoA) were conducted on each dissimilarity matrix, and significant differences between groups were determined using a permutational multivariate analysis of variance (PERMANOVA) using 9,999 permutations and a $P < 0.05$ cutoff. Permutation test for multivariate dispersion (PERMDISP) was conducted to test for differences in variance among community samples. Linear discriminant analysis effect size (LEfSe) were performed on the Galaxy server (http://huttenhower.sph.harvard.edu/galaxy/).

# APPENDIX

**Table A1.1: Summary of bacterial culture collection from Oregon newts.** Taxonomic identification based on the 16S rRNA gene. Bacteria were classified to the genus level using the Ribosomal Database Project classifier (64) and classification within higher taxonomic levels was derived from the List of Prokaryotic Names with Standing in Nomenclature at bacterio.net. Cultivation media and colony pigmentation are also included.

| Phylum | Class | Order | Family | RDP Classification | Strain ID | Culture Medium | Pigmentation |
|---|---|---|---|---|---|---|---|
| Actinobacteria | Actinobacteria | Actinomycetales | Nocardiaceae | *Gordonia* | TG109025 | R2A | Red |
| Actinobacteria | Actinobacteria | Actinomycetales | Nocardiaceae | *Gordonia* | TG109030 | R2A | Orange |
| Actinobacteria | Actinobacteria | Actinomycetales | Nocardiaceae | *Rhodococcus* | TX144010 | R2A | Yellow/green |
| Actinobacteria | Actinobacteria | Actinomycetales | Nocardioidaceae | *Nocardioides* | TX009004 | R2A | Yellow |
| Actinobacteria | Actinobacteria | Actinomycetales | Nocardioidaceae | *Nocardioides* | TX009005 | R2A | Yellow |
| Actinobacteria | Actinobacteria | Actinomycetales | Nocardioidaceae | *Nocardioides* | TX009006 | R2A | Yellow |
| Actinobacteria | Actinobacteria | Actinomycetales | Nocardioidaceae | *Nocardioides* | TX009008 | R2A | Yellow |
| Actinobacteria | Actinobacteria | Micrococcales | Dermacoccaceae | *Dermacoccus* | TX108002 | R2A | Orange |
| Actinobacteria | Actinobacteria | Micrococcales | Microbacteriaceae | *Frondihabitans* | TX015023 | R2A | White |
| Actinobacteria | Actinobacteria | Micrococcales | Microbacteriaceae | *Microbacterium* | TG176007 | Blood Agar | Yellow |
| Actinobacteria | Actinobacteria | Micrococcales | Microbacteriaceae | *Microbacterium* | TX074009 | R2A | Yellow |
| Actinobacteria | Actinobacteria | Micrococcales | Microbacteriaceae | *Microbacterium* | TX109004 | R2A | Yellow |
| Actinobacteria | Actinobacteria | Micrococcales | Microbacteriaceae | *Microbacterium* | TG109012 | R2A | Blue |
| Actinobacteria | Actinobacteria | Micrococcales | Microbacteriaceae | *Microbacterium* | TG109024 | R2A | Orange |
| Actinobacteria | Actinobacteria | Micrococcales | Microbacteriaceae | *Microbacterium* | TG149036 | R2A | Yellow |
| Actinobacteria | Actinobacteria | Micrococcales | Microbacteriaceae | *Microbacterium* | TX000003 | R2A | Yellow |
| Actinobacteria | Actinobacteria | Micrococcales | Microbacteriaceae | *Microbacterium* | TX000004 | R2A | Yellow |
| Actinobacteria | Actinobacteria | Micrococcales | Microbacteriaceae | *Microbacterium* | TX000006 | R2A | Yellow |
| Actinobacteria | Actinobacteria | Micrococcales | Microbacteriaceae | *Microbacterium* | TX000007 | R2A | White/yellow |
| Actinobacteria | Actinobacteria | Micrococcales | Microbacteriaceae | *Microbacterium* | TX000008 | R2A | Yellow |

## Table A1.1 (cont'd):

| Phylum | Class | Order | Family | RDP Classification | Strain ID | Culture Medium | Pigmentation |
|---|---|---|---|---|---|---|---|
| Actinobacteria | Actinobacteria | Micrococcales | Microbacteriaceae | *Microbacterium* | TX073008 | R2A | Yellow |
| Actinobacteria | Actinobacteria | Micrococcales | Microbacteriaceae | *Microbacterium* | TX073010 | R2A | Peach |
| Actinobacteria | Actinobacteria | Micrococcales | Microbacteriaceae | *Microbacterium* | TX079002 | Blood Agar | Yellow |
| Actinobacteria | Actinobacteria | Micrococcales | Microbacteriaceae | *Microbacterium* | TX084001 | Blood Agar | White |
| Actinobacteria | Actinobacteria | Micrococcales | Microbacteriaceae | *Microbacterium* | TX085011 | Blood Agar | Yellow |
| Actinobacteria | Actinobacteria | Micrococcales | Microbacteriaceae | *Microbacterium* | TX115009 | R2A | Orange |
| Actinobacteria | Actinobacteria | Micrococcales | Microbacteriaceae | *Microbacterium* | TX125009 | R2A | Yellow, small |
| Actinobacteria | Actinomycetales | Corynebacterineae | Corynebacteriaceae | *Corynebacterium* | TX080002 | Blood Agar | White |
| Actinobacteria | Actinomycetales | Micrococcales | Micrococcaceae | *Kocuria* | TX080004 | Blood Agar | Pink |
| Bacteroidetes | Cytophagia | Cytophagales | Cytophagaceae | *Flectobacillus* | TG148001 | R2A | Light pink/red |
| Bacteroidetes | Cytophagia | Cytophagales | Cytophagaceae | *Flectobacillus* | TG148009 | R2A | Light pink/red |
| Bacteroidetes | Cytophagia | Cytophagales | Cytophagaceae | *Flectobacillus* | TX126005 | R2A | Pink |
| Bacteroidetes | Cytophagia | Cytophagales | Cytophagaceae | *Hymenobacter* | TX115006 | R2A | Red/orange |
| Bacteroidetes | Cytophagia | Cytophagales | Cytophagaceae | *Lacihabitans* | TX196012 | R2A | Orange |
| Bacteroidetes | Cytophagia | Cytophagales | Cytophagaceae | *Lacihabitans* | TX196015 | R2A | Orange |
| Bacteroidetes | Cytophagia | Cytophagales | Cytophagaceae | *Leadbetterella* | TG149024 | R2A | Orange |
| Bacteroidetes | Cytophagia | Cytophagales | Cytophagaceae | *Leadbetterella* | TG149026 | R2A | Orange |
| Bacteroidetes | Cytophagia | Cytophagales | Cytophagaceae | *Leadbetterella* | TG149027 | R2A | Orange |
| Bacteroidetes | Cytophagia | Cytophagales | Cytophagaceae | *Leadbetterella* | TG149030 | R2A | Orange |
| Bacteroidetes | Cytophagia | Cytophagales | Cytophagaceae | *Leadbetterella* | TG149034 | R2A | Orange |
| Bacteroidetes | Cytophagia | Cytophagales | Cytophagaceae | *Leadbetterella* | TG149041 | R2A | Orange |
| Bacteroidetes | Cytophagia | Cytophagales | Cytophagaceae | *Leadbetterella* | TX000001 | R2A | Orange |
| Bacteroidetes | Cytophagia | Cytophagales | Cytophagaceae | *Leadbetterella* | TX000002 | R2A | Orange |

## Table A1.1 (cont'd):

| Phylum | Class | Order | Family | RDP Classification | Strain ID | Culture Medium | Pigmentation |
|---|---|---|---|---|---|---|---|
| Bacteroidetes | Cytophagia | Cytophagales | Cytophagaceae | *Leadbetterella* | TX015014 | R2A | Red/orange |
| Bacteroidetes | Cytophagia | Cytophagales | Cytophagaceae | *Leadbetterella* | TX015016 | R2A | Red/orange |
| Bacteroidetes | Cytophagia | Cytophagales | Cytophagaceae | *Leadbetterella* | TX015018 | R2A | Orange |
| Bacteroidetes | Cytophagia | Cytophagales | Cytophagaceae | *Leadbetterella* | TX015019 | R2A | Orange |
| Bacteroidetes | Cytophagia | Cytophagales | Cytophagaceae | *unclassified* | TX015026 | R2A | White |
| Bacteroidetes | Flavobacteriia | Flavobacteriales | Cryomorphaceae | *Fluviicola* | TX015021 | R2A | Orange |
| Bacteroidetes | Flavobacteriia | Flavobacteriales | Cryomorphaceae | *Fluviicola* | TX144008 | R2A | White, thin |
| Bacteroidetes | Flavobacteriia | Flavobacteriales | Enterobacteriaceae | *Escherichia/Shigella* | TX143010 | R2A | Green |
| Bacteroidetes | Flavobacteriia | Flavobacteriales | Enterobacteriaceae | *Serratia* | TX068009 | MacConkey | Pink/purple |
| Bacteroidetes | Flavobacteriia | Flavobacteriales | Enterobacteriaceae | *Serratia* | TX076002 | MacConkey | Pink/purple |
| Bacteroidetes | Flavobacteriia | Flavobacteriales | Enterobacteriaceae | *Serratia* | TX086007 | MacConkey | Pink |
| Bacteroidetes | Flavobacteriia | Flavobacteriales | Enterobacteriaceae | *Serratia* | TX087001 | R2A | White |
| Bacteroidetes | Flavobacteriia | Flavobacteriales | Enterobacteriaceae | *Serratia* | TX087015 | Blood Agar | White |
| Bacteroidetes | Flavobacteriia | Flavobacteriales | Flavobacteriaceae | *Chryseobacterium* | TX001006 | R2A | Orange |
| Bacteroidetes | Flavobacteriia | Flavobacteriales | Flavobacteriaceae | *Chryseobacterium* | TX001021 | R2A | Yellow |
| Bacteroidetes | Flavobacteriia | Flavobacteriales | Flavobacteriaceae | *Chryseobacterium* | TX001037 | R2A | Orange |
| Bacteroidetes | Flavobacteriia | Flavobacteriales | Flavobacteriaceae | *Chryseobacterium* | TX001038 | R2A | Orange |
| Bacteroidetes | Flavobacteriia | Flavobacteriales | Flavobacteriaceae | *Chryseobacterium* | TX001039 | R2A | Orange |
| Bacteroidetes | Flavobacteriia | Flavobacteriales | Flavobacteriaceae | *Chryseobacterium* | TX001045 | R2A | Orange |
| Bacteroidetes | Flavobacteriia | Flavobacteriales | Flavobacteriaceae | *Chryseobacterium* | TX001046 | R2A | Orange |
| Bacteroidetes | Flavobacteriia | Flavobacteriales | Flavobacteriaceae | *Chryseobacterium* | TX001047 | R2A | Yellow |
| Bacteroidetes | Flavobacteriia | Flavobacteriales | Flavobacteriaceae | *Chryseobacterium* | TX001048 | R2A | Yellow |
| Bacteroidetes | Flavobacteriia | Flavobacteriales | Flavobacteriaceae | *Chryseobacterium* | TX015002 | R2A | Orange |

## Table A1.1 (cont'd):

| Phylum | Class | Order | Family | RDP Classification | Strain ID | Culture Medium | Pigmentation |
|---|---|---|---|---|---|---|---|
| Bacteroidetes | Flavobacteriia | Flavobacteriales | Flavobacteriaceae | *Chryseobacterium* | TX028001 | R2A | Yellow |
| Bacteroidetes | Flavobacteriia | Flavobacteriales | Flavobacteriaceae | *Chryseobacterium* | TX028002 | R2A | Yellow |
| Bacteroidetes | Flavobacteriia | Flavobacteriales | Flavobacteriaceae | *Chryseobacterium* | TX065001 | R2A | White |
| Bacteroidetes | Flavobacteriia | Flavobacteriales | Flavobacteriaceae | *Chryseobacterium* | TX066016 | R2A | Yellow/orange |
| Bacteroidetes | Flavobacteriia | Flavobacteriales | Flavobacteriaceae | *Chryseobacterium* | TX066017 | R2A | Yellow |
| Bacteroidetes | Flavobacteriia | Flavobacteriales | Flavobacteriaceae | *Chryseobacterium* | TX086001 | R2A | Yellow |
| Bacteroidetes | Flavobacteriia | Flavobacteriales | Flavobacteriaceae | *Chryseobacterium* | TX087004 | R2A | Yellow |
| Bacteroidetes | Flavobacteriia | Flavobacteriales | Flavobacteriaceae | *Chryseobacterium* | TX146002 | R2A | Yellow |
| Bacteroidetes | Flavobacteriia | Flavobacteriales | Flavobacteriaceae | *Chryseobacterium* | TX186001 | R2A | Orange, small |
| Bacteroidetes | Flavobacteriia | Flavobacteriales | Flavobacteriaceae | *Cloacibacterium* | TX150004 | R2A | Yellow |
| Bacteroidetes | Flavobacteriia | Flavobacteriales | Flavobacteriaceae | *Epilithonimonas* | TX086004 | R2A | Yellow |
| Bacteroidetes | Flavobacteriia | Flavobacteriales | Flavobacteriaceae | *Flavobacterium* | TX156006 | 10% newt extract R2A | Peach |
| Bacteroidetes | Flavobacteriia | Flavobacteriales | Flavobacteriaceae | *Flavobacterium* | TG175009 | R2A | Pink |
| Bacteroidetes | Flavobacteriia | Flavobacteriales | Flavobacteriaceae | *Flavobacterium* | TX066005 | R2A | White |
| Bacteroidetes | Flavobacteriia | Flavobacteriales | Flavobacteriaceae | *Flavobacterium* | TX066008 | R2A | Peach |
| Bacteroidetes | Flavobacteriia | Flavobacteriales | Flavobacteriaceae | *Flavobacterium* | TX066009 | R2A | Yellow |
| Bacteroidetes | Flavobacteriia | Flavobacteriales | Flavobacteriaceae | *Flavobacterium* | TX066015 | R2A | Orange |
| Bacteroidetes | Flavobacteriia | Flavobacteriales | Flavobacteriaceae | *Flavobacterium* | TX075010 | R2A | Yellow/orange |
| Bacteroidetes | Flavobacteriia | Flavobacteriales | Flavobacteriaceae | *Flavobacterium* | TX142005 | R2A | Green, small |
| Bacteroidetes | Flavobacteriia | Flavobacteriales | Flavobacteriaceae | *Flavobacterium* | TG149028 | R2A | Yellow |
| Bacteroidetes | Flavobacteriia | Flavobacteriales | Flavobacteriaceae | *Flavobacterium* | TG149037 | R2A | Yellow |
| Bacteroidetes | Flavobacteriia | Flavobacteriales | Flavobacteriaceae | *Flavobacterium* | TX001023 | R2A | Yellow |
| Bacteroidetes | Flavobacteriia | Flavobacteriales | Flavobacteriaceae | *Flavobacterium* | TX015011 | R2A | Yellow |

## Table A1.1 (cont'd):

| Phylum | Class | Order | Family | RDP Classification | Strain ID | Culture Medium | Pigmentation |
|---|---|---|---|---|---|---|---|
| Bacteroidetes | Flavobacteriia | Flavobacteriales | Flavobacteriaceae | *Flavobacterium* | TX124001 | R2A | Yellow |
| Bacteroidetes | Flavobacteriia | Flavobacteriales | Flavobacteriaceae | *Flavobacterium* | TX145010 | R2A | White, small |
| Bacteroidetes | Flavobacteriia | Flavobacteriales | Flavobacteriaceae | *Flavobacterium* | TX152005 | 10% newt extract R2A | Orange |
| Bacteroidetes | Flavobacteriia | Flavobacteriales | Flavobacteriaceae | *Flavobacterium* | TX152010 | 10% newt extract R2A | White, bumpy |
| Bacteroidetes | Flavobacteriia | Flavobacteriales | Flavobacteriaceae | *Flavobacterium* | TX153003 | 10% newt extract R2A | White, small |
| Bacteroidetes | Flavobacteriia | Flavobacteriales | Flavobacteriaceae | *Flavobacterium* | TX153004 | 10% newt extract R2A | Orange, thin, flat |
| Bacteroidetes | Flavobacteriia | Flavobacteriales | Flavobacteriaceae | *Flavobacterium* | TX153005 | 10% newt extract R2A | Peach, large |
| Bacteroidetes | Flavobacteriia | Flavobacteriales | Flavobacteriaceae | *Flavobacterium* | TX153006 | 10% newt extract R2A | White, small |
| Bacteroidetes | Flavobacteriia | Flavobacteriales | Flavobacteriaceae | *Flavobacterium* | TX156001 | 10% newt extract R2A | Orange, large |
| Bacteroidetes | Flavobacteriia | Flavobacteriales | Flavobacteriaceae | *Flavobacterium* | TX156002 | 10% newt extract R2A | Orange, large |
| Bacteroidetes | Flavobacteriia | Flavobacteriales | Flavobacteriaceae | *Flavobacterium* | TX156003 | 10% newt extract R2A | White |
| Bacteroidetes | Flavobacteriia | Flavobacteriales | Flavobacteriaceae | *Flavobacterium* | TX156004 | 10% newt extract R2A | White |
| Bacteroidetes | Flavobacteriia | Flavobacteriales | Flavobacteriaceae | *Flavobacterium* | TX156005 | 10% newt extract R2A | White |
| Bacteroidetes | Flavobacteriia | Flavobacteriales | Flavobacteriaceae | *Flavobacterium* | TX156009 | 10% newt extract R2A | Yellow |
| Bacteroidetes | Flavobacteriia | Flavobacteriales | Flavobacteriaceae | *Flavobacterium* | TX156010 | 10% newt extract R2A | White, swarming |
| Bacteroidetes | Flavobacteriia | Flavobacteriales | Flavobacteriaceae | *Flavobacterium* | TX157001 | 10% newt extract R2A | Orange |
| Bacteroidetes | Flavobacteriia | Flavobacteriales | Flavobacteriaceae | *Flavobacterium* | TX157003 | 10% newt extract R2A | Brown |
| Bacteroidetes | Flavobacteriia | Flavobacteriales | Flavobacteriaceae | *Flavobacterium* | TX157009 | 10% newt extract R2A | Orange, large |
| Bacteroidetes | Flavobacteriia | Flavobacteriales | Flavobacteriaceae | *Flavobacterium* | TX196017 | R2A | Yellow |
| Bacteroidetes | Flavobacteriia | Flavobacteriales | Flavobacteriaceae | unclassified | TG148003 | R2A | Yellow |
| Bacteroidetes | Flavobacteriia | Flavobacteriales | Flavobacteriaceae | unclassified | TG148005 | R2A | Yellow |
| Bacteroidetes | Flavobacteriia | Flavobacteriales | Flavobacteriaceae | unclassified | TG176001 | R2A | White |
| Bacteroidetes | Flavobacteriia | Flavobacteriales | Flavobacteriaceae | unclassified | TX028005 | R2A | Yellow |

## Table A1.1 (cont'd):

| Phylum | Class | Order | Family | RDP Classification | Strain ID | Culture Medium | Pigmentation |
|---|---|---|---|---|---|---|---|
| Bacteroidetes | Flavobacteriia | Flavobacteriales | Flavobacteriaceae | unclassified | TX197013 | R2A | White, small |
| Bacteroidetes | Sphingobacteriia | Sphingobacteriales | Chitinophagaceae | *Lacibacter* | TX076005 | R2A | Cream |
| Bacteroidetes | Sphingobacteriia | Sphingobacteriales | Chitinophagaceae | *Lacibacter* | TX079001 | Blood Agar | Orange |
| Bacteroidetes | Sphingobacteriia | Sphingobacteriales | Chitinophagaceae | *Lacibacter* | TX079006 | Blood Agar | White |
| Bacteroidetes | Sphingobacteriia | Sphingobacteriales | Chitinophagaceae | *Lacibacter* | TX080003 | Blood Agar | Yellow |
| Bacteroidetes | Sphingobacteriia | Sphingobacteriales | Sphingobacteriaceae | *Pedobacter* | TG175005 | R2A | Yellow |
| Bacteroidetes | Sphingobacteriia | Sphingobacteriales | Sphingobacteriaceae | *Pedobacter* | TG176008 | Blood Agar | Cream |
| Bacteroidetes | Sphingobacteriia | Sphingobacteriales | Sphingobacteriaceae | *Pedobacter* | TX076006 | R2A | Yellow |
| Bacteroidetes | Sphingobacteriia | Sphingobacteriales | Sphingobacteriaceae | *Pedobacter* | TX087013 | Blood Agar | Pink |
| Bacteroidetes | Sphingobacteriia | Sphingobacteriales | Sphingobacteriaceae | *Pedobacter* | TX088001 | R2A | Cream |
| Bacteroidetes | Sphingobacteriia | Sphingobacteriales | Sphingobacteriaceae | *Pedobacter* | TX088005 | R2A | Pink |
| Bacteroidetes | Sphingobacteriia | Sphingobacteriales | Sphingobacteriaceae | *Pedobacter* | TX108003 | R2A | Pink |
| Bacteroidetes | Sphingobacteriia | Sphingobacteriales | Sphingobacteriaceae | *Pedobacter* | TX109007 | R2A | Pink |
| Bacteroidetes | Sphingobacteriia | Sphingobacteriales | Sphingobacteriaceae | *Sphingobacterium* | TG175006 | R2A | Cream |
| Firmicutes | Bacilli or Firmibacteria | Bacillales | Bacillaceae | (not sequenced to genus) | TX146006 | R2A | Orange |
| Firmicutes | Bacilli or Firmibacteria | Bacillales | Bacillaceae | *Bacillus* | TX115005 | R2A | White |
| Firmicutes | Bacilli or Firmibacteria | Bacillales | Bacillaceae | *Bacillus* | TX145006 | R2A | White, small |
| Firmicutes | Bacilli or Firmibacteria | Bacillales | Bacillaceae | *Falsibacillus* | TX087003 | R2A | White |
| Firmicutes | Bacilli or Firmibacteria | Bacillales | Paenibacillaceae | *Brevibacillus* | TX156008 | 10% newt extract R2A | White |
| Firmicutes | Bacilli or Firmibacteria | Bacillales | Paenibacillaceae | *Brevibacillus* | TX143006 | R2A | White, small |
| Firmicutes | Bacilli or Firmibacteria | Bacillales | Paenibacillaceae | *Brevibacillus* | TX154007 | 10% newt extract R2A | White |
| Firmicutes | Bacilli or Firmibacteria | Bacillales | Paenibacillaceae | *Brevibacillus* | TX154008 | 10% newt extract R2A | White |
| Firmicutes | Bacilli or Firmibacteria | Bacillales | Paenibacillaceae | *Brevibacillus* | TX154009 | 10% newt extract R2A | White |

## Table A1.1 (cont'd):

| Phylum | Class | Order | Family | RDP Classification | Strain ID | Culture Medium | Pigmentation |
|---|---|---|---|---|---|---|---|
| Firmicutes | Bacilli or Firmibacteria | Bacillales | Paenibacillaceae | *Cohnella* | TX139001 | R2A | White, small |
| Firmicutes | Bacilli or Firmibacteria | Bacillales | Paenibacillaceae | *Paenibacillus* | TG149039 | R2A | White |
| Firmicutes | Bacilli or Firmibacteria | Bacillales | Paenibacillaceae | *Paenibacillus* | TG175007 | R2A | White |
| Firmicutes | Bacilli or Firmibacteria | Bacillales | Paenibacillaceae | *Paenibacillus* | TX014010 | R2A | White |
| Firmicutes | Bacilli or Firmibacteria | Bacillales | Paenibacillaceae | *Paenibacillus* | TX014011 | R2A | White |
| Firmicutes | Bacilli or Firmibacteria | Bacillales | Paenibacillaceae | *Paenibacillus* | TX015001 | R2A | White |
| Firmicutes | Bacilli or Firmibacteria | Bacillales | Paenibacillaceae | *Paenibacillus* | TX015001 | R2A | White |
| Firmicutes | Bacilli or Firmibacteria | Bacillales | Paenibacillaceae | *Paenibacillus* | TX015004 | R2A | White |
| Firmicutes | Bacilli or Firmibacteria | Bacillales | Planococcaceae | *Planococcaceae* | TX078001 | Blood Agar | Yellow |
| Firmicutes | Bacilli or Firmibacteria | Bacillales | Staphylococcaceae | *Staphylococcus* | TX115002 | R2A | White |
| Proteobacteria | Alphaproteobacteria | Caulobacterales | Caulobacteraceae | *Asticcacaulis* | TG149019 | R2A | White |
| Proteobacteria | Alphaproteobacteria | Caulobacterales | Caulobacteraceae | *Brevundimonas* | TX074008 | R2A | Peach |
| Proteobacteria | Alphaproteobacteria | Caulobacterales | Caulobacteraceae | *Brevundimonas* | TX065007 | R2A | Red/orange |
| Proteobacteria | Alphaproteobacteria | Caulobacterales | Caulobacteraceae | *Brevundimonas* | TX073007 | R2A | Orange |
| Proteobacteria | Alphaproteobacteria | Caulobacterales | Caulobacteraceae | *Brevundimonas* | TX074010 | R2A | Orange |
| Proteobacteria | Alphaproteobacteria | Caulobacterales | Caulobacteraceae | *Brevundimonas* | TX075009 | R2A | Orange |
| Proteobacteria | Alphaproteobacteria | Caulobacterales | Caulobacteraceae | *Brevundimonas* | TX086002 | R2A | Cream |
| Proteobacteria | Alphaproteobacteria | Caulobacterales | Caulobacteraceae | *Brevundimonas* | TX144003 | R2A | Cream |
| Proteobacteria | Alphaproteobacteria | Caulobacterales | Caulobacteraceae | *Brevundimonas* | TX179004 | Blood Agar | Yellow, small |
| Proteobacteria | Alphaproteobacteria | Caulobacterales | Caulobacteraceae | *Brevundimonas* | TX196019 | R2A | Orange, small |
| Proteobacteria | Alphaproteobacteria | Rhizobiales | Bradyrhizobiaceae | *Bosea* | TX067014 | MacConkey | Purple |
| Proteobacteria | Alphaproteobacteria | Rhizobiales | Bradyrhizobiaceae | *Bosea* | TX075004 | MacConkey | Purple |
| Proteobacteria | Alphaproteobacteria | Rhizobiales | Brucellaceae | *Ochrobactrum* | TX066019 | MacConkey | Purple |

## Table A1.1 (cont'd):

| Phylum | Class | Order | Family | RDP Classification | Strain ID | Culture Medium | Pigmentation |
|---|---|---|---|---|---|---|---|
| Proteobacteria | Alphaproteobacteria | Rhizobiales | Methylobacteriaceae | *Microvirga* | TG105005 | R2A | Blue |
| Proteobacteria | Alphaproteobacteria | Rhizobiales | Methylobacteriaceae | *Microvirga* | TG105009 | R2A | Blue |
| Proteobacteria | Alphaproteobacteria | Rhizobiales | Methylobacteriaceae | *Microvirga* | TG105011 | R2A | White |
| Proteobacteria | Alphaproteobacteria | Rhizobiales | Methylobacteriaceae | *Microvirga* | TG105013 | R2A | Blue |
| Proteobacteria | Alphaproteobacteria | Rhizobiales | Methylobacteriaceae | *Microvirga* | TG105018 | R2A | Peach |
| Proteobacteria | Alphaproteobacteria | Rhizobiales | Methylobacteriaceae | *Microvirga* | TG105019 | R2A | Peach |
| Proteobacteria | Alphaproteobacteria | Rhizobiales | Methylobacteriaceae | *Microvirga* | TG105021 | R2A | Peach |
| Proteobacteria | Alphaproteobacteria | Rhizobiales | Methylobacteriaceae | *Microvirga* | TG105022 | R2A | White |
| Proteobacteria | Alphaproteobacteria | Rhizobiales | Methylobacteriaceae | *Microvirga* | TG105024 | R2A | Peach |
| Proteobacteria | Alphaproteobacteria | Rhizobiales | Methylobacteriaceae | *Microvirga* | TG109002 | R2A | Blue |
| Proteobacteria | Alphaproteobacteria | Rhizobiales | Methylobacteriaceae | *Microvirga* | TG109009 | R2A | White |
| Proteobacteria | Alphaproteobacteria | Rhizobiales | Methylobacteriaceae | *Microvirga* | TG109014 | R2A | Blue |
| Proteobacteria | Alphaproteobacteria | Rhizobiales | Phyllobacteriaceae | *Phyllobacterium* | TG178001 | MacConkey | Pink |
| Proteobacteria | Alphaproteobacteria | Rhizobiales | Rhizobiaceae | *Rhizobium* | TX109008 | R2A | White |
| Proteobacteria | Alphaproteobacteria | Rhizobiales | Rhizobiaceae | *Rhizobium* | TX114005 | R2A | Yellow |
| Proteobacteria | Alphaproteobacteria | Rhizobiales | Rhizobiaceae | *Rhizobium* | TG176004 | MacConkey | Purple |
| Proteobacteria | Alphaproteobacteria | Rhizobiales | Rhizobiaceae | *Rhizobium* | TG176005 | MacConkey | Brown |
| Proteobacteria | Alphaproteobacteria | Rhizobiales | Rhizobiaceae | *Rhizobium* | TX065012 | MacConkey | Purple |
| Proteobacteria | Alphaproteobacteria | Rhizobiales | Rhizobiaceae | *Rhizobium* | TX065015 | MacConkey | Purple |
| Proteobacteria | Alphaproteobacteria | Rhizobiales | Rhizobiaceae | *Rhizobium* | TX067016 | MacConkey | Pink/purple |
| Proteobacteria | Alphaproteobacteria | Rhizobiales | Rhizobiaceae | *Rhizobium* | TX071002 | MacConkey | Pink/purple |
| Proteobacteria | Alphaproteobacteria | Rhizobiales | Rhizobiaceae | *Rhizobium* | TX073003 | MacConkey | Pink/Purple |
| Proteobacteria | Alphaproteobacteria | Rhizobiales | Rhizobiaceae | *Rhizobium* | TX075003 | MacConkey | Purple |

## Table A1.1 (cont'd):

| Phylum | Class | Order | Family | RDP Classification | Strain ID | Culture Medium | Pigmentation |
|---|---|---|---|---|---|---|---|
| Proteobacteria | Alphaproteobacteria | Rhizobiales | Rhizobiaceae | *Rhizobium* | TX081006 | R2A | White |
| Proteobacteria | Alphaproteobacteria | Rhizobiales | Rhizobiaceae | *Rhizobium* | TX115004 | R2A | Pink |
| Proteobacteria | Alphaproteobacteria | Rhizobiales | Rhizobiaceae | *Rhizobium* | TX148008 | R2A | White |
| Proteobacteria | Alphaproteobacteria | Rhizobiales | Rhizobiaceae | *Rhizobium* | TX148009 | R2A | White |
| Proteobacteria | Alphaproteobacteria | Rhizobiales | Rhizobiaceae | unclassified | TX157006 | 10% newt extract R2A | White, small |
| Proteobacteria | Alphaproteobacteria | Rhodobacterales | Rhodobacteraceae | *Catellibacterium* | TX080005 | Blood Agar | Peach |
| Proteobacteria | Alphaproteobacteria | Rhodobacterales | Rhodobacteraceae | *Defluviimonas* | TX151006 | R2A | White, small |
| Proteobacteria | Alphaproteobacteria | Rhodobacterales | Rhodobacteraceae | *Labrenzia* | TG149023 | R2A | White |
| Proteobacteria | Alphaproteobacteria | Rhodobacterales | Rhodobacteraceae | *Labrenzia* | TG149033 | R2A | White |
| Proteobacteria | Alphaproteobacteria | Rhodobacterales | Rhodobacteraceae | unclassified | TX155008 | 10% newt extract R2A | Brown, large |
| Proteobacteria | Alphaproteobacteria | Rhodobacterales | Rhodobacteraceae | unclassified | TX155009 | 10% newt extract R2A | Brown, large |
| Proteobacteria | Alphaproteobacteria | Rhodobacterales | Rhodobacteraceae | unclassified | TX155010 | 10% newt extract R2A | Yellow |
| Proteobacteria | Alphaproteobacteria | Sphingomonadales | Sphingomonadaceae | *Novosphingobium* | TX082001 | R2A | Yellow/orange |
| Proteobacteria | Alphaproteobacteria | Sphingomonadales | Sphingomonadaceae | *Novosphingobium* | TX083003 | R2A | Yellow |
| Proteobacteria | Alphaproteobacteria | Sphingomonadales | Sphingomonadaceae | *Novosphingobium* | TX085004 | R2A | Yellow |
| Proteobacteria | Alphaproteobacteria | Sphingomonadales | Sphingomonadaceae | *Sphingobium* | TX149001 | R2A | Yellow, small |
| Proteobacteria | Alphaproteobacteria | Sphingomonadales | Sphingomonadaceae | *Sphingomonas* | TG148011 | R2A | Yellow |
| Proteobacteria | Alphaproteobacteria | Sphingomonadales | Sphingomonadaceae | *Sphingomonas* | TG149008 | R2A | Yellow |
| Proteobacteria | Alphaproteobacteria | Sphingomonadales | Sphingomonadaceae | *Sphingomonas* | TG149014 | R2A | White |
| Proteobacteria | Alphaproteobacteria | Sphingomonadales | Sphingomonadaceae | *Sphingomonas* | TG184001 | R2A | Yellow/orange |
| Proteobacteria | Alphaproteobacteria | Sphingomonadales | Sphingomonadaceae | *Sphingomonas* | TX016003 | R2A | Yellow |
| Proteobacteria | Alphaproteobacteria | Sphingomonadales | Sphingomonadaceae | *Sphingomonas* | TX016004 | R2A | Yellow |
| Proteobacteria | Alphaproteobacteria | Sphingomonadales | Sphingomonadaceae | *Sphingomonas* | TX143008 | R2A | Cream, large |

## Table A1.1 (cont'd):

| Phylum | Class | Order | Family | RDP Classification | Strain ID | Culture Medium | Pigmentation |
|---|---|---|---|---|---|---|---|
| Proteobacteria | Alphaproteobacteria | Sphingomonadales | Sphingomonadaceae | *Sphingomonas* | TX158003 | 10% newt extract R2A | Brown/white |
| Proteobacteria | Alphaproteobacteria | Sphingomonadales | Sphingomonadaceae | *Sphingomonas* | TX158009 | 10% newt extract R2A | Yellow, rough |
| Proteobacteria | Alphaproteobacteria | Sphingomonadales | Sphingomonadaceae | *Sphingopyxis* | TX150006 | R2A | Yellow |
| Proteobacteria | Alphaproteobacteria | Sphingomonadales | Sphingomonadaceae | *Sphingopyxis* | TX114010 | R2A | Orange |
| Proteobacteria | Alphaproteobacteria | Sphingomonadales | Sphingomonadaceae | *Sphingopyxis* | TG149025 | R2A | Yellow |
| Proteobacteria | Alphaproteobacteria | Sphingomonadales | Sphingomonadaceae | *Sphingopyxis* | TG149032 | R2A | Yellow |
| Proteobacteria | Alphaproteobacteria | Sphingomonadales | Sphingomonadaceae | *Sphingopyxis* | TG149035 | R2A | Yellow |
| Proteobacteria | Alphaproteobacteria | Sphingomonadales | Sphingomonadaceae | *Sphingopyxis* | TX015007 | R2A | Yellow |
| Proteobacteria | Alphaproteobacteria | Sphingomonadales | Sphingomonadaceae | *Sphingopyxis* | TX141001 | R2A | White, small |
| Proteobacteria | Alphaproteobacteria | Sphingomonadales | Sphingomonadaceae | *Sphingopyxis* | TX144006 | R2A | Green, small |
| Proteobacteria | Alphaproteobacteria | Sphingomonadales | Sphingomonadaceae | *Sphingopyxis* | TX153008 | 10% newt extract R2A | Orange |
| Proteobacteria | Betaproteobacteria | Burkholderiales | (unassigned) | *Methylibium* | TX140007 | R2A | |
| Proteobacteria | Betaproteobacteria | Burkholderiales | Burkholderiaceae | *Pandoraea* | TX076004 | R2A | White |
| Proteobacteria | Betaproteobacteria | Burkholderiales | Burkholderiaceae | *Pandoraea* | TX084006 | R2A | cream |
| Proteobacteria | Betaproteobacteria | Burkholderiales | Burkholderiaceae | *Ralstonia* | TG148013 | R2A | White |
| Proteobacteria | Betaproteobacteria | Burkholderiales | Burkholderiaceae | *Ralstonia* | TG149006 | R2A | White |
| Proteobacteria | Betaproteobacteria | Burkholderiales | Burkholderiaceae | *Ralstonia* | TG149007 | R2A | White |
| Proteobacteria | Betaproteobacteria | Burkholderiales | Burkholderiaceae | *Ralstonia* | TG149012 | R2A | White |
| Proteobacteria | Betaproteobacteria | Burkholderiales | Burkholderiaceae | *Ralstonia* | TG149016 | R2A | White |
| Proteobacteria | Betaproteobacteria | Burkholderiales | Burkholderiaceae | *Ralstonia* | TG178003 | Blood Agar | Cream |
| Proteobacteria | Betaproteobacteria | Burkholderiales | Comamonadaceae | *Acidovorax* | TX144001 | R2A | Pink, small |
| Proteobacteria | Betaproteobacteria | Burkholderiales | Comamonadaceae | *Acidovorax* | TX144002 | R2A | Cream |
| Proteobacteria | Betaproteobacteria | Burkholderiales | Comamonadaceae | *Acidovorax* | TX144005 | R2A | Orange |

## Table A1.1 (cont'd):

| Phylum | Class | Order | Family | RDP Classification | Strain ID | Culture Medium | Pigmentation |
|---|---|---|---|---|---|---|---|
| Proteobacteria | Betaproteobacteria | Burkholderiales | Comamonadaceae | *Pseudacidovorax* | TX153010 | 10% newt extract R2A | Yellow, large |
| Proteobacteria | Betaproteobacteria | Burkholderiales | Comamonadaceae | *Ramlibacter* | TX115008 | R2A | Orange |
| Proteobacteria | Betaproteobacteria | Burkholderiales | Comamonadaceae | *unclassified* | TX157008 | 10% newt extract R2A | White, small |
| Proteobacteria | Betaproteobacteria | Burkholderiales | Comamonadaceae | *unclassified* | TX015008 | R2A | White |
| Proteobacteria | Betaproteobacteria | Burkholderiales | Comamonadaceae | *Variovorax* | TX071001 | MacConkey | Cream |
| Proteobacteria | Betaproteobacteria | Burkholderiales | Comamonadaceae | *Variovorax* | TX155006 | 10% newt extract R2A | Clear, small |
| Proteobacteria | Betaproteobacteria | Burkholderiales | Comamonadaceae | *Variovorax* | TX157002 | 10% newt extract R2A | Yellow, small |
| Proteobacteria | Betaproteobacteria | Burkholderiales | Oxalobacteraceae | *Herbaspirillum* | TX081004 | R2A | Clear/white |
| Proteobacteria | Betaproteobacteria | Burkholderiales | Oxalobacteraceae | *Massilia* | TX115007 | R2A | Multicolor |
| Proteobacteria | Betaproteobacteria | Neisseriales | Chromobacteriaceae | *Aquitalea* | TX069010 | MacConkey | Purple |
| Proteobacteria | Betaproteobacteria | Neisseriales | Chromobacteriaceae | *Deefgea* | TX150003 | R2A | White |
| Proteobacteria | Betaproteobacteria | Neisseriales | Chromobacteriaceae | *Vogesella* | TX114006 | R2A | Pink |
| Proteobacteria | Betaproteobacteria | Neisseriales | Chromobacteriaceae | *Vogesella* | TX110003 | Blood Agar | Gray |
| Proteobacteria | Betaproteobacteria | Neisseriales | Chromobacteriaceae | *Vogesella* | TX138004 | R2A | White, large |
| Proteobacteria | Betaproteobacteria | Neisseriales | Chromobacteriaceae | *Vogesella* | TX138005 | R2A | White, swarming |
| Proteobacteria | Betaproteobacteria | Neisseriales | Chromobacteriaceae | *Vogesella* | TX139002 | R2A | White, large |
| Proteobacteria | Betaproteobacteria | Neisseriales | Chromobacteriaceae | *Vogesella* | TX139008 | R2A | White |
| Proteobacteria | Betaproteobacteria | Neisseriales | Chromobacteriaceae | *Vogesella* | TX150002 | R2A | White |
| Proteobacteria | Betaproteobacteria | Neisseriales | Chromobacteriaceae | *Vogesella* | TX151005 | R2A | Swarming |
| Proteobacteria | Betaproteobacteria | Neisseriales | Chromobacteriaceae | *Vogesella* | TX196011 | R2A | White |
| Proteobacteria | Betaproteobacteria | Neisseriales | Chromobacteriaceae | *Vogesella* | TX197008 | Blood Agar | Peach/white |
| Proteobacteria | Gammaproteobacteria | Aeromonadales | Aeromonadaceae | *Aeromonas* | TX196002 | Blood Agar | Yellow |
| Proteobacteria | Gammaproteobacteria | Aeromonadales | Aeromonadaceae | *Aeromonas* | TX074007 | R2A | Cream |

## Table A1.1 (cont'd):

| Phylum | Class | Order | Family | RDP Classification | Strain ID | Culture Medium | Pigmentation |
|---|---|---|---|---|---|---|---|
| Proteobacteria | Gammaproteobacteria | Aeromonadales | Aeromonadaceae | *Aeromonas* | TX001022 | R2A | White |
| Proteobacteria | Gammaproteobacteria | Aeromonadales | Aeromonadaceae | *Aeromonas* | TX174006 | R2A | Clear/white, small |
| Proteobacteria | Gammaproteobacteria | Aeromonadales | Aeromonadaceae | *Aeromonas* | TX196007 | Blood Agar | White |
| Proteobacteria | Gammaproteobacteria | Aeromonadales | Aeromonadaceae | *Aeromonas* | TX196009 | Blood Agar | White |
| Proteobacteria | Gammaproteobacteria | Aeromonadales | Aeromonadaceae | *Aeromonas* | TX196014 | R2A | White |
| Proteobacteria | Gammaproteobacteria | Aeromonadales | Aeromonadaceae | *Aeromonas* | TX196016 | R2A | White, large |
| Proteobacteria | Gammaproteobacteria | Aeromonadales | Aeromonadaceae | *Aeromonas* | TX196018 | R2A | White |
| Proteobacteria | Gammaproteobacteria | Alteromonadales | Shewanellaceae | *Shewanella* | TX140004 | R2A | White |
| Proteobacteria | Gammaproteobacteria | Alteromonadales | Shewanellaceae | *Shewanella* | TX180013 | Blood Agar | Peach |
| Proteobacteria | Gammaproteobacteria | Alteromonadales | Shewanellaceae | *Shewanella* | TX111005 | Blood Agar | Brown |
| Proteobacteria | Gammaproteobacteria | Alteromonadales | Shewanellaceae | *Shewanella* | TX114002 | R2A | Yellow |
| Proteobacteria | Gammaproteobacteria | Alteromonadales | Shewanellaceae | *Shewanella* | TX114004 | R2A | White |
| Proteobacteria | Gammaproteobacteria | Alteromonadales | Shewanellaceae | *Shewanella* | TX114008 | R2A | Yellow |
| Proteobacteria | Gammaproteobacteria | Alteromonadales | Shewanellaceae | *Shewanella* | TX001005 | R2A | Peach |
| Proteobacteria | Gammaproteobacteria | Alteromonadales | Shewanellaceae | *Shewanella* | TX001014 | MacConkey | White |
| Proteobacteria | Gammaproteobacteria | Alteromonadales | Shewanellaceae | *Shewanella* | TX001054 | MacConkey | Maroon |
| Proteobacteria | Gammaproteobacteria | Alteromonadales | Shewanellaceae | *Shewanella* | TX001062 | MacConkey | Maroon |
| Proteobacteria | Gammaproteobacteria | Alteromonadales | Shewanellaceae | *Shewanella* | TX124002 | R2A | White |
| Proteobacteria | Gammaproteobacteria | Alteromonadales | Shewanellaceae | *Shewanella* | TX125008 | R2A | Clear |
| Proteobacteria | Gammaproteobacteria | Alteromonadales | Shewanellaceae | *Shewanella* | TX174005 | R2A | Orange, small |
| Proteobacteria | Gammaproteobacteria | Alteromonadales | Shewanellaceae | *Shewanella* | TX179005 | Blood Agar | Brown, large |
| Proteobacteria | Gammaproteobacteria | Alteromonadales | Shewanellaceae | *Shewanella* | TX185004 | R2A | Peach |
| Proteobacteria | Gammaproteobacteria | Alteromonadales | Shewanellaceae | *Shewanella* | TX186002 | R2A | Peach, small |

## Table A1.1 (cont'd):

| Phylum | Class | Order | Family | RDP Classification | Strain ID | Culture Medium | Pigmentation |
|---|---|---|---|---|---|---|---|
| Proteobacteria | Gammaproteobacteria | Chromatiales | Chromatiaceae | *Rheinheimera* | TX000005 | R2A | Yellow |
| Proteobacteria | Gammaproteobacteria | Chromatiales | Chromatiaceae | *Rheinheimera* | TX197003 | Blood Agar | Peach, swarming |
| Proteobacteria | Gammaproteobacteria | Enterobacteriales | Enterobacteriaceae | *Citrobacter* | TX115003 | R2A | White |
| Proteobacteria | Gammaproteobacteria | Enterobacteriales | Enterobacteriaceae | *Citrobacter* | TX065011 | MacConkey | Pink |
| Proteobacteria | Gammaproteobacteria | Enterobacteriales | Enterobacteriaceae | *Citrobacter* | TX073002 | MacConkey | Pink |
| Proteobacteria | Gammaproteobacteria | Enterobacteriales | Enterobacteriaceae | *Citrobacter* | TX073004 | MacConkey | Pink/Purple |
| Proteobacteria | Gammaproteobacteria | Enterobacteriales | Enterobacteriaceae | *Enterobacter* | TX073005 | MacConkey | Pink |
| Proteobacteria | Gammaproteobacteria | Enterobacteriales | Enterobacteriaceae | *Hafnia* | TX115001 | R2A | Yellow |
| Proteobacteria | Gammaproteobacteria | Enterobacteriales | Enterobacteriaceae | *Hafnia* | TX085007 | MacConkey | Pink/purple |
| Proteobacteria | Gammaproteobacteria | Pseudomonadales | Moraxellaceae | *Acinetobacter* | TX074006 | MacConkey | Purple |
| Proteobacteria | Gammaproteobacteria | Pseudomonadales | Moraxellaceae | *Acinetobacter* | TG178002 | MacConkey | Purple |
| Proteobacteria | Gammaproteobacteria | Pseudomonadales | Moraxellaceae | *Acinetobacter* | TX001003 | R2A | White |
| Proteobacteria | Gammaproteobacteria | Pseudomonadales | Moraxellaceae | *Acinetobacter* | TX073009 | R2A | White |
| Proteobacteria | Gammaproteobacteria | Pseudomonadales | Moraxellaceae | *Acinetobacter* | TX075006 | MacConkey | Purple |
| Proteobacteria | Gammaproteobacteria | Pseudomonadales | Moraxellaceae | *Acinetobacter* | TX126006 | R2A | White |
| Proteobacteria | Gammaproteobacteria | Pseudomonadales | Moraxellaceae | *Acinetobacter* | TX153001 | 10% newt extract R2A | White |
| Proteobacteria | Gammaproteobacteria | Pseudomonadales | Moraxellaceae | *Psychrobacter* | TX179007 | Blood Agar | White, small |
| Proteobacteria | Gammaproteobacteria | Pseudomonadales | Pseudomonadaceae | *Pseudomonas* | TX111003 | Blood Agar | White |
| Proteobacteria | Gammaproteobacteria | Pseudomonadales | Pseudomonadaceae | *Pseudomonas* | TX111008 | Blood Agar | Gray |
| Proteobacteria | Gammaproteobacteria | Pseudomonadales | Pseudomonadaceae | *Pseudomonas* | TX111009 | Blood Agar | pink |
| Proteobacteria | Gammaproteobacteria | Pseudomonadales | Pseudomonadaceae | *Pseudomonas* | TX135003 | R2A | White |
| Proteobacteria | Gammaproteobacteria | Pseudomonadales | Pseudomonadaceae | *Pseudomonas* | TX135004 | R2A | White |
| Proteobacteria | Gammaproteobacteria | Pseudomonadales | Pseudomonadaceae | *Pseudomonas* | TX174011 | R2A | Yellow, small |

## Table A1.1 (cont'd):

| Phylum | Class | Order | Family | RDP Classification | Strain ID | Culture Medium | Pigmentation |
|---|---|---|---|---|---|---|---|
| Proteobacteria | Gammaproteobacteria | Pseudomonadales | Pseudomonadaceae | *Pseudomonas* | TG176002 | MacConkey | Purple |
| Proteobacteria | Gammaproteobacteria | Pseudomonadales | Pseudomonadaceae | *Pseudomonas* | TG176003 | MacConkey | Clear/brown |
| Proteobacteria | Gammaproteobacteria | Pseudomonadales | Pseudomonadaceae | *Pseudomonas* | TG176006 | Blood Agar | Yellow |
| Proteobacteria | Gammaproteobacteria | Pseudomonadales | Pseudomonadaceae | *Pseudomonas* | TX075001 | MacConkey | Grey/purple |
| Proteobacteria | Gammaproteobacteria | Pseudomonadales | Pseudomonadaceae | *Pseudomonas* | TX110004 | Blood Agar | Orange |
| Proteobacteria | Gammaproteobacteria | Pseudomonadales | Pseudomonadaceae | *Pseudomonas* | TX111002 | Blood Agar | White |
| Proteobacteria | Gammaproteobacteria | Pseudomonadales | Pseudomonadaceae | *Pseudomonas* | TX111007 | Blood Agar | Brown |
| Proteobacteria | Gammaproteobacteria | Pseudomonadales | Pseudomonadaceae | *Pseudomonas* | TX114009 | R2A | White |
| Proteobacteria | Gammaproteobacteria | Pseudomonadales | Pseudomonadaceae | *Pseudomonas* | TX135002 | R2A | Clear, rough |
| Proteobacteria | Gammaproteobacteria | Pseudomonadales | Pseudomonadaceae | *Pseudomonas* | TX137003 | R2A | Yellow |
| Proteobacteria | Gammaproteobacteria | Pseudomonadales | Pseudomonadaceae | *Pseudomonas* | TX140001 | R2A | Yellow, swarming |
| Proteobacteria | Gammaproteobacteria | Pseudomonadales | Pseudomonadaceae | *Pseudomonas* | TG148002 | R2A | Light pink/red |
| Proteobacteria | Gammaproteobacteria | Pseudomonadales | Pseudomonadaceae | *Pseudomonas* | TG148010 | R2A | White |
| Proteobacteria | Gammaproteobacteria | Pseudomonadales | Pseudomonadaceae | *Pseudomonas* | TX001010 | MacConkey | Peach |
| Proteobacteria | Gammaproteobacteria | Pseudomonadales | Pseudomonadaceae | *Pseudomonas* | TX001016 | MacConkey | Peach |
| Proteobacteria | Gammaproteobacteria | Pseudomonadales | Pseudomonadaceae | *Pseudomonas* | TX001053 | MacConkey | Yellow |
| Proteobacteria | Gammaproteobacteria | Pseudomonadales | Pseudomonadaceae | *Pseudomonas* | TX001055 | MacConkey | Maroon |
| Proteobacteria | Gammaproteobacteria | Pseudomonadales | Pseudomonadaceae | *Pseudomonas* | TX015022 | R2A | White |
| Proteobacteria | Gammaproteobacteria | Pseudomonadales | Pseudomonadaceae | *Pseudomonas* | TX028003 | R2A | White |
| Proteobacteria | Gammaproteobacteria | Pseudomonadales | Pseudomonadaceae | *Pseudomonas* | TX028004 | R2A | White |
| Proteobacteria | Gammaproteobacteria | Pseudomonadales | Pseudomonadaceae | *Pseudomonas* | TX035003 | MacConkey | White |
| Proteobacteria | Gammaproteobacteria | Pseudomonadales | Pseudomonadaceae | *Pseudomonas* | TX036008 | MacConkey | Purple |
| Proteobacteria | Gammaproteobacteria | Pseudomonadales | Pseudomonadaceae | *Pseudomonas* | TX065005 | R2A | White |

## Table A1.1 (cont'd):

| Phylum | Class | Order | Family | RDP Classification | Strain ID | Culture Medium | Pigmentation |
|---|---|---|---|---|---|---|---|
| Proteobacteria | Gammaproteobacteria | Pseudomonadales | Pseudomonadaceae | *Pseudomonas* | TX066020 | MacConkey | Brown |
| Proteobacteria | Gammaproteobacteria | Pseudomonadales | Pseudomonadaceae | *Pseudomonas* | TX067015 | MacConkey | Brown |
| Proteobacteria | Gammaproteobacteria | Pseudomonadales | Pseudomonadaceae | *Pseudomonas* | TX067017 | MacConkey | Clear |
| Proteobacteria | Gammaproteobacteria | Pseudomonadales | Pseudomonadaceae | *Pseudomonas* | TX069009 | MacConkey | Purple |
| Proteobacteria | Gammaproteobacteria | Pseudomonadales | Pseudomonadaceae | *Pseudomonas* | TX073006 | MacConkey | Purple |
| Proteobacteria | Gammaproteobacteria | Pseudomonadales | Pseudomonadaceae | *Pseudomonas* | TX073012 | R2A | White |
| Proteobacteria | Gammaproteobacteria | Pseudomonadales | Pseudomonadaceae | *Pseudomonas* | TX075005 | MacConkey | Grey |
| Proteobacteria | Gammaproteobacteria | Pseudomonadales | Pseudomonadaceae | *Pseudomonas* | TX075008 | R2A | White |
| Proteobacteria | Gammaproteobacteria | Pseudomonadales | Pseudomonadaceae | *Pseudomonas* | TX088007 | MacConkey | Purple |
| Proteobacteria | Gammaproteobacteria | Pseudomonadales | Pseudomonadaceae | *Pseudomonas* | TX110006 | Blood Agar | Gray |
| Proteobacteria | Gammaproteobacteria | Pseudomonadales | Pseudomonadaceae | *Pseudomonas* | TX110007 | Blood Agar | Orange |
| Proteobacteria | Gammaproteobacteria | Pseudomonadales | Pseudomonadaceae | *Pseudomonas* | TX125001 | R2A | White |
| Proteobacteria | Gammaproteobacteria | Pseudomonadales | Pseudomonadaceae | *Pseudomonas* | TX125005 | R2A | White |
| Proteobacteria | Gammaproteobacteria | Pseudomonadales | Pseudomonadaceae | *Pseudomonas* | TX125007 | R2A | Clear, large |
| Proteobacteria | Gammaproteobacteria | Pseudomonadales | Pseudomonadaceae | *Pseudomonas* | TX137002 | R2A | Yellow, small |
| Proteobacteria | Gammaproteobacteria | Pseudomonadales | Pseudomonadaceae | *Pseudomonas* | TX154001 | 10% newt extract R2A | Peach, large |
| Proteobacteria | Gammaproteobacteria | Pseudomonadales | Pseudomonadaceae | *Pseudomonas* | TX154004 | 10% newt extract R2A | White |
| Proteobacteria | Gammaproteobacteria | Pseudomonadales | Pseudomonadaceae | *Pseudomonas* | TX155007 | 10% newt extract R2A | White, large, thin |
| Proteobacteria | Gammaproteobacteria | Pseudomonadales | Pseudomonadaceae | *Pseudomonas* | TX187011 | Blood Agar | Clear/white |
| Proteobacteria | Gammaproteobacteria | Pseudomonadales | Pseudomonadaceae | unclassified | TX152004 | 10% newt extract R2A | White |
| Proteobacteria | Gammaproteobacteria | Pseudomonadales | Pseudomonadaceae | unclassified | TX186006 | R2A | Peach, small |

**Table A1.2: Pairwise comparison of 16S rRNA sequences between TTX-producing strains of *Pseudomonas* spp. identified in this study.** Nucleotide identities are shown as percentages (%) for each pairwise sequence comparison. Sequence groups with > 99% nucleotide identities are indicated through color coding and were considered replicate isolates of the same bacterial strains.

| | TX180010 | TX174011 | TX135004 | TX135003 | TX111009 | TX111008 | TX111003 |
|---|---|---|---|---|---|---|---|
| TX180010 | | 99.532 | 96.046 | 96.048 | 96.982 | 97.505 | 99.792 |
| TX174011 | 99.532 | | 95.786 | 96.048 | 96.722 | 97.141 | 99.532 |
| TX135004 | 96.046 | 95.786 | | 99.76 | 98.127 | 97.401 | 96.046 |
| TX135003 | 96.048 | 96.048 | 99.76 | | 97.725 | 97.485 | 95.928 |
| TX111009 | 96.982 | 96.722 | 98.127 | 97.725 | | 97.193 | 96.982 |
| TX111008 | 97.505 | 97.141 | 97.401 | 97.485 | 97.193 | | 97.401 |
| TX111003 | 99.792 | 99.532 | 96.046 | 95.928 | 96.982 | 97.401 | |

**Table A1.3: The top 20 most relatively abundant bacterial OTUs found among toxic and non-toxic newts.** The relative abundance of each bacterial OTU within a sample was calculated and averaged across all samples for each population. These data are shown below as percentages. Taxonomy was assigned using the Ribosomal Database Project (64) and a confidence threshold of 80%. OTUs shared between the two populations are in bold.

**Oregon (toxic):**

| OTU | Taxonomic Classification | Relative Abundance (%) |
|---|---|---|
| 00002 | *Rhodoferax* | 19.45 |
| 00001 | Unclassified Flavobacteriaceae | 10.74 |
| **00003** | ***Rhodoferax*** | **6.85** |
| **00004** | **Unclassified Proteobacteria** | **3.49** |
| 00006 | Unclassified Verrucomicrobiales | 3.35 |
| **00005** | ***Romboutsia*** | **3.08** |
| 00022 | Unclassified Fusobacteriaceae | 2.59 |
| 00025 | Unclassified Bacteria | 2.42 |
| 00038 | *Arthrobacter* | 2.10 |
| **00007** | ***Clostridium* sensu stricto** | **2.06** |
| 00029 | Unclassified Bacteria | 1.66 |
| 00015 | *Methylophilus* | 1.16 |
| 00014 | Unclassified Burkholderiales | 1.53 |
| 00034 | *Flavobacterium* | 1.32 |
| 00008 | Unclassified Bacteria | 1.29 |
| 00017 | Unclassified SR1 | 1.23 |
| 00042 | *Pseudomonas* | 0.99 |
| **00011** | **Unclassified Comamonadaceae** | **0.88** |
| 00031 | Unclassified Peptostreptococcaceae | 0.85 |
| 00027 | *Aeromonas* | 0.74 |
| | Other genera | 32.22 |

## Table A1.3 (cont'd):

**Idaho (non-toxic):**

| OTU | Taxonomic Classification | Relative Abundance (%) |
|---|---|---|
| **00004** | **Unclassified Proteobacteria** | **7.98** |
| **00003** | ***Rhodoferax*** | **6.55** |
| **00008** | **Unclassified Bacteria** | **5.25** |
| **00007** | ***Clostridium* sensu stricto** | **4.18** |
| 00012 | Unclassified Burkholderiales | 3.07 |
| 00010 | Unclassified Comamonadaceae | 2.97 |
| 00013 | Unclassified Betaproteobacteria | 2.70 |
| 00009 | Unclassified Methylococcaceae | 2.61 |
| **00005** | ***Romboutsia*** | **2.40** |
| **00011** | **Unclassified Comamonadaceae** | **2.24** |
| 00016 | Unclassified Burkholderiales | 1.66 |
| 00020 | Verrucomicrobiaceae | 1.52 |
| **00014** | **Unclassified Burkholderiales** | **1.43** |
| 00019 | Unclassified Sphingobacteriales | 1.33 |
| 00024 | Unclassified Methylococcaceae | 1.17 |
| **00015** | ***Methylophilus*** | **1.16** |
| 00023 | *Thiodictyon* | 1.09 |
| 00033 | Unclassified Opitutae | 1.03 |
| 00028 | *Rhodoferax* | 0.99 |
| 00018 | Unclassified Bacteria | 0.90 |
| | Other genera | 47.77 |

**Table A1.4: Variation in alpha diversity between newt populations and sampling sites across the bodies of individual newts.** Each value is shown as mean ± SEM.

| Population | Body Site | Sample Size | Good's Coverage | Number of OTUs | Chao1 Richness | Simpson Index (1-D) |
|---|---|---|---|---|---|---|
| Oregon | Dorsal | 11 | 0.964 ± 0.013 | 397 ± 105 | 655 ± 214 | 0.921 ± 0.039 |
| | Ventral | 10 | 0.965 ± 0.008 | 389 ± 85 | 634 ± 135 | 0.908 ± 0.038 |
| | Cloaca | 12 | 0.968 ± 0.006 | 325 ± 65 | 593 ± 117 | 0.850 ± 0.035 |
| | Chin | 8 | 0.967 ± 0.012 | 391 ± 132 | 612 ± 177 | 0.894 ± 0.066 |
| Idaho | Dorsal | 15 | 0.904 ± 0.019 | 828 ± 159 | 1766 ± 339 | 0.965 ± 0.018 |
| | Ventral | 14 | 0.918 ± 0.019 | 697 ± 160 | 1509 ± 351 | 0.943 ± 0.027 |
| | Cloaca | 13 | 0.922 ± 0.024 | 738 ± 196 | 1392 ± 424 | 0.957 ± 0.030 |
| | Chin | 15 | 0.928 ± 0.022 | 635 ± 187 | 1283 ± 406 | 0.912 ± 0.031 |

**Table A1.5: Differences in alpha diversity estimators between Oregon and Idaho newts.** Student's t-test comparisons of corresponding body sites between the two populations (e.g. Oregon cloaca vs. Idaho cloaca) reveal significant difference in both the number of bacterial OTUs present (richness) and the relative abundance of each OTU across the community (evenness as characterized through the Simpson index). Mean values for both richness and evenness were higher in the Idaho than the Oregon newts.

| **OTU Richness** | **d.f.** | **t statistic** | **p-value** |
|---|---|---|---|
| Dorsal skin | 22.44 | 4.9188 | <0.0001 |
| Ventral skin | 18.81 | 3.7049 | 0.0015 |
| Cloaca | 14.56 | 4.3463 | 0.0006 |
| Chin gland | 20.84 | 2.3544 | 0.0284 |
| | | | |
| **OTU Evenness** | | | |
| Dorsal skin | 23.19 | 3.2173 | 0.0038 |
| Ventral skin | 21.89 | 4.9188 | 0.0486 |
| Cloaca | 18.75 | 5.1457 | <0.0001 |
| Chin gland | 15.83 | 0.8307 | 0.4185 |

**Table A1.6: Reaction mixture for colony PCR.** Reactions were prepared on ice, and individual bacterial colonies were picked and submerged into each reaction for PCR amplification of the 16S rRNA gene.

| | Volume in 25 µl Reaction (µl) | Final Concentration |
|---|---|---|
| Nuclease-free water | 18.55 | -- |
| 10x PCR buffer | 2.5 | 1x |
| 50 mM $MgCl_2$ | 0.75 | 1.5 mM |
| 10 mM dNTP mix | 0.5 | 0.2 mM (each dNTP) |
| 10 µM 16S rRNA 8F primer | 0.6 | 0.24 µM |
| 10 µM 16S rRNA 1492R primer | 0.6 | 0.24 µM |
| 1% NP-40 | 1.25 | 0.05% |
| Taq polymerase | 0.25 | 1.25U |

**Table A1.7: Sequences of V4 primers used in 16S rRNA gene amplicon sequencing.** Target-specific primers anneal to the V4 region of the 16S rRNA gene in the first phase of PCR, and barcoded index primers that recognize the overhang adaptor sequence were added in the second phase.

| **Target** | **Overhang Adaptor Sequence** | **Target-Specific Sequence** |
|---|---|---|
| 515F | ACACTGACGACATGGTTCTACA | GTGCCAGCMGCCGCGGTAA |
| 806R | TACGGTAGCAGAGACTTGGTCT | TGGACTACHVGGGTWTCTAAT |

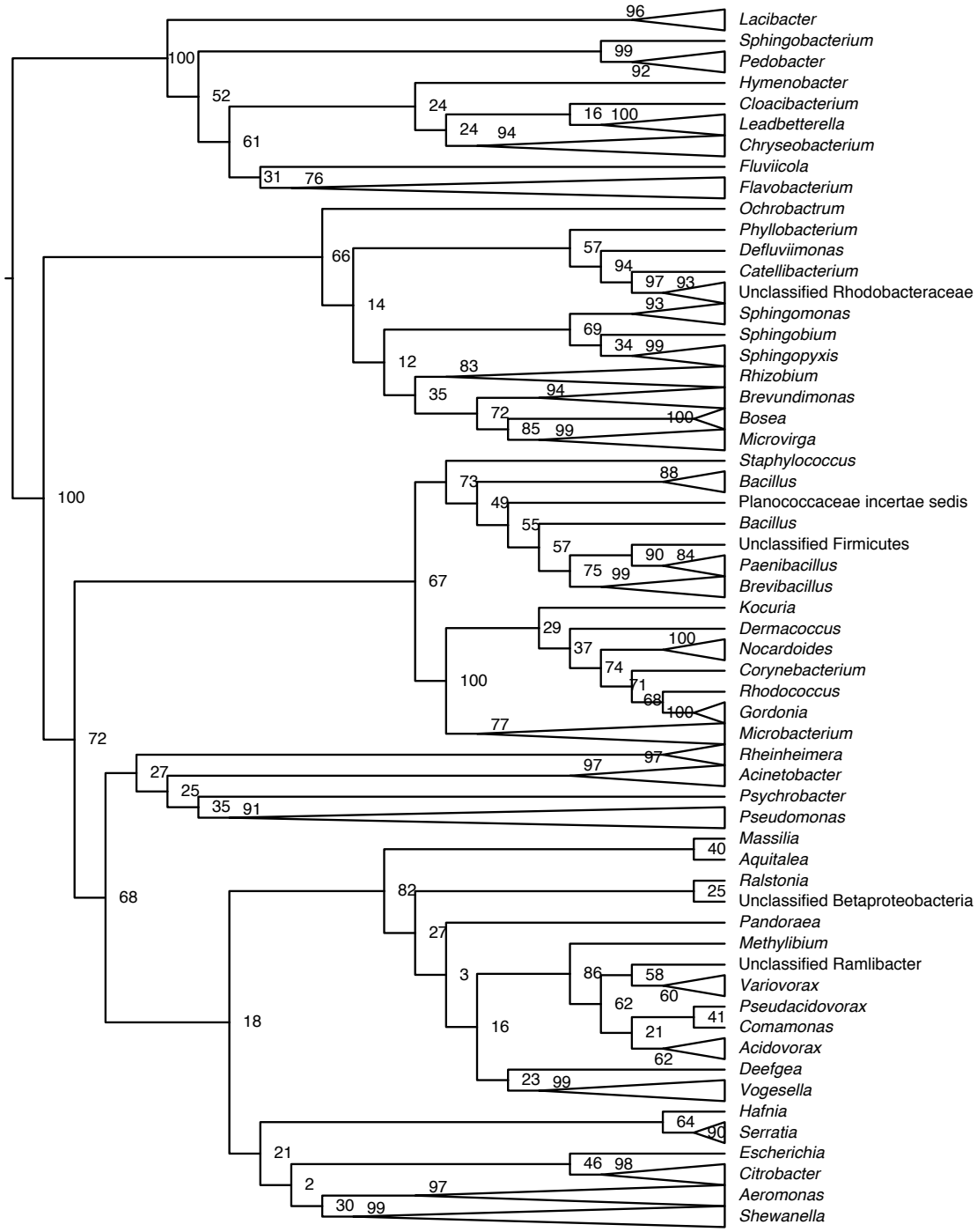


**Figure A1.1: Phylogenetic tree of symbiotic bacteria cultivated from the skin of toxic rough-skinned newts.** Evolutionary relationships were determined by aligning newt bacterial 16S rRNA gene sequences to the SILVA Ribosomal RNA database (65) using mothur v1.40.3 (107). Trees were constructed using randomized axelerated

**Figure A1.1 (cont'd)** maximum likelihood (RAxML) with 1,000 bootstrap replicates (108) in Geneious v11.0.5 (109). Clades with multiple sequences are represented with triangles and bootstrap support is shown on each node.

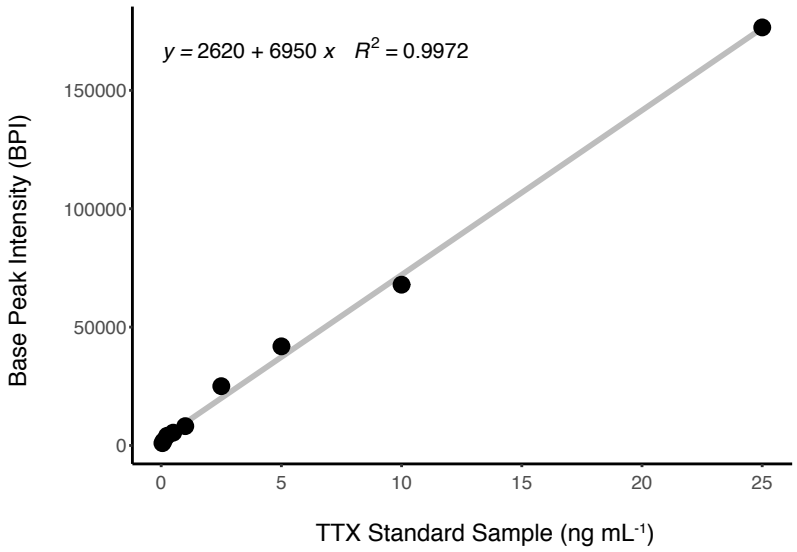


**Figure A1.2: Representative calibration curve for TTX standards.** A linear serial dilution of purified TTX was performed and analyzed by HILIC-MS/MS along with bacterial culture extracts in each run. Our limit of detection was approximately 0.1 ng/ml and our limit of quantification was 0.5 ng/ml.

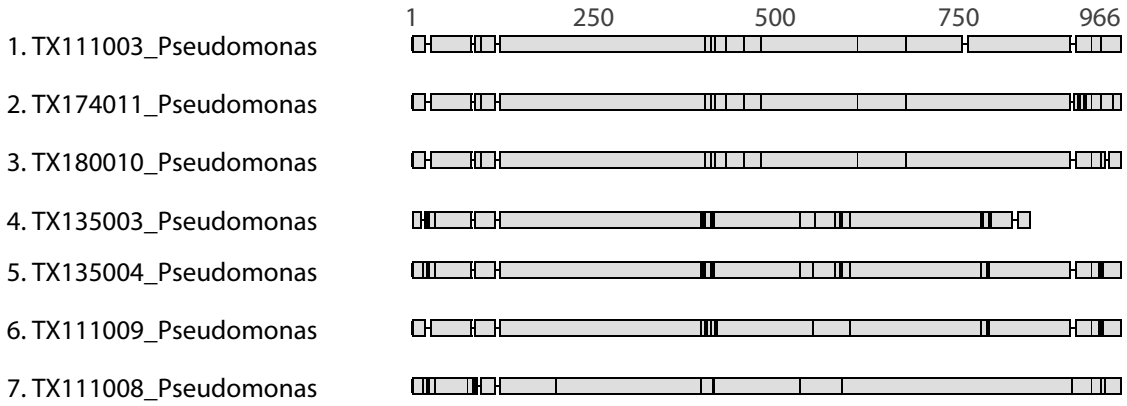


**Figure A1.3: Comparison of 16S rRNA gene structure among TTX-producing strains of *Pseudomonas* spp.** Grey regions represent invariable sites, while black bars show mutations. Strains 1-3 and strains 4-5 share > 99% pairwise nucleotide identities, but the two groups appear to be distinct from each other. Sequence 6 and 7 share around 95% nucleotide identities with the other two groups, but each possess unique mutations indicating that they are possibly distinct strains of *Pseudomonas*.

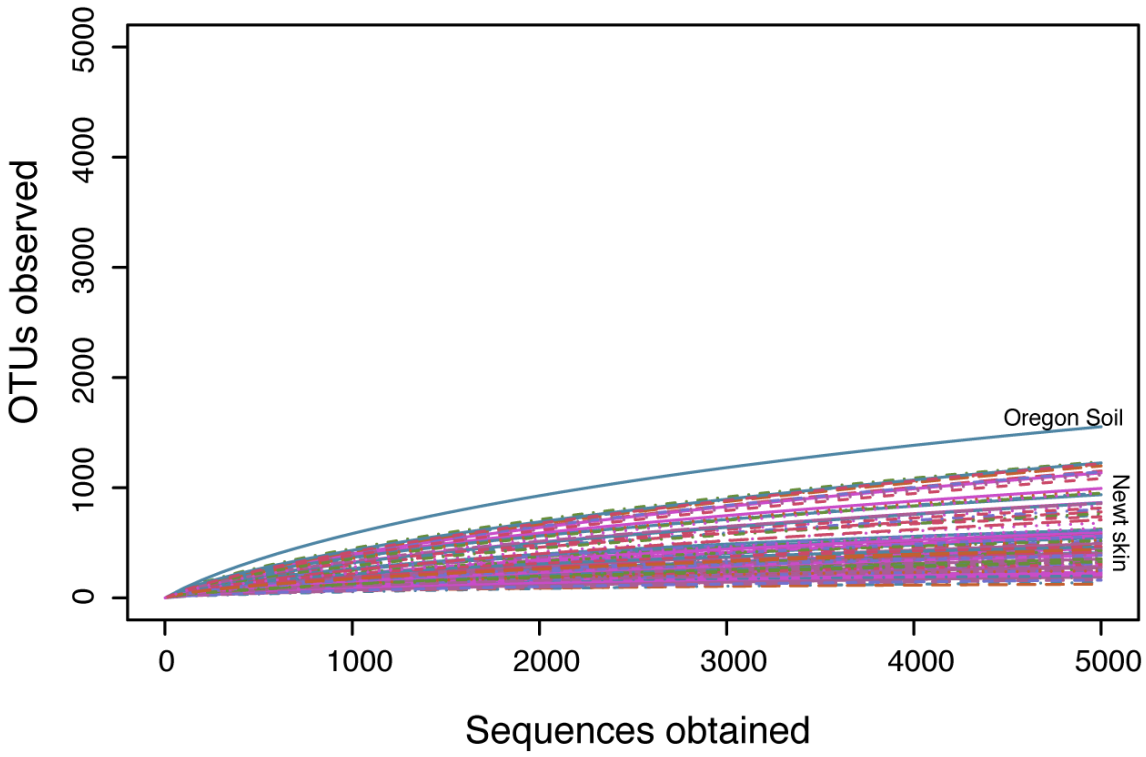


**Figure A1.4: Rarefaction plot showing estimated species diversity as a function of sample size.** In this study, 16S amplicon data were subsampled to 5,000 sequences per sample. Rarefaction curves approach saturation for nearly all samples, indicating that subsampling to 5,000 sequences is sufficient to capture OTU diversity within samples.

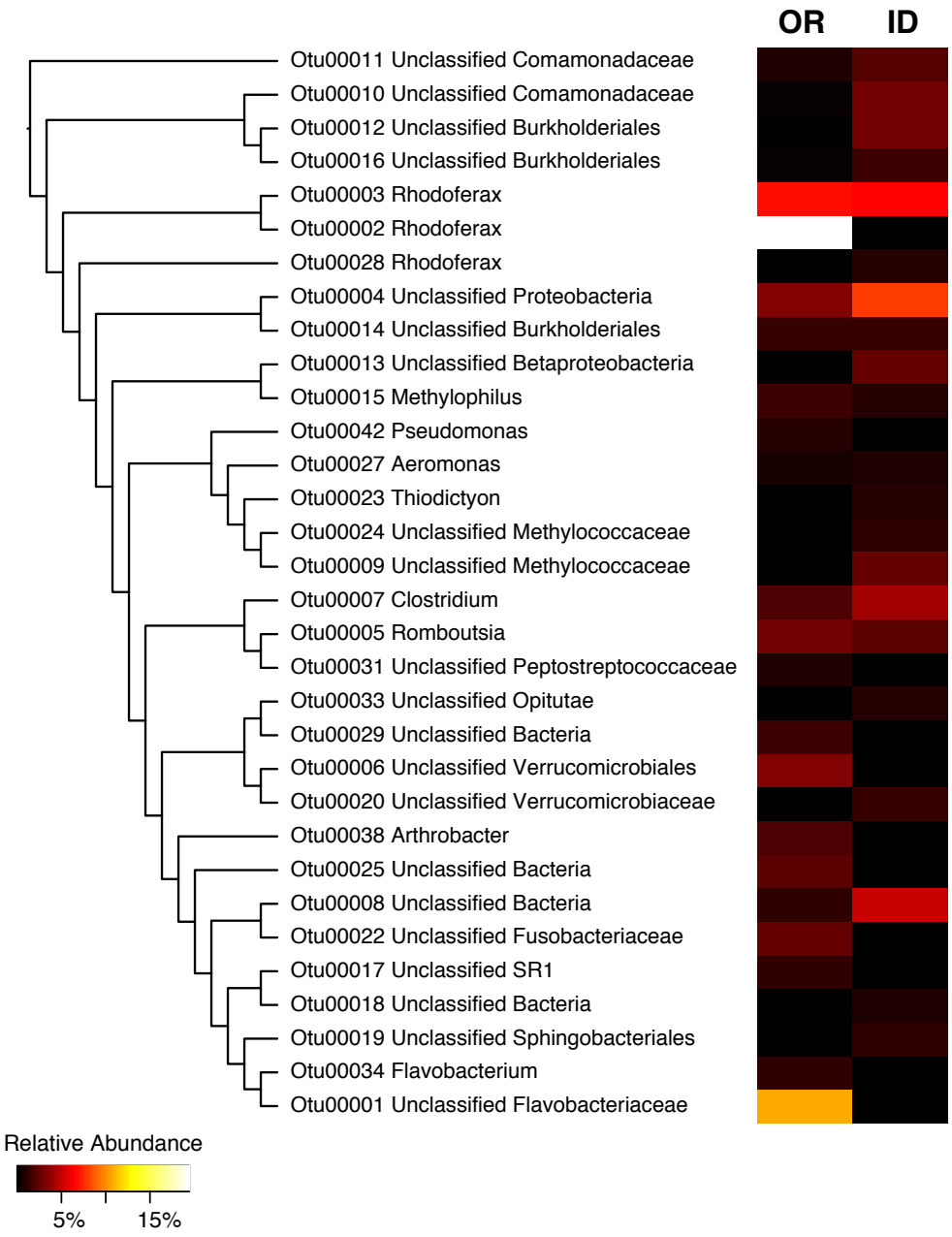


**Figure A1.5: Neighbor-joining phylogenetic tree of the top 20 most relatively abundant OTUs from each population.** Heatmap displays the mean relative abundance of each OTU in Oregon and Idaho newts. 12 of these OTUs are unique to one population, while 8 OTUs are shared between both populations.

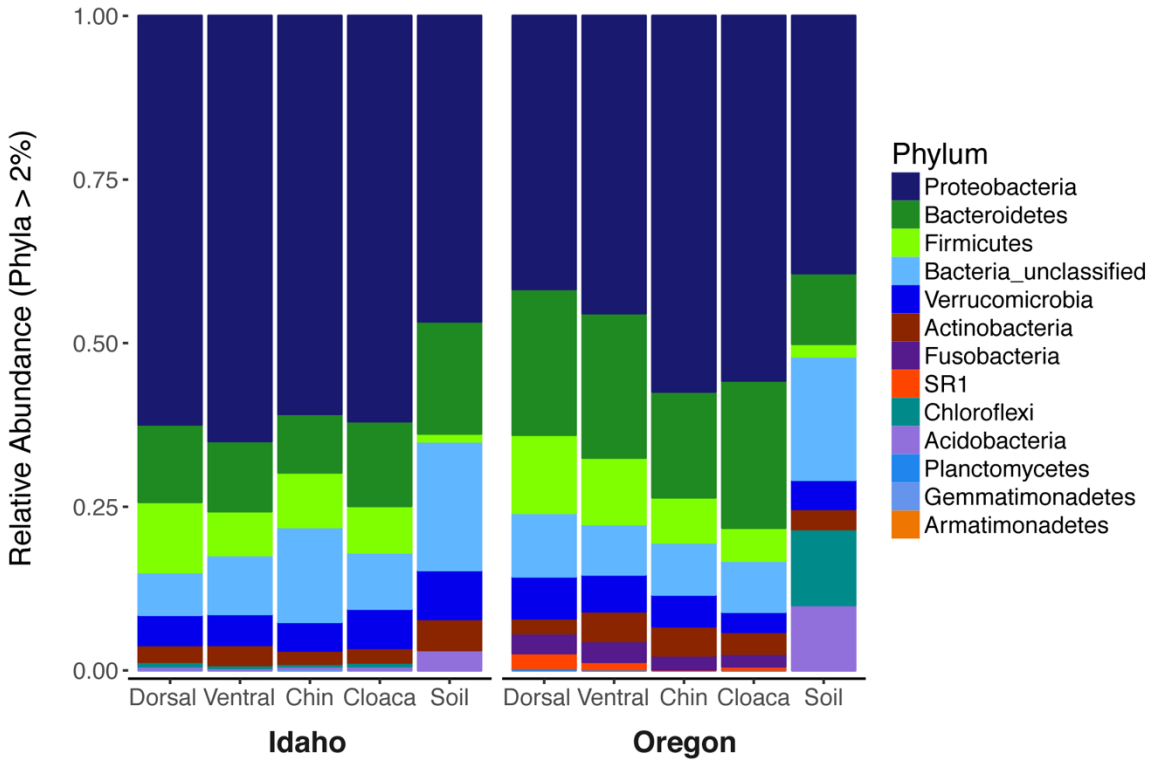


**Figure A1.6: Relative abundance of newt-associated bacteria at the phylum level.** Newt skin communities are diverse, with bacterial OTUs from 12 distinct phyla present at >2% relative abundance. Proteobacteria are most abundant in newts from both study populations, followed by Bacteroidetes and Firmicutes.

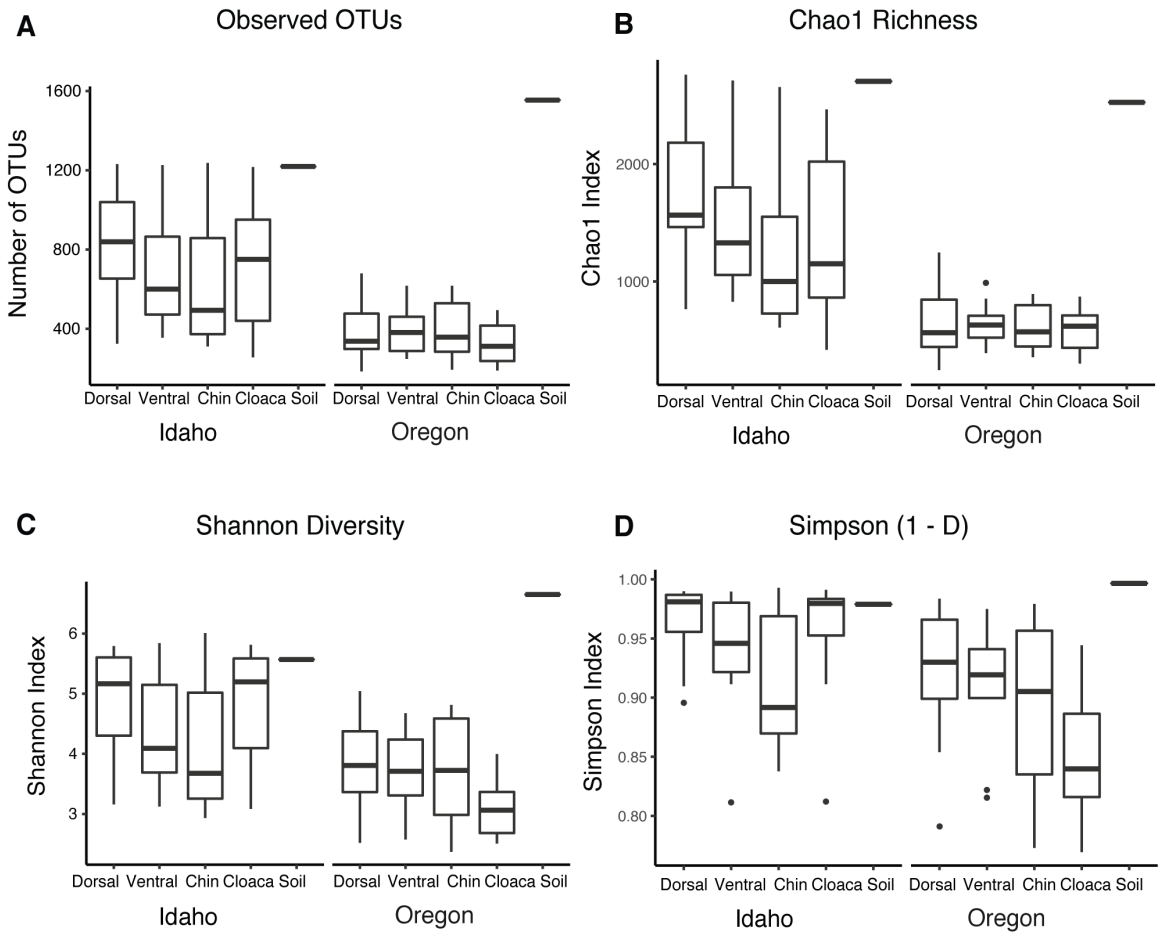


**Figure A1.7: Variation in the alpha diversities of newt-associated bacterial communities.** Boxplots show **(A)** the observed number of OTUs, **(B)** OTU richness estimate, **(C)** Shannon diversity, and **(D)** Simpson diversity. Values for corresponding soil samples are shown as black bars.

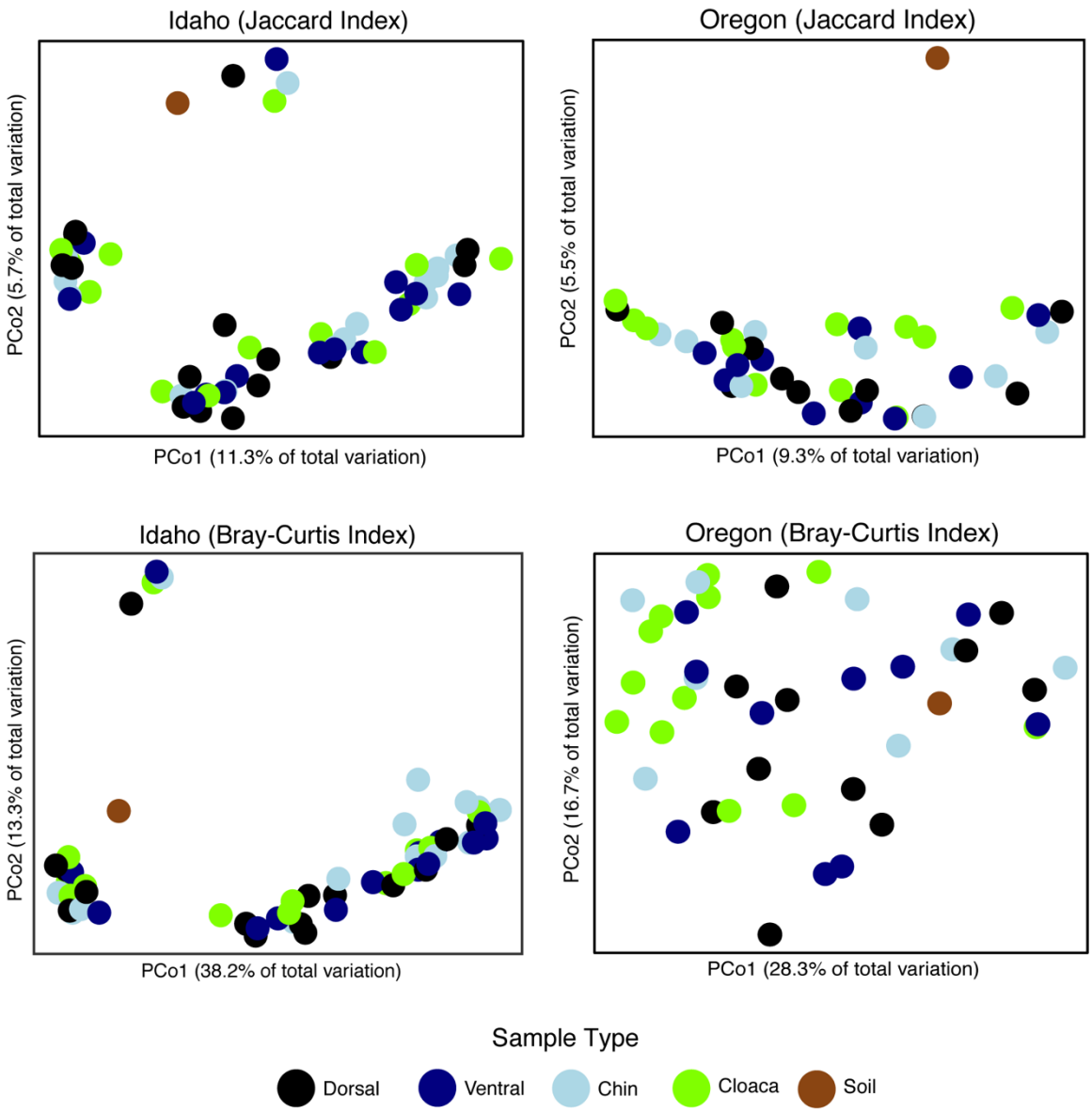


**Figure A1.8: Beta diversity across body sites within each population**. Principal coordinates analysis of bacterial diversity, estimated by Jaccard and Bray-Curtis dissimilarity indices, show no strong patterns of differentiation among samples collected from different body sites.

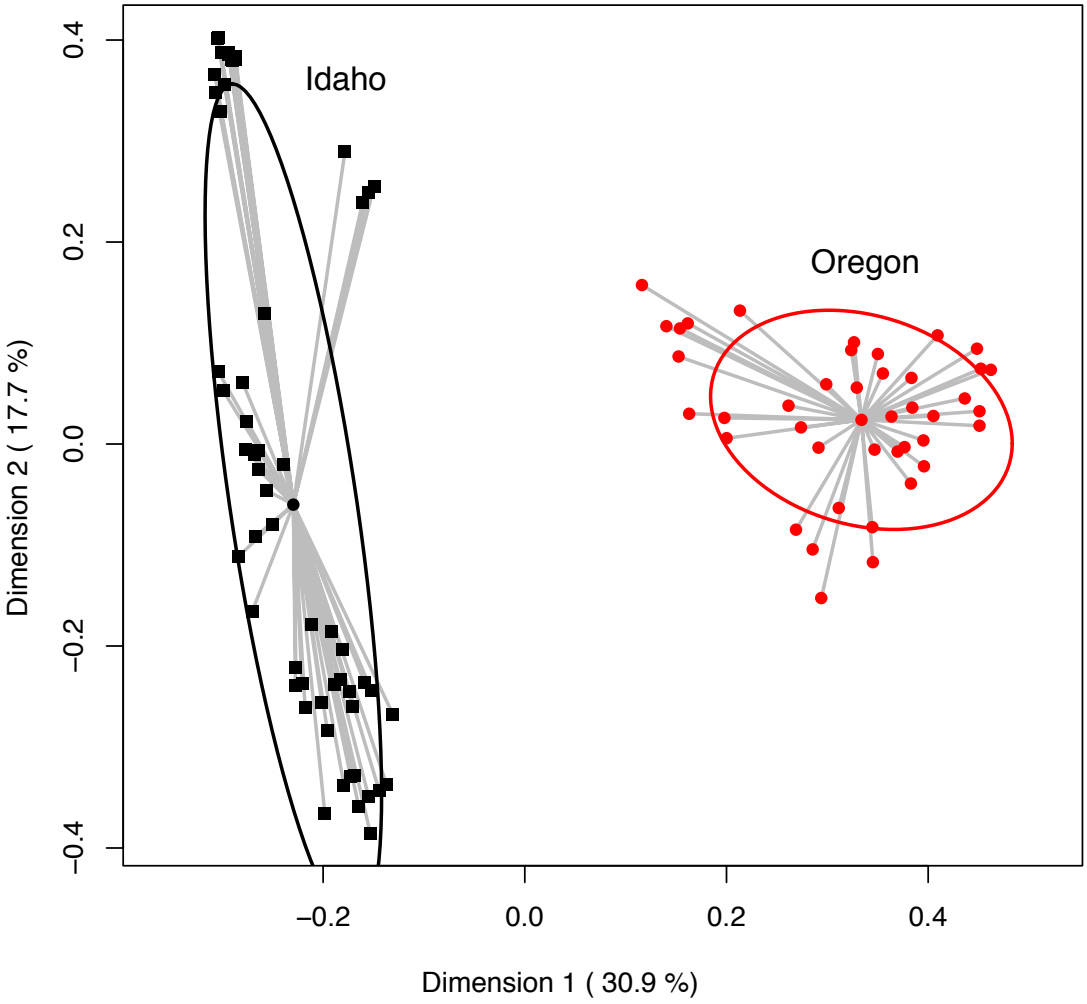


**Figure A1.9: Principal coordinates analysis highlighting variation in bacterial community structure.** Variation in Bray-Curtis indices for newt skin microbiota in Oregon (red circles) and Idaho (black squares). Dispersion (i.e. variance) of individual samples are shown as grey lines from the mean centroid, and 95% confidence ellipses are shown for each group. Permutation test of multivariate homogeneity of group dispersion (PERMDISP) indicates a significant difference between the two populations (P = 0.0053).

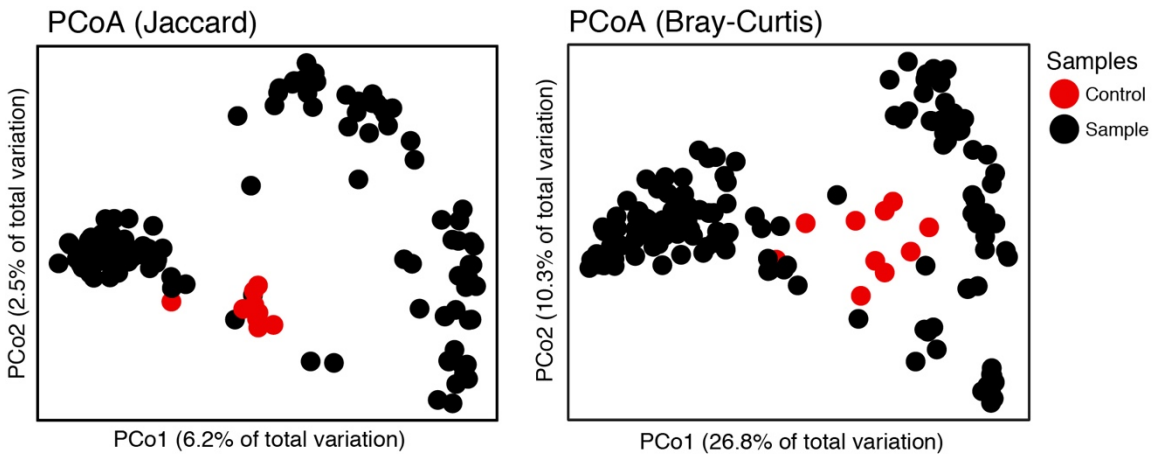


**Figure A1.10: Newt bacterial communities differ significantly from DNA extraction and PCR controls.** Principal coordinates analysis show that while certain OTUs are present in both controls and samples from newts (Jaccard), the abundances of these OTUs (Bray-Curtis) differ significantly between controls and newt samples. Non-parametric multivariate analysis of variance (PERMANOVA) of both Jaccard ($F= 5.855$, $p = <0.0001$) and Bray-Curtis ($F = 10.441$, $p = <0.0001$) diversity indices support for these differences.

# REFERENCES

## REFERENCES


1. Chau R, Kalaitzis JA, Neilan BA (2011) On the origins and biosynthesis of tetrodotoxin. Aquat Toxicol 104(1-2):61–72.

2. Bane V, Lehane M, Dikshit M, O'Riordan A, Furey A (2014) Tetrodotoxin: Chemistry, toxicity, source, distribution and detection. Toxins 6(2):693–755.

3. Tsuda K, Kawamura M (1952) The constituents of the ovaries of globefish. VII. Yakugaku Zasshi 72(6):771–773.

4. Woodward RB (1964) The structure of tetrodotoxin. J Applied Chem 9(1):49–74.

5. Tsuda K, et al. (1964) On the structure of tetrodotoxin. Chem Pharm Bull 12(11):1357–1374.

6. Goto T, Kishi Y, S T, Hirata Y (1965) Tetrodotoxin. Tetrahedron 21(8):2059–2088.

7. Noguchi T, et al. (1983) Occurence of tetrodotoxin as the major toxin in a xanthid crab Atergatis floridus. Bulletin Japanese Soc Sci Fisheries 49(12):1887–1892.

8. Kungsuwan A, et al. (1987) Tetrodotoxin in the horseshoe crab Carcinoscorpius rotundicauda inhabiting Thailand. Nippon Suisan Gakkaishi 53(2):261–266.

9. Maruyama J, et al. (1985) Occurrence of tetrodotoxin in a starfish, Astropecten scoparius. Agri and Biol Chem 49(10):3069–3070.

10. Miyazawa K, et al. (1986) Occurrence of tetrodotoxin in the flatworm Planocera multitentaculata. Toxicon 24(7):645–650.

11. Ali AE, et al. (1990) Tetrodotoxin and related substances in a ribbon worm Cephalothrix linearis (Nemertean). Toxicon 28(9):1083–1093.

12. Thuesen EV, Kogure K, Hashimoto K, Nemoto T (1988) Poison arrowworms: a tetrodotoxin venom in the marine phylum Chaetognatha. J Exp Marine Biol and Ecol 116(3):249–256.

13. Noguchi T, Maruyama J, Narita H, Toxicon HK, 1984 (1984) Occurrence of tetrodotoxin in the gastropod mollusk Tutufa lissostoma (frog shell). Toxicon 22(2):219–226.

14. Hwang DF, Chueh CH, Jeng SS (1990) Occurrence of tetrodotoxin in the gastropod mollusk Natica lineata (lined moon shell). Toxicon 28(1):21–27.

15. Hwang DF, Tai KP, Chueh CH, Lin LC, Jeng SS (1991) Tetrodotoxin and derivatives in several species of the gastropod Naticidae. Toxicon 29(8):1019–1024.

16. Scheumack DD, Howden ME, Spence I, Quinn RJ (1978) Maculotoxin: a neurotoxin from the venom glands of the octopus Hapalochlaena maculosa identified as tetrodotoxin. Science 199:188–189.

17. Lin S-J, Hwang D-F, Shao K-T, Jeng S-S (2000) Toxicity of taiwanese gobies. Fisheries Sci 66(3):547–552.

18. Kim YH, Brown GB, Mosher FA (1975) Tetrodotoxin: Occurrence in atelopid frogs of Costa Rica. Science 189(4197):151–152.

19. Mebs D, Yotsu-Yamashita M, Yasumoto T, Lötters S, Schlüter A (1995) Further report of the occurrence of tetrodotoxin in Atelopus species (family: Bufonidae). Toxicon 33(2):246–249.

20. Daly JW, Gusovsky F, Myers CW, Yotsu-Yamashita M, Yasumoto T (1994) First occurrence of tetrodotoxin in a dendrobatid frog (Colostethus inguinalis), with further reports for the bufonid genus Atelopus. Toxicon 32(3):279–285.

21. Tanu MB, Mahmud Y, Tsuruda K, Arakawa O, Noguchi T (2001) Occurrence of tetrodotoxin in the skin of a rhacophoridid frog Polypedates sp. from Bangladesh. Toxicon 39(7):937–941.

22. Brown MS, Mosher HS (1963) Tarichatoxin: isolation and purification. Science 140(3564):295–296.

23. Mosher HS, Fuhrman FA, Buchwald HD, Fischer HG (1964) Tarichatoxin-tetrodotoxin: a potent neurotoxin. Science 144(3622):1100–1110.

24. Miyazawa K, Noguchi T (2001) Distribution and origin of tetrodotoxin. Toxin Reviews 20(1):11–33.

25. Daly JW (2004) Marine toxins and nonmarine toxins: Convergence or symbiotic organisms? J Nat Prod 67(8):1211–1215.

26. Hanifin CT (2010) The chemical and evolutionary ecology of tetrodotoxin (TTX) toxicity in terrestrial vertebrates. Marine Drugs 8(3):577–593.

27. Narahashi T, Moore JW, Scott WR (1964) Tetrodotoxin blockage of sodium conductance increase in lobster giant axons. J Gen Physiol 47(5):965–974.

28. Fozzard HA, Lipkind GM (2010) The tetrodotoxin binding site is within the outer vestibule of the sodium channel. Marine Drugs 8(2):219–234.

29. Shen H, et al. (2018) Structural basis for the modulation of voltage-gated sodium channels by animal toxins. Science 362(6412):1–8.

30. Zimmer T (2010) Effects of tetrodotoxin on the mammalian cardiovascular system. Marine Drugs 8(3):741–762.

31. Stevens M, Peigneur S, Tytgat J (2011) Neurotoxins and their binding areas on voltage-gated sodium channels. Front Pharmacol 2(71):1–13.

32. Narahashi T (2008) Tetrodotoxin—A brief history—. Proc of the Japan Acad B 84(5):147.

33. Nieto FR, et al. (2012) Tetrodotoxin (TTX) as a therapeutic agent for pain. Marine Drugs 10(12):281–305.

34. Melnikova D, Khotimchenko Y, Magarlamov T (2018) Addressing the issue of tetrodotoxin targeting. Marine Drugs 16(352):1–14.

35. Liu J, et al. (2015) Production level of tetrodotoxin in Aeromonas is associated with the copy number of a plasmid. Toxicon 101:27–34.

36. Chau J, Ciufolini MA (2011) The chemical synthesis of tetrodoxin: An ongoing quest. Marine Drugs 9(12):2046–2074.

37. Pratheepa V, Vasconcelos V (2013) Microbial diversity associated with tetrodotoxin production in marine organisms. Environ Toxicol Pharmacol 36(3):1046–1054.

38. Jal S, Khora SS (2015) An overview on the origin and production of tetrodotoxin, a potent neurotoxin. J Appl Microbiol 119(4):907–916.

39. Noguchi T (2008) Tetrodotoxin – Distribution and accumulation in aquatic organisms, and cases of human intoxication. Marine Drugs 6(2):220–242.

40. Do HK, et al. (1991) Tetrodotoxin production of actinomycetes isolated from marine sediment. J Appl Microbiol 70(6):464–468.

41. Do HK, et al. (1993) Presence of tetrodotoxin and tetrodotoxin-producing bacteria in freshwater sediments. Appl and Environ Microbiol 59(11):3934–3937.

42. Brodie ED, Ridenhour BJ, Brodie ED (2002) The evolutionary response of predators to dangerous prey: hotspots and coldspots in the geographic mosaic of coevolution between garter snakes and newts. Evolution 56(10):2067–2082.

43. Geffeney S, Brodie ED, Ruben PC (2002) Mechanisms of adaptation in a predator-prey arms race: TTX-resistant sodium channels. Science 297(5585):1336–1339.

44. Geffeney SL, Fujimoto E, Brodie ED, Ruben PC (2005) Evolutionary diversification of TTX-resistant sodium channels in a predator-prey interaction. Nature 434(7034):759–763.

45. Hanifin CT, Brodie ED (2008) Phenotypic mismatches reveal escape from arms-race coevolution. PLoS Biol 6(3):e60.

46. Feldman CR, Brodie ED, Pfrender ME (2009) The evolutionary origins of beneficial alleles during the repeated adaptation of garter snakes to deadly prey. Proc Natl Acad Sci USA 106(32):13415–13420.

47. McGlothlin JW, et al. (2014) Parallel evolution of tetrodotoxin resistance in three voltage-gated sodium channel genes in the garter snake *Thamnophis sirtalis*. Mol Biol and Evol 31(11):2836–2846.

48. Williams BL, Brodie ED Jr., Brodie ED III (2004) A resistant predator and its toxic prey: persistence of newt toxin leads to poisonous (not venomous) snakes. J Chem Ecol 30(10):1901–1919.

49. Hanifin CT, Brodie ED (2002) Tetrodotoxin levels of the rough-skin newt, *Taricha granulosa*, increase in long-term captivity. Toxicon 40(8):1149–1153.

50. Cardall BL, Brodie ED Jr., Brodie ED III, Hanifin CT (2004) Secretion and regeneration of tetrodotoxin in the rough-skin newt (*Taricha granulosa*). Toxicon 44(8):933–938.

51. Shimizu Y, Kobayashi M (1983) Apparent lack of tetrodotoxin biosynthesis in captured Taricha torosa and *Taricha granulosa*. Chem Pharm Bull 31(10):3625–3631.

52. Lehman EM, Brodie ED Jr., Brodie ED III (2004) No evidence for an endosymbiotic bacterial origin of tetrodotoxin in the newt *Taricha granulosa*. Toxicon 44(3):243–249.

53. Brodie ED III, et al. (2005) Parallel arms races between garter snakes and newts involving tetrodotoxin as the phenotypic interface of coevolution. J Chem Ecol 31(2):343–356.

54. Gall BG, Stokes AN, French SS, Brodie ED III, Brodie ED Jr. (2012) Female newts (*Taricha granulosa*) produce tetrodotoxin laden eggs after long term captivity. Toxicon 60(6):1057–1062.

55. Gall BG, Brodie ED III, Brodie ED Jr. (2011) Survival and growth of the caddisfly Limnephilus flavastellusafter predation on toxic eggs of the Rough-skinned Newt (*Taricha granulosa*). Canadian J Zool 89(6):483–489.

56. Hanifin CT, Gilly WF (2014) Evolutionary history of a complex adaptation: Tetrodotoxin resistance in salamanders. Evolution 69(1):232–244.

57. Magarlamov T, Melnikova D, Chernyshev A (2017) Tetrodotoxin-producing bacteria: Detection, distribution and migration of the toxin in aquatic systems. Toxins 9(166):1–20.

58. Vartoukian SR, Palmer RM, Wade WG (2010) Strategies for culture of “unculturable” bacteria. FEMS Microbiology Letters 309:1–7.

59. Stewart EJ (2012) Growing unculturable bacteria. J Bacteriol 194(16):4151–4160.

60. Theis KR, et al. (2016) Getting the hologenome concept right: An eco-evolutionary framework for hosts and their microbiomes. mSystems 1(2):1–6.

61. Hanifin CT, Yotsu-Yamashita M, Yasumoto T, Brodie ED III, Brodie ED Jr. (1999) Toxicity of dangerous prey: variation of tetrodotoxin levels within and among populations of the newt *Taricha granulosa*. J Chem Ecol 25(9):2161–2175.

62. Wakely JF, Fuhrman GJ, Fuhrman FA, Fischer HG, Mosher HS (1966) The occurrence of tetrodotoxin (tarichatoxin) in amphibia and the distribution of the toxin in the organs of newts (*Taricha*). Toxicon 3(3):195–203.

63. Yotsu M, Iorizzi M, Yasumoto T (1990) Distribution of tetrodotoxin, 6-epitetrodotoxin, and 11-deoxytetrodotoxin in newts. Toxicon 28(2):238–241.

64. Cole JR, et al. (2013) Ribosomal Database Project: Data and tools for high throughput rRNA analysis. Nucleic Acids Research 42:D633–D642.

65. Quast C, et al. (2012) The SILVA ribosomal RNA gene database project: improved data processing and web-based tools. Nucleic Acids Research 41(D1):D590–D596.

66. Toledo RC, Jared C (1995) Cutaneous granular glands and amphibian venoms. Comp Biochem and Physiol Part A 111(1):1–29.

67. Saporito RA, Donnelly MA, Spande TF, Garraffo HM (2011) A review of chemical ecology in poison frogs. Chemoecology 22(3):159–168.

68. Tsuruda K, Arakawa O, Kawatsu K, Hamano Y (2002) Secretory glands of tetrodotoxin in the skin of the Japanese newt Cynops pyrrhogaster. Toxicon 40:131–136.

69. Mebs D, Arakawa O, Yotsu-Yamashita M (2010) Tissue distribution of tetrodotoxin in the red-spotted newt Notophthalmus viridescens. Toxicon 55(7):1353–1357.

70. Hanifin CT, Brodie ED III, Brodie ED Jr. (2004) A predictive model to estimate total skin tetrodotoxin in the newt *Taricha granulosa*. Toxicon 43(3):243–249.

71. Kozich JJ, Westcott SL, Baxter NT, Highlander SK, Schloss PD (2013) Development of a dual-index sequencing strategy and curation pipeline for analyzing amplicon sequence data on the MiSeq Illumina sequencing platform. Appl and Environ Microbiol 79(17):5112–5120.

72. Good IJ (1953) The population frequencies of species and the estimation of population parameters. Biometrika 40(3-4):237–264.

73. Rosenberg E, Zilber-Rosenberg I (2014) The Hologenome Concept: Human, Animal and Plant Microbiota (Springer Science & Business Media).

74. Gall BG, et al. (2014) Tetrodotoxin concentrations within a clutch and across embryonic development in eggs of the rough-skinned newts (*Taricha granulosa*). Toxicon 90(C):249–254.

75. Brodie ED Jr. (1968) Investigations on the skin toxin of the red-spotted newt, Notophthalmus viridescens viridescens. American Midland Naturalist 80(1):276–280.

76. Brodie ED Jr., Hensel JL Jr, Johnson JA (1974) Toxicity of the urodele amphibians Taricha, Notophthalmus, Cynops and Paramesotriton (salamandridae). Copeia:506–511.

77. Yotsu-Yamashita M, Mebs D, Kwet A, Schneider M (2007) Tetrodotoxin and its analogue 6-epitetrodotoxin in newts (Triturus spp.; Urodela, Salamandridae) from southern Germany. Toxicon 50(2):306–309.

78. Yotsu-Yamashita M, Toennes SW, Mebs D (2017) Tetrodotoxin in Asian newts (Salamandridae). Toxicon 134:14–17.

79. Yotsu-Yamashita M, Tateki E (2010) First report on toxins in the Panamanian toads Atelopus limosus, A. glyphus and A. certus. Toxicon 55(1):153–156.

80. Kim YH, Kim YB, Yotsu-Yamashita M (2003) Potent neurotoxins: Tetrodotoxin, chiriquitoxin, and zetekitoxin from Atelopus frogs in Central America. Toxin Reviews 22(4):521–532.

81. Tanu MB, Mahmud Y, Tsuruda K, Arakawa O, Noguchi T (2001) Occurrence of tetrodotoxin in the skin of a rhacophoridid frog Polypedates sp. from Bangladesh. Toxicon 39(7):937–941.

82. Yotsu-Yamashita M, Mebs D (2003) Occurrence of 11-oxotetrodotoxin in the red-spotted newt, Notophthalmus viridescens, and further studies on the levels of tetrodotoxin and its analogues in the newt's efts. Toxicon 41(7):893–897.

83. Stokes AN, et al. (2014) Confirmation and distribution of tetrodotoxin for the first time in terrestrial invertebrates: Two terrestrial flatworm species (Bipalium adventitium and Bipalium kewense). PLoS ONE 9(6):1–6.

84. Conlon JM (2010) The contribution of skin antimicrobial peptides to the system of innate immunity in anurans. Cell Tissue Res 343(1):201–212.

85. Rollins-Smith LA (2009) The role of amphibian antimicrobial peptides in protection of amphibians from pathogens linked to global amphibian declines. Biochimica et Biophysica Acta 1788:1593–1599.

86. Mangoni ML, et al. (2007) Comparative analysis of the bactericidal activities of amphibian peptide analogues against multidrug-resistant nosocomial bacterial strains. Antimicrobial Agents and Chemotherapy 52(1):85–91.

87. Colombo BM, Scalvenzi T, Benlamara S, Pollet N (2015) Microbiota and mucosal immunity in amphibians. Front Immunol 6(111):1–15.

88. McKenzie VJ, Bowers RM, Fierer N, Knight R, Lauber CL (2011) Co-habiting amphibian species harbor unique skin bacterial communities in wild populations. ISME Journal 6(3):588–596.

89. Brodie ED Jr. (1968) Investigations on the skin toxin of the adult rough-skinned newt, *Taricha granulosa*. Copeia:307–313.

90. Brodie ED III, Brodie ED Jr. (1999) Predator-prey arms races. BioScience 49(7):557–568.

91. Feldman CR, Brodie ED, Pfrender ME (2012) Constraint shapes convergence in tetrodotoxin-resistant sodium channels of snakes. Proc Natl Acad Sci USA 109(12):4556–4561.

92. McFall-Ngai M, et al. (2013) Animals in a bacterial world, a new imperative for the life sciences. Proc Natl Acad Sci USA 110(9):3229–3236.

93. Maynard CL, Elson CO, Hatton RD, Weaver CT (2012) Reciprocal interactions of the intestinal microbiota and immune system. Nature 489(7415):231–241.

94. Koch H, Schmid-Hempel P (2011) Socially transmitted gut microbiota protect bumble bees against an intestinal parasite. Proc Natl Acad Sci USA 108(48):19288–19292.

95. Ezenwa VO, Gerardo NM, Inouye DW, Medina M, Xavier JB (2012) Animal Behavior and the Microbiome. Science 338(6104):198–199.

96. Lizé A, McKay R, Lewis Z (2013) Gut microbiota and kin recognition. Trends Ecol Evol 28(6):325–326.

97. Theis KR, et al. (2013) Symbiotic bacteria appear to mediate hyena social odors. Proc Natl Acad Sci USA 110(49):19832–19837.

98. Stamatakis A (2014) RAxML version 8: a tool for phylogenetic analysis and post-analysis of large phylogenies. Bioinformatics 30(9):1312–1313.

99. Kearse M, et al. (2012) Geneious Basic: An integrated and extendable desktop software platform for the organization and analysis of sequence data. Bioinformatics 28(12):1647–1649.

100. Bucciarelli GM, Li A, Kats LB, Green DB (2014) Quantifying tetrodotoxin levels in the California newt using a non-destructive sampling method. Toxicon 80:87–93.

101. O'Leary MA, Schneider JJ, Isbister GK (2004) Use of high performance liquid chromatography to measure tetrodotoxin in serum and urine of poisoned patients. Toxicon 44(5):549–553.

102. Jen H-C, et al. (2008) Tetrodotoxin poisoning evidenced by solid-phase extraction combining with liquid chromatography–tandem mass spectrometry. J Chromatography B 871(1):95–100.

103. Schloss PD, Gevers D, Westcott SL (2011) Reducing the effects of PCR amplification and sequencing artifacts on 16S rRNA-based studies. PLoS ONE 6(12):1–14.

104. McMurdie PJ, Holmes S (2013) phyloseq: An R package for reproducible interactive analysis and graphics of microbiome census data. PLoS ONE 8(4):1–11.

105. Oksanen J, et al. vegan: Community Ecology Package. R package version. Available at: https://CRAN.R-project.org/package=vegan.

106. Ramette A (2015) Multivariate analyses in microbial ecology. FEMS Microbiology Ecology 62(2):142–160.

107. Schloss PD, et al. (2009) Introducing mothur: Open-Source, Platform-Independent, Community-Supported Software for Describing and Comparing Microbial Communities. Applied and Environmental Microbiology 75(23):7537–7541.

108. Stamatakis A (2014) RAxML version 8: a tool for phylogenetic analysis and post-analysis of large phylogenies. Bioinformatics 30(9):1312–1313.

109. Kearse M, et al. (2012) Geneious Basic: An integrated and extendable desktop software platform for the organization and analysis of sequence data. Bioinformatics 28(12):1647–1649.

# CHAPTER 2: Parallel Evolution of Tetrodotoxin Resistance Across the Voltage-Gated Sodium Channel Gene Family in Poisonous Rough-skinned Newts (*Taricha granulosa*)


## ABSTRACT

Rough-skinned newts (*Taricha granulosa*) are poisonous salamanders that possess tetrodotoxin (TTX), a potent neurotoxin that inhibits sodium ion ($Na^+$) conductance in neurons and muscle cells through selective block of voltage-gated sodium channels ($Na_v$s). TTX blocks the $Na_v$ channel pore through electrostatic interactions with the outer vestibule and $Na^+$ selectivity filter, evolutionarily conserved regions that are critical for proper $Na_v$ channel function. Populations of *T. granulosa* in the Pacific Northwest possess extremely high concentrations of TTX for defense against predators, but the molecular basis of TTX resistance across the $Na_v$ gene family in newts has not been investigated. Newts possess six $Na_v$ gene paralogs that are expressed in different excitable tissues, and each $Na_v$ has unique physiological properties that contribute to proper neural and muscular function. Here, we show that newts possess several amino acid substitutions in the evolutionarily conserved S5-S6 pore loop regions (P-loops) of all six $Na_v$ gene paralogs. One substitution occurs at an identical locus in four of the six $Na_v$ channels, suggesting a limited adaptive landscape for the evolution of TTX resistance in this critical gene family. Neural subtype $Na_v1.6$ is ubiquitously expressed in the both the central and peripheral nervous systems and we used this channel as a model for understanding the functional consequences of P-loop mutations identified in newts. We used site-directed mutagenesis to insert the three newt mutations into the

TTX-sensitive mouse ortholog $Na_v1.6$ and examined their effects on TTX binding by heterologous expression and electrophysiological recording in *Xenopus laevis* oocytes. We found that each individual mutation increased TTX resistance, but the triple mutant was extremely resistant to TTX concentrations exceeding 100 μM. Overall, our results show that TTX resistance has evolved through limited convergent mutations, providing an exemplar of parallel adaptive evolution across an entire gene family in the nervous system.

## INTRODUCTION

Coevolution is a central process driving the origin of novel, adaptive phenotypes (1-4). Adaptations arising in one species can destabilize the fitness landscape of competing species, shifting selective pressures and potentially giving rise to counter adaptations. This is often true for predator-prey interactions, in which prey species may possess morphological, physiological, or behavioral traits that negatively impact foraging success for predators, thereby driving increased selection for predators to overcome prey defenses (5-8). Although predator-prey interactions may drive coevolutionary dynamics in competing species, the traits under selection are often complex and arise from multifaceted interactions among genetic, molecular, and environmental forces.

Chemically-mediated interactions between predators and prey offer a tractable opportunity to study coevolutionary processes, particularly if the chemical compound(s) (selective agent) and molecular or pharmacological target(s) are known. Chemical defenses, including noxious or toxic compounds, have evolved across diverse

organisms including protists, plants, fungi, and animals, and these toxins often target evolutionarily conserved proteins in potential predators (9-13). In the case of animal predators, many defensive compounds target ion channels, transporters, or receptors in the nervous system, which can limit reciprocal counter-adaptation in potential predators, as mutations that impact toxin-binding can also affect canonical protein function (14). This results in a narrow fitness landscape by which the evolution of toxin resistance can only occur through a constrained, stepwise accumulation of beneficial mutations (15-17).

One frequent target of animal neurotoxins is the family of voltage-gated sodium ($Na^+$) channels (gene: SCN; protein: $Na_v$) expressed in neurons, muscles, and other excitable cells (18). $Na_v$ channels are highly-conserved transmembrane protein complexes consisting of one large α subunit (~270 kD) and two accessory β subunits (~32-35 kD) (19). The α subunit contains four homologous domains (DI-DIV), each with six transmembrane segments (S1-S6) that fold together to produce a $Na^+$ selective pore in the membrane (19). The inner vestibule and selectivity filter of the channel are formed by highly conserved sequences between the S5 and S6 segments called pore-loops (P-loops). The base of each P-loop contains one critical amino acid (D, E, K, or A) that ensure $Na^+$ selectivity (Figure1A). β subunits (β1 – β4) bind extracellularly to DI and DIV and are involved in modulating channel activity and regulating tissue-specific and subcellular expression patterns (20-22). Together, $Na_v$ channels form a $Na^+$ selective permeation pathway that is critical for inward flow of $Na^+$ ions during action potentials in most excitable cells (18, 23, 24). Consequently, many animals, including pufferfishes, poison frogs, sea anemones, cone snails, spiders, and scorpions have evolved small

molecule and/or peptide neurotoxins that target and disrupt $Na_v$ channel function (25, 26).

Perhaps the most famous and well-characterized $Na_v$ neurotoxin is tetrodotoxin (TTX), a small-molecule guanidinium alkaloid that is notoriously associated with toxic pufferfishes (27). TTX inhibits $Na^+$ currents in neurons and muscles through selective block of the $Na_v$ channel pore (28-30). The positively-charged guanidinium moiety of TTX interacts with electronegative amino acids of the outer vestibule of the channel, which is thought to attract $Na^+$ to the channel's selectivity filter (29). TTX then binds directly to the aspartate (Asp-D) and glutamate (Glu-E) of the $Na^+$ selectivity filter, preventing the flow of $Na^+$ ions necessary for membrane depolarization and the generation of action potentials (30).

Consequently, TTX is a highly effective chemical defense against nearly all predators in coevolutionary interactions among species. The evolution of TTX resistance would necessarily involve amino acid substitutions in the highly conserved P-loops of the $Na_v$ channel to reduce or eliminate TTX binding, but such mutations might have pleiotropic effects on other channel properties. Nevertheless, TTX resistance has evolved independently several times, and its molecular basis has been described in some species. In vertebrates, TTX resistance has evolved in the skeletal muscle-specific isoform $Na_v1.4$ of pufferfishes (31), garter snakes (32-35), and salamanders (36). Further investigations have documented TTX resistance in other $Na_v$ gene paralogs expressed in the brain, heart, and peripheral sensory fibers of the dorsal root ganglia (37-40). In all cases, target-site insensitivity is thought to arise from amino acid substitutions within the critical P-loop regions.

Two studies have examined TTX resistance in salamander $Na_v$s: the first characterized a TTX-resistant $Na_v$ expressed in the retina of the firebelly newt (*Cynops pyrrhogaster*) (41), and the second focused on the skeletal muscle isoform ($Na_v1.4$) from representative species across Salamandridae, the family of amphibians that contains all newts (36). However, amphibians possess at least six $Na_v$ isoforms, $Na_v1.1$ – $Na_v1.6$, encoded by genes SCN1A – 5A and SCN8A, respectively. Investigations into the mammalian orthologs of each isoform have shown that the channels possesses different physiological properties and that they are differentially expressed across various tissues (42, 43). $Na_v1.1$, $Na_v1.2$, and $Na_v1.3$ are specifically expressed in the central nervous system (CNS) (44). $Na_v1.1$ is expressed in GABAergic inhibitory neurons, and several human channelopathies are known to arise from mutations in the isoform (45); $Na_v1.2$ is expressed in the axon initial segment (AIS), where its high threshold for the voltage dependence of activation ensures the directionality of action potentials and prevents backpropagation up the soma (46); and $Na_v1.3$ is expressed in peripheral nociceptive pain pathways, where expression levels dramatically increase to amplify pain signals following tissue damage (47). $Na_v1.4$ and $Na_v1.5$ are muscle-specific isoforms, which in tetrapods are expressed in skeletal muscle and cardiac muscle, respectively (44); however both isoforms are partially expressed in the cardiac muscle of some fishes (48). $Na_v1.6$ is perhaps the most widely expressed channel, occurring in the dendrites, AIS, and nodes of Ranvier of several neural subtypes including cortical pyramidal and cerebellar Purkinje neurons, dorsal root ganglia of the afferent sensory pathways, and motor neurons (46, 49, 50). This channel exhibits substantial persistent and resurgent currents, both of which facilitate sustained,

repetitive neuronal firing (51, 52). Further, the localized expression of $Na_v1.6$ at the nodes of Ranvier along myelinated axons in vertebrates facilitates rapid saltatory conduction of action potentials, increasing the speed of neural transmission and decoupling the trade-off between axon diameter and signaling speed that exists across most invertebrate nervous systems (53). Finally, the persistent currents from $Na_v1.6$ can also tune spike timing in cerebellar granule cells, the most abundant neuronal cell type in mammals, and are responsible for autonomous pacemaker activity in neurons from the globus pallidus (54, 55).

While the subcellular expression patterns for CNS-specific isoforms have not been thoroughly investigated in amphibians, tissue-level expression patterns (i.e. neural, cardiac, or skeletal muscle) are consistent between amphibians and mammals, as shown by examination of SCN gene expression in *Xenopus laevis* EST databases (43). In newts, TTX is present throughout the body including the skin, muscles, blood, liver, intestines, and reproductive organs (56-59). Furthermore, the retinal $Na_v$ of fire-belly newts has been shown to be TTX-resistant (60), suggesting that channels in the CNS are exposed to TTX. Thus, the evolution of neural and muscular resistance in newts would necessarily involve all six $Na_v$ channel subtypes.

In this study, we investigated the evolution of tetrodotoxin resistance across the $Na_v$ family in a highly toxic population of rough-skinned newts (*Taricha granulosa*) from Western Oregon (61). We found numerous amino acid substitutions in the P-loop regions of all channels in the newt $Na_v$ gene family. Several mutations occur across previously characterized TTX binding sites, including a parallel substitution in DI and several additional mutations in DIII and DIV. To evaluate whether P-loop mutations

conferred TTX resistance in newts, we focused on the widely expressed subtype $Na_v1.6$. We used site-directed mutagenesis (SDM) to modify $Na_v1.6$ from the house mouse (*Mus musculus*) to possess three substitutions found in the orthologous $Na_v1.6$ of newts and found that one mutation in DI (Y371A) conferred significant resistance, as predicted by studies of the Y401N mutation in pufferfish (31, 37). Two additional mutations in DIII (V1407I) and DIV (I1699V) individually contribute mild TTX resistance. However, the triple mutant channel with all three substitutions was far more resistant than the Y371A mutation alone, indicating that these mutations interact additively to increase resistance. Interestingly, the DIII and DIV mutations are also present in Mexican axolotls (*Ambystoma mexicanum*), a salamander that lacks TTX. These mutations may have served as pre-adaptations, providing mild resistance that enabled an adaptive walk towards higher toxicity. Taken together, our results demonstrate that newts have evolved auto-resistance to TTX through substitutions across the entire $Na_v$ channel gene family, demonstrating a remarkable instance of parallel molecular evolution in the nervous system.

## MATERIALS AND METHODS

All procedures involving animals were approved by and conducted under the supervision of the Institutional Animal Care and Use Committee at Michigan State University (approval no. 10/15-154-00) in accordance with guidelines established by the US Public Health Service.

**Research animals**

Adult male rough-skinned newts (*Taricha granulosa*) were collected from ponds in Lincoln Country, Oregon, USA and maintained in our animal facility at Michigan State University. Newts were housed in aquaria containing 100% Holtfreter's solution (60 mM NaCl, 0.67 mM KCl, 0.81 mM MgSO4, and 0.68 mM CaCl2; pH 7.5) maintained at 20˚C with a 14:10 light dark cycle and fed live blackworms (*Lumbriculus variegatus*) or frozen bloodworms (chironomid larvae) 2-3 times weekly.

**RNA isolation**

Newts were euthanized by immersion in pH-corrected 0.1% MS-222, and tissue samples including brain, nose, heart, and skeletal muscle were collected and stored in RNAlater (ThermoFisher Scientific, Waltham, MA) at -20˚C. Total RNA was extracted from newt tissues using TRIzol (ThermoFisher Scientific) following manufacturer's instructions. Briefly, each tissue was aseptically dissected and placed into a sterile tube containing 1 mL TRIzol reagent. Tissues were homogenized in TRIzol using a TissueRuptor (Qiagen, Hilden, Germany), then incubated at room temperature for 5 min. 0.2 mL chloroform was added to each sample, mixed, and incubated for an additional 2-3 min at room temperature. Samples were then centrifuged at 12,000 x g for 15 min at 4˚C. The colorless upper layer of aqueous supernatant containing RNA was then transferred to a new tube. To recover the extracted RNA, 0.5 mL 100% isopropanol was added to the sample and incubated at room temperature for 10 min. Samples were then centrifuged at 12,000 x g for 10 min at 4˚C. The supernatant was discarded and the pellet was washed with 75% ethanol and re-centrifuged. The clean

RNA pellet was resuspended in 50 µL tris-EDTA buffer (pH 8.0) and total RNA yield was quantified by fluorescence using a Qubit fluorometer (ThermoFisher Scientific).

**Transcriptome sequencing**

We generated reference transcriptomes from the brain and nose of *T. granulosa* for identification of SCN genes. Non-excitable tissues including liver and skin were included in the sequencing run but were not used for analysis in this study. Poly-adenylated RNA was purified from total RNA samples (previous section) using the NEXTflex PolyA Bead kit (Bioo Scientific, Austin, TX) according to manufacturer instructions. Lack of contaminating ribosomal RNA was confirmed using the Agilent 2100 Bioanalyzer. Strand-specific libraries for each sample were prepared using the dUTP NEXTflex RNAseq Directional kit (Bioo Scientific), which includes magnetic bead-based size selection, resulting in an average library size of 462 bp. Libraries were pooled in equimolar amounts after quantification using the fluorometric Qubit dsDNA high sensitivity assay kit (Life Technologies) according to manufacturer instructions. Libraries were sequenced on an Illumina HiSeq 2000 (Harvard University, Cambridge, MA) in one lane to obtain 503,241,123 paired-end 100bp reads .

**Transcriptome assembly and annotation**

We first corrected errors in the Illumina reads using Rcorrector (62); parameters: run_rcorrector.pl -k 31) and then applied quality and adaptor trimming using Trim Galore! (http://www.bioinformatics.babraham.ac.uk/projects/trim_galore/; parameters: trim_galore --paired --phred33 --length 36 -q 5 --stringency 5 --illumina -e 0.1). After

filtering and trimming, a total of 500,631,191 reads remained for de novo assembly. We created the newt transcriptome de novo assembly using Trinity (63), parameters: --seqType fq --SS_lib_type RF). The raw Trinity assembly produced 2,559,666 contigs (N50: 399 bp). To reduce redundancy in the assembly, we ran cd-hit-est (64), parameters: -c 0.97) resulting in 2,208,791 contigs (N50: 390 bp). As the sequences were obtained from a wild-caught newt, we next filtered the assembly to remove parasites, microbes, and other contaminants. To accomplish this, we used BLAST to compare each contig with proteins in the Uniprot SwissProt database (e-value threshold of 1e-5); specifically, we used non-vertebrate reference genomes, including those of arthropods (*Drosophila*), microbes (fungi, *Saccharomyces*; bacteria, *Pseudomonas*), and parasites (*Caenorhabditis*) to identify potential contaminants, resulting in the removal of 61,185 contigs. For the purposes of our study, we only retained contigs with homologs to vertebrate proteins based on this BLAST search of the Swiss Prot database; our final draft assembly of the newt transcriptome contained 77,535 contigs with an N50 of 3025 bp. We assessed the completeness of this final assembly by examining vertebrate ortholog representation using BUSCO (65), which showed 86% of BUSCO groups represented in the assembly.

**PCR and cloning**

To evaluate SCN gene sequence assembly and confirm the presence of P-loop mutations, we used sequence-specific or degenerate PCR primers to amplify SCN gene fragments from newt RNA, followed by Sanger sequencing. Degenerate PCR primers were designed based on conserved amino acid sequences identified in vertebrate $Na_v$

protein alignments. cDNA templates were synthesized from newt RNA using the SuperScript III First-Strand Synthesis kit following manufacturer's instructions (Invitrogen, Carlsbad, CA). RNA (0.5 – 1 µg) was primed with oligo$(dT)_{20}$ primers, targeting the mRNA poly(A)+ tail to enhance synthesis of expressed mRNA transcripts. cDNA samples were stored at -20˚C until use. PCR reactions were performed using Q5 High-Fidelity 2X master mix (New England Biolabs, Ipswich, MA) and analyzed by gel electrophoresis on 0.8% w/v agarose gel in tris-acetate-EDTA buffer (pH 8.0). Amplified DNA was either sequenced directly from PCR products or cloned into the pGEM-T DNA vector (Promega, Madison, WI). In the latter case, PCR products were first purified by spin column using the DNA Clean & Concentrator kit (Zymo Research, Irvine, CA), then A-tailed using GoTaq (Promega) by combining 10 µL purified PCR product, 2.5 µL 10X buffer, 5 µL dATP (1 mM), 0.2 µL Taq polymerase, and 7.3 µL nuclease-free water to a total volume of 25 µL, and then incubated at 72˚C for 20 min. A-tailed products were used for TA cloning using the pGEM Easy Vector system (Promega). Ligated PCR products were transformed into STBL2 competent E. coli cells by heat shock at 42˚C for 45 seconds, and 950 µL of SOC media was added to each sample. The following procedures were then adjusted specifically for SCN gene cloning based on recommendations in (66): samples were incubated at 30˚C for 60 min and plated on ½ strength antibiotic Luria-Bertani (LB) agar plates (50 µg/mL ampicillin or 7.5 µg/mL tetracycline). Plates were incubated at 30˚C for two days, and smaller colonies were preferentially selected over large colonies. Plasmid DNA was recovered using the QIAprep Spin Miniprep kit (Qiagen) and quantified using a Qubit fluorometer. Aliquots of transformed competent cells in LB were combined with equal volumes of 50% glycerol

and stored at -80˚C. PCR products or cloned PCR amplicons were submitted for Sanger Sequencing at the Michigan State University Genomics Core Facility (East Lansing, MI).

**Sequence analysis**

SCN gene sequences were analyzed in Geneious v11.0.5 (Biomatters Inc., Newark, NJ). We assessed the quality of sequence base calls by peak shape in the sequence electropherogram files. High-quality sequences were aligned to either transcriptomic reference sequences or orthologous gene sequences of related species downloaded from Genbank (NCBI). Functional protein annotations were added to each sequence using the reference human $Na_v$ ortholog from UniProt. We then aligned all $Na_v$ protein sequences using MUSCLE (v3.8.425) and extracted the P-loop regions for analysis of *T. granulosa* mutations. Finally, we constructed maximum-likelihood phylogenetic trees from $Na_v$ sequence alignments using RAxML with a GAMMA BLOSUM62 protein substitution model and 1,000 bootstrap replicates.

**Immunohistochemistry**

Newts were euthanized in pH-corrected 0.1% MS-222 and perfused with 4% paraformaldehyde in 0.1M phosphate buffer (PB). The brain was removed and post-fixed in 4% paraformaldehyde in 0.1M PB for 2 hours at 4˚C, then cryoprotected by overnight incubation in 20% sucrose in 0.1M PB at 4˚C. The brain was then frozen in M-1 embedding medium (Thermo Fisher Scientific) and cryosectioned at 16 µm. Brain sections were collected on Superfrost Plus slides (Thermo Fisher Scientific) and dried for 1 hr on a slide warmer at 35˚C.

For antibody labeling, brain sections were first rinsed 6x with phosphate buffered saline (PBS) to remove fixative and incubated in blocking solution containing 2% TritonX-100, 10% goat serum, and 0.05% sodium azide in PBS. We then incubated brain sections with a primary monoclonal antibody generated against a 97 amino acid antigen directed against the C-terminus of mouse $Na_v1.6$ (Sigma Aldrich, St. Louis, MO; product number WH0006334M4; antigen sequence: RVLGDSGELDILRQQMEERFVASNPSKVSYEPITTTLRRKQEEVSAVVLQRAYRGHLA RRGFICKKTTSNKLENGGTHREKKESTPSTASLPSYDSVT). The antibody was used at a concentration of 10 μg $mL^{-1}$. After three days incubation at 4˚C, sections were rinsed 8x with PBS and incubated in secondary antibody (goat anti-mouse IgG Alexa Fluor 488, Thermo Fisher Scientific) at 1 μg $mL^{-1}$ for 60 mins. Slides were then rinsed 6x to remove residual secondary antibody and counterstained with Hoechst 33258 (Sigma Aldrich) for 2 mins.

Brain sections were dehydrated through an ethanol gradient: 1 min at 70%, 1 min at 95%, 2 mins at 100%, and an additional 2 mins at 100%. Slides were then incubated in three baths of xylene for 5 mins each and coverslipped with DPX (Sigma Aldrich). Images were collected using an Olympus BX53 fluorescence microscope outfitted with FITC (excitation 488 nm) and DAPI (excitation 405 nm) filters using Cell Sens software and a Qi-Click 12 Bit cooled camera.

**Site-directed mutagenesis**

Characterization of the effects of three individual mutations in *T. granulosa* $Na_v1.6$ on TTX binding were examined by heterologous expression and

electrophysiological recording in *Xenopus laevis* oocytes. We introduced these mutations into an orthologous *M. musculus* SCN8A construct (mSCN8A), kindly provided by Dr. Al Goldin (51), to create a chimeric newt-mouse SCN8A construct. The mSCN8A construct contained an upstream T7 promotor and a downstream NotI restriction enzyme site for plasmid linearization. Site-directed mutagenesis (SDM) was performed using the Q5 SDM kit (New England Biolabs). SDM primers containing the target mutation were produced using the NEBase Changer tool (https://nebasechanger.neb.com). After PCR amplification, PCR products were treated with kinase-ligase-DpnI enzyme mix (New England Biolabs), then purified by spin column using the DNA Clean & Concentrator kit (Zymo Research). Mutated plasmid DNA was cloned into STBL2 *E. coli* competent cells by heat shock at 42˚C for 45 secs. Incubation and colony selection was performed following the protocol of (66); specifically, all incubations were performed at 30˚C using ½ antibiotic (ampicillin: 50 mg $L^{-1}$; tetracycline: 5 mg $L^{-1}$) and two-day incubation periods. Colonies were picked and submerged in LB for overnight incubation, and plasmid DNA was recovered by mini-prep (Qiagen). Samples of each culture were combined with an equal volume of 50% glycerol and stored at -80˚C.

Because rearrangements and other replication errors are common with sodium channel sequences (66), each plasmid was screened by restriction enzyme (RE) digest using BamH1 and IgIII (New England Biolabs) and run on a 0.8% w/v agarose gel to ensure the correct fragmentation pattern was present. Samples with the correct RE pattern were inoculated in 400 mL of LB and incubated overnight, and plasmid DNA was recovered using the Qiagen plasmid maxi-prep kit (Qiagen). Maxi-prepped DNA

was quantified using a Qubit fluorometer and the mSCN8A reading frame was sequenced at the MSU Genomics Core Facility to ensure the correct substitution was made and that no other mutations were introduced into the construct.

**cRNA synthesis**

Capped mRNA (cRNA) was synthesized from linearized DNA templates. Plasmid DNA containing the unmutated mSCN8A, individual mutations, or the triple-mutant construct was linearized by overnight digestion using the NotI restriction enzyme in the presence of calf intestinal alkaline phosphatase (New England Biolabs). 10% SDS and proteinase K were added to each reaction and incubated at 50˚C for 1 hr. Two volumes of phenol were added and mixed into each sample prior to centrifugation at 12,000 x g at 4˚C for 10 min, and the upper aqueous layer was transferred to a new tube. Linearized DNA was precipitated by the addition of two volumes of ice cold 100% ethanol, 20 µL of 3M sodium acetate, and 1 µL of glycogen, followed by overnight incubation at -20˚C. Samples were then centrifuged at 12,000 x g at 4˚C for 20 min, the supernatant discarded, and the DNA pellet washed with 0.5 mL 75% ethanol by brief vortexing and re-centrifugation. The supernatant was discarded, and the DNA pellet air-dried and resuspended in 10 µL nuclease-free water. cRNA was produced using the T7 mMessage mMachine kit following manufacturer's instructions (ThermoFisher Scientific). Reaction components were combined with 250 ng of linearized template DNA and incubated at 37˚C for 2-8 hours. Synthesized RNA was recovered by lithium chloride precipitation with the addition of 1 µL glycogen. RNA pellets were resuspended

in 20 µL nuclease-free water and aliquots at 50 ng/µL concentration were produced for injection into oocytes. Aliquots were stored at -80˚C.

**Expression in Xenopus oocytes**

Ovaries of adult Xenopus laevis were purchased from Xenopus 1 (Dexter, MI) for electrophysiological recordings. Individual oocytes were collected from the ovary by enzymatic digestion using collagenase (0.4 mg $mL^{-1}$, type II activity 255 µ/mg) in $Ca^{2+}$-free ND96 solution (in mM: 96 NaCl, 2 KCl, 1.8 CaCl2, 1 MgCl2, and 5 HEPES adjusted to pH 7.5 and supplemented with 0.1 mg/ml gentamycin, 0.55 mg/ml pyruvate, and 0.5 mM theophylline). After 90 min incubation, treated ovaries were washed 5X with normal ND96, and Stage 5 and 6 oocytes were selected for injection.

Oocytes were injected with cRNA samples using a Nanoject III (Drummond Scientific, Broomall, PA). Nanoject glass capillaries (Drummond, 3-000-203-G/X) were pulled into pipettes using a Sutter P-97 micropipette puller (Sutter Instruments Co., Novato, CA) using the following conditions: Heat=ramp+5, Pull=100, Velocity=50, Delay=50, Pressure=500. Pipettes were backfilled with mineral oil and placed onto the Nanoject. A 4-µL droplet of each cRNA sample (50 ng/µL) was front loaded into the pipette, and oocytes were injected with either 10, 25, or 50 nL of cRNA (0.5 – 2.5 ng/oocyte). Oocytes were incubated at 14˚C and used for recording within 2-10 days.

**Electrophysiology**

Macroscopic sodium currents were measured by two-electrode voltage clamp using a Warner Instruments Oocyte Clamp (model OC-725C). Borosilicate glass

pipettes (1B120F-4, World Precision Instruments, Sarasota, FL) pulled to a 1 or 2 MΩ tip (Heat = Ramp + 5, Pull = 100, Vel = 50, Time = 50, on a Sutter Instruments P-97 puller) served as current and voltage electrodes, respectively. Pipettes were filled with 3M KCl and 0.5% agarose. Oocytes were recorded in a RC-26Z diamond bath recording chamber with a chamber volume of 350 µL (Warner Instruments, Hamden, CT) in filter-sterilized ND96 recording solution (96 mM NaCL, 2 mM KCl, 1.8mM CaCal2, 1mM MgCl2, and 10mM HEPES; pH 7.5) at room temperature (20˚-22˚C). Purified TTX (Sigma Aldrich or Abcam, Cambridge, UK) was diluted in recording solution and perfused through the chamber for experimental applications. $Na^+$ current traces were digitized at 10 kHz using a Digidata 1550B (Molecular Devices, San Jose, CA) and recorded in pCLAMP v10.7 (Molecular Devices). Leak currents were subtracted by P/4 correction.

The electrophysiological properties measured from each construct (wildtype, triple mutant, and three individual mutants of mSCN8A) include peak $Na^+$ current ($I_{max}$), conductance, and the voltage-dependence of fast inactivation. Current-voltage (I/V) relationships for each mSCN8A construct were determined using an activation protocol where each oocyte was clamped to a membrane potential of -100 mV and depolarized from -80 to +65 mV in 5 mV steps. The pulse duration was 50 ms with an inter-pulse interval of 5 secs. Fast inactivation was measured by clamping the membrane at increasingly depolarized membrane potentials from -100 mV to +10 mV in 5 mV steps for 100 ms, followed by a 50 ms test pulse at 0 mV. In such a protocol, the current generated during the test pulse is inversely related to the population of inactivated channels (18).

To measure the effects of TTX on $I_{max}$, conductance, and fast inactivation, 10 volumes (3.5 mLs) of ND96 recording solution containing experimental concentrations of TTX (100 nM, 1 μM, and 10 μM) were perfused over the oocyte at a flow rate of 5 mL per min. TTX block was monitored by delivering a 50 ms test pulse of 0 mV from a holding potential of -100 mV every 10 secs. Steady-state block was achieved with ten consecutive pulses without a change in peak current, typically around 5 mins after the application of TTX. Step activation and fast inactivation were then measured in the presence of TTX using the protocols described above. To determine whether TTX was responsible for reductions in $I_{max}$, all oocytes were then washed for 5-10 mins with normal ND96 and re-recorded by the same protocols. Recordings were discontinued if the membrane leak potential increased more than 0.1 mV during the recording or if $I_{max}$ did not recover during the wash.

To determine half maximal inhibitory concentration ($IC_{50}$) of TTX for each mutant construct, we followed the protocol described in (67). Peak currents were measured every 10 secs using a 50 ms depolarization from -100 to 0 mV. Baseline recordings ($I_{max}$) were taken for 1-2 mins, then TTX was applied by continual perfusion over the oocyte until steady-state block was reached ($I_{TTX}$), defined by at least 10 pulses without a change in peak current. The TTX concentration used in each experiment was adjusted to achieve between 40-80% block of $I_{max}$: for wild-type mSCN8A, DIII, and DIV mutants, 5 μM TTX used, and for DI and triple mutant constructs, 100 μM TTX was used. TTX was then washed off by perfusion with normal ND96 until the current returned to $I_{max}$, typically within 3 mins. The rates of TTX binding ($\tau_{on}$) and unbinding ($\tau_{off}$) were calculated from these recordings for analysis.

**Data analysis**

Data were extracted from $Na^+$ current traces in Clampfit v10.7 (Molecular Devices) and exported for analysis in R Studio v3.6.0. $Na^+$ currents elicited by each voltage step in the presence and absence of TTX were normalized relative to the peak current ($I_{max}$) recorded for each oocyte prior to the addition of TTX. Statistical differences in peak current in the presence and absence of TTX were determined using one-way repeated measures analysis of variance (ANOVA) at the -20 mV depolarization step, at which $I_{max}$ was typically largest.

Normalized conductance curves for each oocyte were determined by $G_{Na} = I_{max}/(V-V_{Na})$, where $I_{max}$ is the peak current, V is the voltage step, and $V_{Na}$ is the $Na^+$ reversal potential. $V_{Na}$ was assessed empirically for each oocyte from the corresponding I/V curve. Conductance-voltage plots were fit with a single Boltzman equation, $G_{Na} = 1/(1 + \exp[ -(V – V_{1/2}) / k])$, where V is the voltage step, $V_{1/2}$ is the voltage required for half-maximal activation, and k is the slope of the Boltzmann fit. The voltage-dependence of fast inactivation was assessed by plotting normalized $I/I_{max}$ and fitting with a single Boltzman equation, $I = 1/(1 + \exp[(V – V_{1/2}) / -k])$, where I is the peak current measured during the test pulse, V is the pre-pulse voltage, $V_{1/2}$ is the voltage required for half-maximal inactivation, and k is the slope of the Boltzmann fit.

The $IC_{50}$ for TTX binding was determined from the ratio of peak currents in the presence and absence of TTX by a single-site Langmuir equation, $IC_{50} = [TTX](I_{TTX}/I_{max}) / (1 – (I_{TTX}/I_{max}))$, where $I_{max}$ is the peak current recorded under control conditions and $I_{TTX}$ is the current recorded for a given concentration of TTX. Values for $IC_{50}$ are shown

as mean ± SEM, and statistical differences between constructs were assessed by one-way ANOVA.

## RESULTS

### All newt $Na_v$s possess amino acid substitutions in conserved S5-S6 pore-loops

From our brain and nose transcriptomes, we obtained full length or partial sequences for all five target SCN genes (genes: SCN1A, SCN2A, SCN3A, SCN5A, SCN8A; proteins: $Na_v1.1$, $Na_v1.2$, $Na_v1.3$, $Na_v1.5$, $Na_v1.6$, respectively). We identified full length coding sequences for genes SCN3A, SCN5A, and SCN8A and partial sequences for SCN1A and SCN2A. Our sequence for SCN2A encodes all four transmembrane domains and P-loop regions, but the sequence for SCN1A only encodes DIII and DIV of the channel. The DI-DIV transmembrane sequences of each gene identified in the transcriptomes were PCR amplified from brain or nose cDNA and resequenced to verify that the assembled sequences were correct, particularly in the critical S5-S6 P-loop regions. Consensus sequences for each gene will be submitted to GenBank upon approval of the manuscript. The sequence for *T. granulosa* $Na_v1.4$ was obtained from GenBank (KP118969.1) for comparison with other newt channels.

To identify mutations in newt $Na_v$ channels, sequences were translated and aligned with orthologous $Na_v$ sequences from representative vertebrate taxa: human (*Homo sapiens*), mouse (*Mus musculus*), chicken (*Gallus gallus*), green anole (*Anolis carolinensis*), and the two amphibians for which complete SCN gene sequence data were available in GenBank, the Western clawed frog (*Xenopus tropicalis*) and Tibetan frog (*Nanorana parkeri*) (**Figure A2.1**). We also constructed maximum-likelihood gene

trees based on the vertebrate $Na_v$ alignment to evaluate the ancestral state of P-loop sequences and determine whether newt mutations are unique to *T. granulosa* or synapomorphic among amphibians (**Figure A2.2**). In the following discussion, mutations are annotated and numbered by reference to the homologous amino acid site in the mouse $Na_v1.6$ channel (GenBank: U26707.1).

Overall, although the amphibian S5-S6 P-loop sequences are highly conserved across the $Na_v$ gene family, several amino acid substitutions are present in the P-loops of all six $Na_v$ channels in *T. granulosa* (**Figure 2.1**). In DI, one site at Tyr-371 has mutated independently across four channels: $Na_v1.2$, $Na_v1.3$, $Na_v1.5$, and $Na_v1.6$. This parallel substitution involves a replacement from an aromatic Tyr or Phe to a non-aromatic amino acid, either Cys, Ser, or Ala, and mutations at this locus in other $Na_v$s have been shown to provide up to 2,500-fold resistance to TTX (31, 37, 68). An additional mutation is found at N374T in $Na_v1.5$; interestingly, this site is also mutated in the TTX-resistant cardiac channel ($Na_v1.5$) of mammals, but not in *Xenopus* (48), indicating that these mutations are convergent.

In DII, only one substitution is present at T938S, and only in $Na_v1.3$. This locus is adjacent to the electronegative Glu-937 that directly binds the positively charged guanidinium group of TTX (30). This region is otherwise well conserved across vertebrates (**Figure A2.1**), suggesting that the DII P-loop sequence is under strong purifying selection. Three sites are mutated in DIII including V1407I, M1414T, and A1419P in $Na_v1.6$, $Na_v1.4$, and $Na_v1.1$, respectively. The M1414T mutation is remarkably widespread and has evolved convergently across several $Na_v$ paralogs in puffer fishes, several species of newts, one garter snake (*Thamnophis couchii*), and a

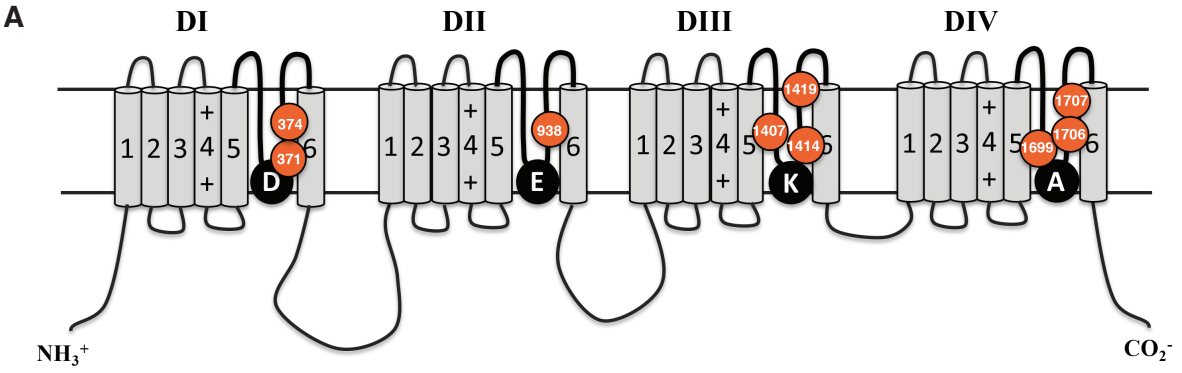


B

| | | Consensus: SLFRLMTQ**D**YWENLYQL | IVFRVLCG**E**WIETMWDC | ALLQVATF**K**GWMDIMYA | CLFQITTS**A**GWDGLLA |
|---|---|---|---|---|---|
| $Na_v1.1$ | *N. parkeri* | .....D..... | .....E..... | .....K..... | .....A..... |
| | *X. tropicalis* | .....D..... | .....E..... | .....K..... | .....A..... |
| | *T. granulosa* | | | .....K.....P | ...E....A...R... |
| $Na_v1.2$ | *N. parkeri* | .....D.....MK | .....E..... | .....K...P.... | ...M....A...L... |
| | *X. tropicalis* | .....DC..... | .....E..... | .....K...P.... | .....A...L..E |
| | *T. granulosa* | .....DC.....Q | .....E..... | .....K..... | .....G...V..S |
| $Na_v1.3$ | *N. parkeri* | .....D.....M. | .....E..... | .....K..... | ...M....A..... |
| | *X. tropicalis* | .....DF..... | .....E..... | .....K...E.... | .....A..... |
| | *T. granulosa* | .....DA..... | .....E...S.... | .....K..... | ...M....A..... |
| $Na_v1.4$ | *N. parkeri* | A.....D.....F.. | ....I...E..... | S.....K..... | ...E....A.....N |
| | *X. tropicalis* | .....DF....F.. | ....I...E..... | S.....K..... | .....A.....N |
| | *T. granulosa* | .....D.....F.. | ....I...E..... | S.....K..T..... | ....S...A..SD..I |
| $Na_v1.5$ | *X. tropicalis* | .....D.....Q | .....E..... | .....K..... | .....A.....N |
| | *T. granulosa* | A.....DS..T...Q | .....E..... | .....K..... | .....A.....N |
| $Na_v1.6$ | *N. parkeri* | A.....DF..... | .....E..... | ....I...K..... | .....A.....L |
| | *X. tropicalis* | A.....DF..... | .....E..... | .....K..... | .....A.....L |
| | *T. granulosa* | A.....DA..... | .....E..... | ....I...K..... | ....V...A.....L |

**Figure 2.1: Amino acid substitutions in the S5-S6 P-loops across the $Na_v$ gene family in amphibians.**

(A) The structure of the $Na_v$ α subunit is comprised of four homologous domains (DI–DIV) each with six transmembrane segments (S1–S6) that form the central pore of the channel. The S5 and S6 pore-loops (P-loops) for the outer vestibule and inner pore of the channel, and the DEKA motif at the base of the P-loops form the selectivity filter. The approximate locations of mutations are shown as orange circles, and the amino acid site of each mutation is numbered based on $Na_v1.6$ from Mus musculus.
(B) Multiple sequence alignment of S5-S6 P-loops from *T. granulosa* and two other amphibians. The residues from the DEKA motif are shown in bold. Amino acid substitutions are shown relative to the P-loop consensus sequence generated across all $Na_v$ channels shown here. Putative TTX resistance mutations are highlighted. Mutations not highlighted are either synapomorphic in a gene clade or are present in TTX sensitive channels. Data are missing for DI and DII of $Na_v1.1$ in *T. granulosa* and $Na_v1.5$ from *N. parkeri*.

mite (*Varroa destructor*) (35, 36, 38, 69). This substitution, inserted into rat $Na_v1.4$, was shown to increase TTX resistance 15-fold when expressed in *Xenopus laevis* oocytes (38). The effects of the other two DIII mutations on TTX binding are unknown, but the V1407I mutation is present in the TTX-resistant newt retinal channel and the skeletal muscle of the pufferfish *Fugu pardalis*, suggesting that it may be involved in TTX binding and resistance. Thus, we examined the functional consequences of this mutation in $Na_v1.6$, as described below (41, 70).

Finally, in DIV mutations occur across four sites, including a substitution of A1703G in the selectivity filter DEKA motif in $Na_v1.2$. Although Asp-1703 is thought to be critical for $Na^+$ selectivity and therefore might be presumed to be invariant, this mutation occurs naturally in pufferfish Nav1.1b, Nav1.4a, and Nav1.6b of pufferfishes (71). Heterologous expression studies have shown that this mutation does not affect monovalent cation selectivity, but does increase TTX resistance 1.5-fold, as well as increasing single channel conductance (38, 71). Two other mutations that have been shown to increase resistance 2-fold in garter snakes occur at Ile-1699 in $Na_v1.4$ and $Na_v1.6$ (33). Another mutation occurs at D1706S in $Na_v1.4$, which is also present in TTX resistant mites (69). This site was also recently shown to bind directly to the guanidinium group of TTX (30). Last, Gly-1707 is mutated across $Na_v1.1$, $Na_v1.2$, and $Na_v1.4$, and this replacement confers up to 250-fold resistance in garter snake skeletal muscle (33).

**Newts and TTX resistant snakes from Oregon possess parallel mutations in the neural subtype $Na_v1.6$**

TTX resistance has evolved independently in several populations of garter snakes (*Thamnophis sirtalis spp.*) that prey on toxic newts. Substitutions in the garter snake skeletal muscle $Na_v1.4$ isoform dramatically reduce sensitivity to TTX (32, 33), and $Na_v1.4$ resistance has evolved independently in several populations of *T. sirtalis*, as well as other snake species (34, 35). However, mutations in two neural subtypes, $Na_v1.6$ and $Na_v1.7$, preceded the evolution of skeletal muscle resistance in snakes, and the ancestral resistance of peripheral nerves is thought to have facilitated the initiation of a coevolutionary arms race between toxic newts and resistant snakes (40). Interestingly, when we compared $Na_v1.6$ sequences in newts and snakes, we found that the channels share two identical substitutions in DIII V1407I and DIV 1699V P-loops (**Figure 2.2**). Both newt and snake sequences were derived from wild-caught individuals living in Benton County, OR, where predator-prey coevolution has driven TTX toxicity and resistance to extreme levels (61, 72). The DIV I1699V mutation is also found in $Na_v1.6$ of red-spotted newts (Notophthalmus viridescens), which possess high levels of TTX during their juvenile red eft stage (73), as well as in the retinal $Na_v$ from C. pyrrhogaster (41).

The presence of two identical substitutions in both TTX-resistant newts and snakes provided an opportunity to investigate convergent molecular evolution between both predators and prey responding to the same selection pressure. Parallel mutations may reflect a constrained adaptive walk towards resistance, and/or a unique aspect of the amphibian-specific TTX toxin profile, which consists of a mixture of TTX and

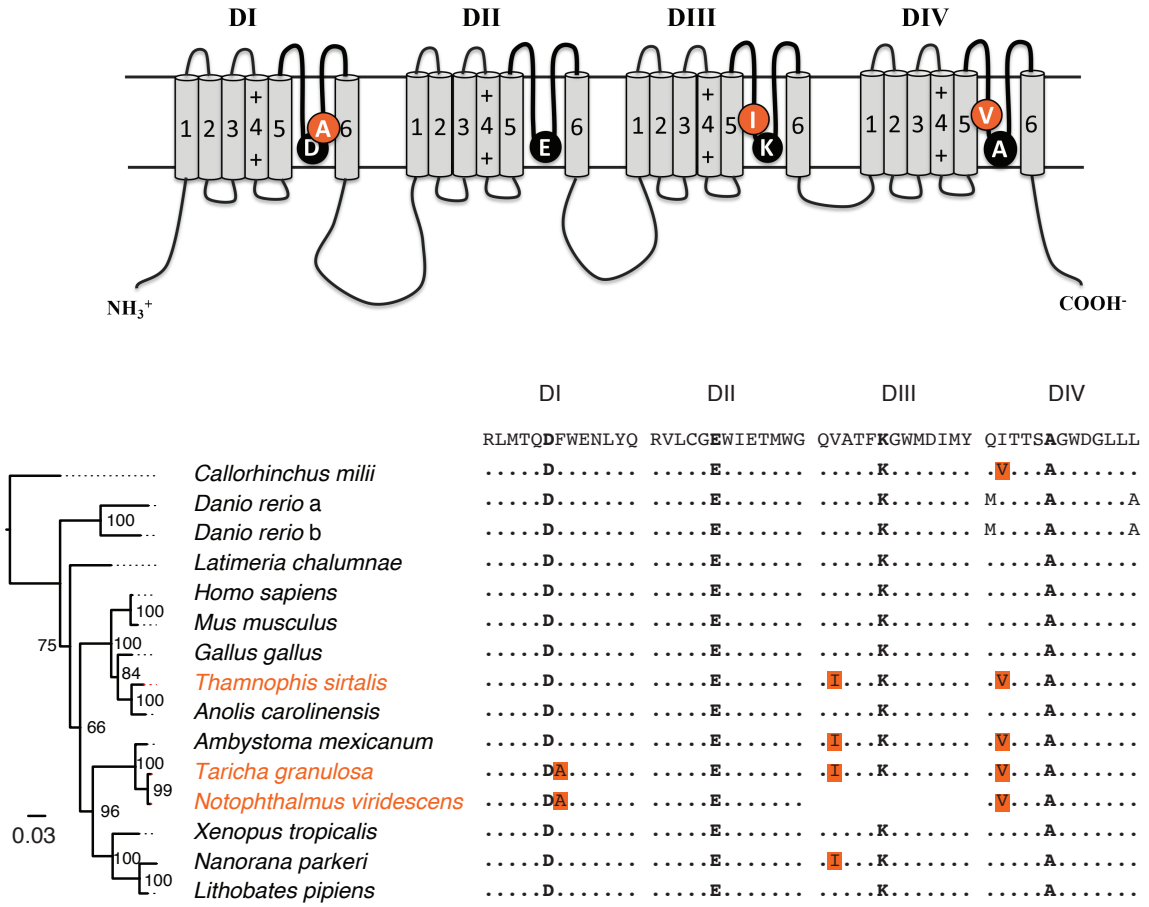


**Figure 2.2: Parallel evolution of DIII and DIV P-loop substitutions in $Na_v1.6$ of toxic newts and TTX resistant garter snakes.**

Multiple sequence alignment of $Na_v1.6$ across representative vertebrate taxa. The consensus sequence is shown above the alignment. Phylogenetic relationships are based on full-length $Na_v1.6$ assessed by RAxML with 1,000 bootstrap replicates. Support values are shown on each node, and the scale bar reflects the mean number of nucleotide substitutions per site. Taxa that either possess TTX or consume TTX-laden prey, as well as convergent amino acid substitutions occurring among these taxa, are labeled in orange. The location of these mutations relative to the DEKA motif is shown in the $Na_v$ illustration above the alignment.

congeners such as 6- or 8-epiTTX that are not present in marine animals (74). Both mutations are also present in the TTX-sensitive Mexican axolotl (*Ambystoma mexicanum)* and may be synapomorphic in $Na_v1.6$ among salamanders.

If the DIII and DIV mutations provide low levels of TTX resistance, they may have served as preadaptations facilitating the initial steps of the adaptive walk towards increased toxicity. We therefore investigated the physiological effects of these three mutations on TTX binding and resistance in a chimeric newt-mouse $Na_v1.6$ construct expressed in X. laevis oocytes; we also used immunocytochemistry to verify that it is abundantly expressed in axons in the CNS (**Supplemental Figure 2.3**).

**Newt pore-loop mutations increase TTX resistance in mouse $Na_v1.6$**

To assess the functional consequences of newt P-loop mutations on TTX resistance in $Na_v1.6$, we investigated the physiological properties of a chimeric mouse $Na_v1.6$ channel that possessed one of three single amino acid replacements, DI Y371A, DIII V1407I, or DIV I1699V, as well as a triple mutant channel that contained all three mutations. We expressed each channel in X. laevis oocytes and recorded peak $Na^+$ currents under control conditions or in the presence of 1 μM or 10 μM TTX (**Figure 2.3A**). Our results show that $Na^+$ currents were inhibited by TTX in a dose-dependent manner in wild-type (n=16), DIII V1407I (n=11), and DIV I1699V (n=11) channels, but that the DI Y371A construct was significantly more resistant than the other channels (n=10) (**Figure 2.3B-E**). Our results also verify that the mutations do not alter channel conductance or fast inactivation (**Supplemental Figure 2.4**).

In the wild-type mouse channel, one-way repeated measures ANOVA on normalized peak current elicited by a step depolarization to -15 mV indicates a global effect of TTX concentration ($F = 148.07$, $P < 0.0001$). Tukey's multiple comparisons of means test with Bonferroni correction reveals that this effect arises from the comparison

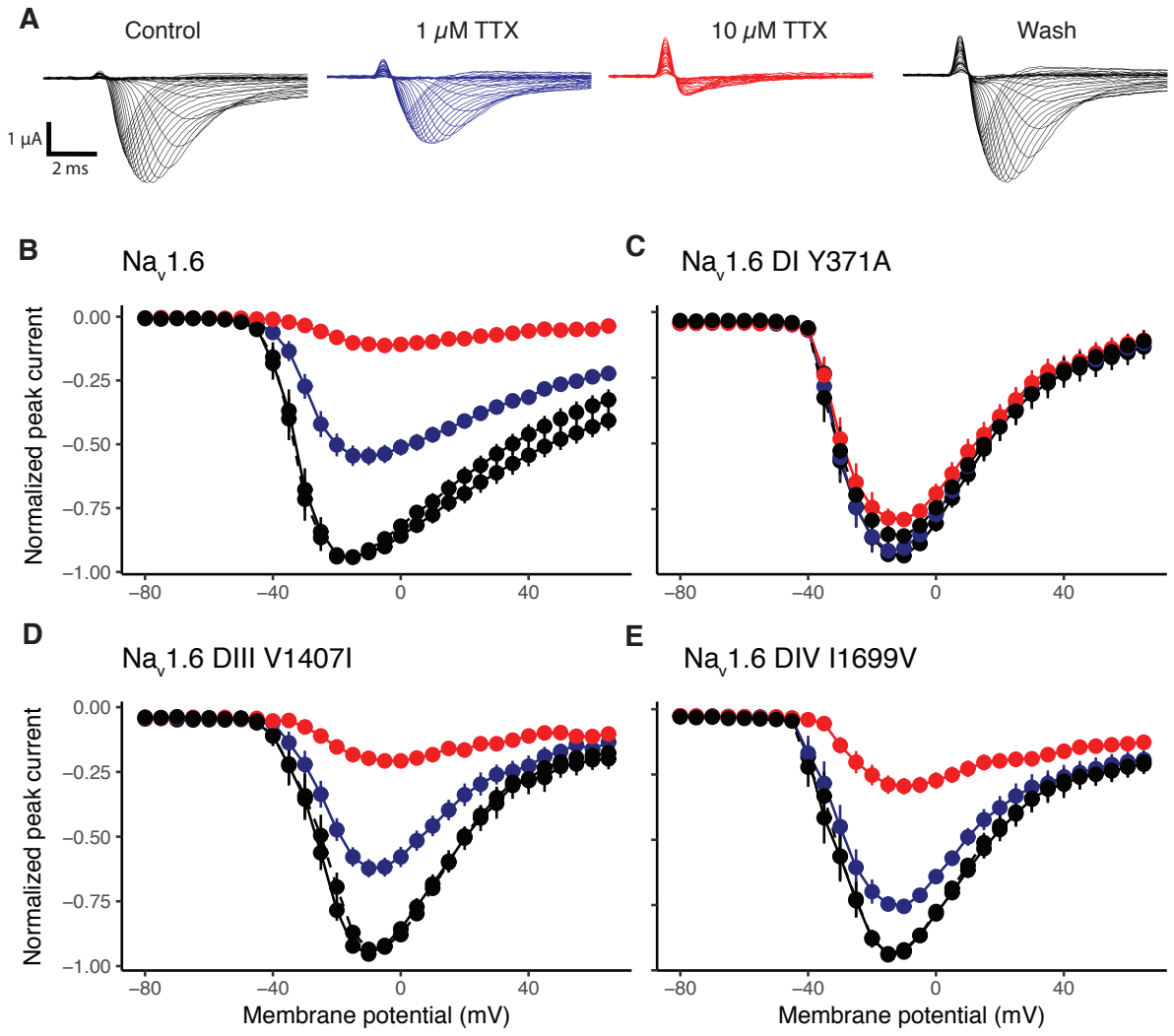


**Figure 2.3: Effect of newt $Na_v1.6$ mutations on TTX sensitivity in mouse $Na_v1.6$.**

(A) Overview of our experimental procedure. $Na^+$ currents elicited by 5 mV step depolarizations from a holding potential of -100 mV to a set of pulses from -80 to +65 mV in control solution (ND96) (black), 1 μM TTX (blue), 10 μM TTX (red), and wash (black). The pulse duration was 50 ms. I/V curves of normalized peak $Na^+$ currents measured for (B) wild-type mouse $Na_v1.6$ and mutant constructs (C) DI Y371A, (D) DIII V1407I, and (E) DIV I1699V containing one of three mutations in the presence of the control solution (black), 1 μM TTX (blue), and 10 μM TTX (red). Each construct was coexpressed with rat β1 and β2 subunits. Data are shown as peak currents normalized to the maximum current recorded for each oocyte. Dotted lines indicate current after washing TTX from the oocyte. The construct containing the DI mutation was largely unaffected by TTX at 1 or 10 μM (n=10); DIII (n=11) and DIV (n=11) were more sensitive, but each channel shows reduced sensitivity relative to the wild-type channel.

of control vs. 1 μM TTX ($z = -9.06$, $P < 0.0001$) and control vs. 10 μM TTX ($z = -18.99$, $P < 0.0001$). The difference between pre-TTX control and wash conditions was not significant ($z = -1.89$, $P = 0.352$), demonstrating that our recordings were stable over the course of the experiment (**Figure 2.3B**).

Each of the three newt mutations reduces the proportion of blocked $Na^+$ current relative to the wild-type mouse channel. The DI Y371A mutation has the most dramatic effect and reduces TTX sensitivity such that the channel cannot be blocked with 10 μM TTX (control vs. 10 μM, $z = -1.352$, $P = 0.175$) (**Figure 2.3C**). The effect of the other two mutations were milder: $Na^+$ currents in each construct were significantly blocked when comparing control conditions to 1 μM TTX for DIII ($z = -7.432$, $P < 0.0001$) and DIV constructs ($z = -4.58$, $P < 0.0001$) (**Figure 2.3D-E**). However, the proportion of the $Na^+$ current remaining in the presence of 10 μM TTX was significantly greater for the DIII V1407I ($z = 3.05$, $P = 0.023$) and DIV I1699V ($z = 6.51$, $P < 0.0001$) constructs than in the wild-type channel (**Figure A2.5**).

Thus, the DI mutation alone has a dramatic effect on TTX resistance, but the DIII and DIV mutations also contribute mild resistance to the channel. Our sequence data show that convergent mutations are present in the DI site across four $Na_v$ channels in newts, and this mutation has also been reported in other TTX-resistant species such as pufferfishes and fire-belly newts. Replacements at this site reduce TTX sensitivity when expressed in other TTX-sensitive channels such as $Na_v1.2$ and $Na_v1.4$ in rats (31, 37, 68). Our results confirm the effect of this mutation in a neural subtype, $Na_v1.6$, which has not previously been evaluated.

**Pore-loop mutations interact to increase TTX resistance**

Finally, we examined the combined effect of all three mutations on TTX resistance and compared the result with those of the individual mutant constructs. Like the DI Y371A mutant alone, the triple mutant was highly resistant to TTX: the magnitude of the $Na^+$ current did not differ significantly between the control and 10 μM TTX solutions ($F = 0.223$, $P = 0.879$) (**Figure 2.4**). However, despite the resistance conferred by the DI mutation individually, estimates of the half-maximal inhibitory concentration ($IC_{50}$) of TTX for all constructs indicates that the triple mutant is far more resistant than the DI mutation alone (**Table 2.1**). Dose-response analysis of each channel exposed to 0.1, 1, or 10 μM TTX shows that the three single mutations all have an increased $IC_{50}$ relative to wild-type channels (**Figure 2.5**). The DIII and DIV mutations provide 1.2-fold and 2-fold increases in resistance, while the DI mutation provides a 609-fold increase in resistance. In contrast, the triple mutant provides a 2,832-fold increase in resistance. Indeed, we were unable to block current through the triple mutant channel even with 100 μM TTX ($n = 3$; data not shown). Thus, it appears the three mutations interact to further increase TTX resistance beyond the robust resistance provided by the DI Y371A mutation. These results show that the three P-loop mutations present in newt $Na_v1.6$ provide resistance to extreme concentrations of TTX exceeding any amount detected in TTX-laden animals, and that these substitutions are more than sufficient to confer resistance within any biologically relevant range of TTX toxicity.

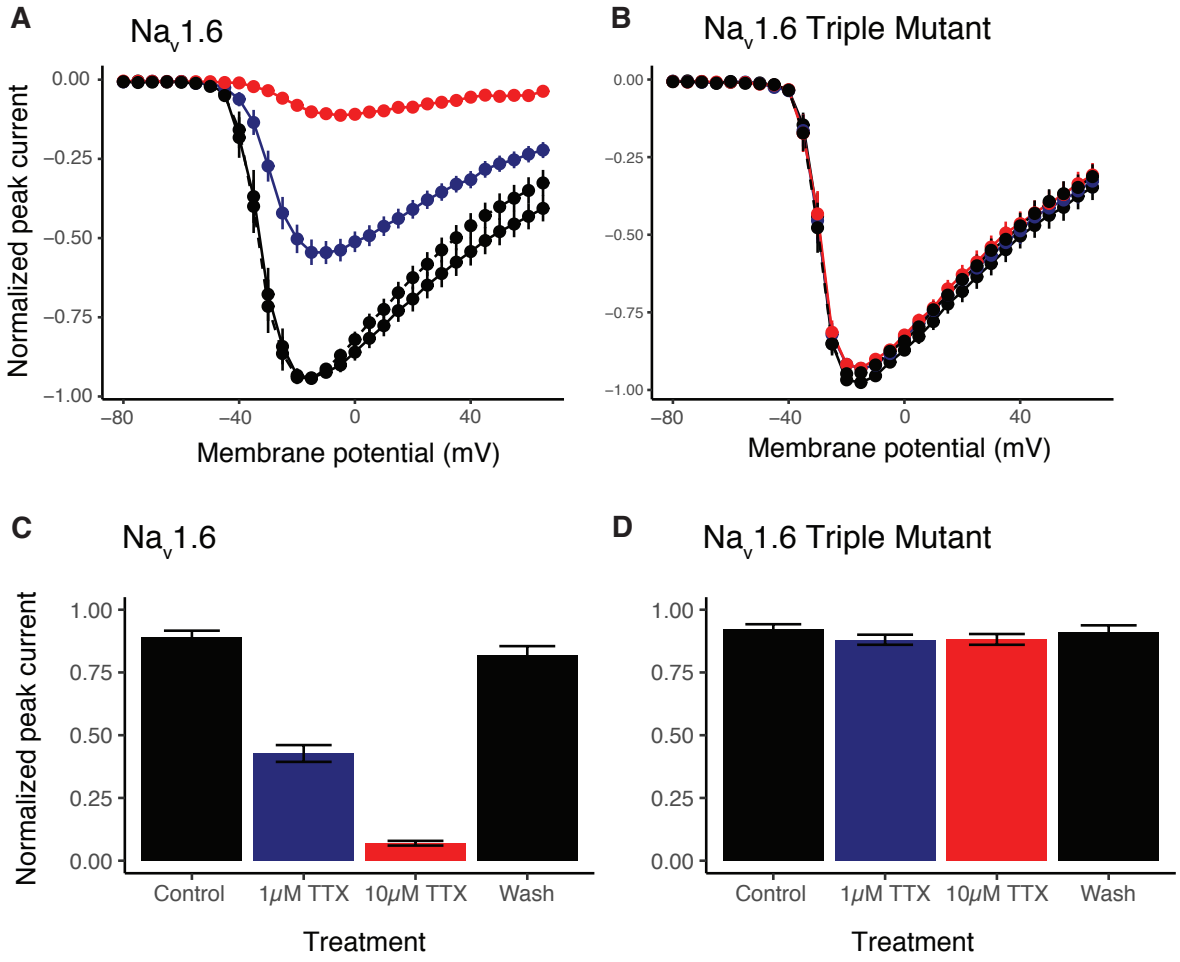


**Figure 2.4: Effect of TTX on Na⁺ currents in triple mutant channels.**

I/V curves illustrating the effect of TTX on normalized peak $Na^+$ currents in (A) wild-type or (B) mutated $Na_v1.6$ co-expressed with β1 and β2 subunits. Wild-type channels (n=16) are blocked in a dose-dependent manner and are almost completely blocked at 10 μM TTX. The triple mutant channel (n=13) is unaffected by even the highest concentration of TTX. $Na^+$ currents recovered in the wash (dotted line).

Difference in normalized peak $Na^+$ current elicited by a step depolarization to -15 mV in (C) wild-type and (D) triple mutant channels. One-way repeated measures ANOVA shows a strong statistical effect of TTX treatment in the reduction of peak $Na^+$ currents for wild-type channels ($F = 148.07$, $P < 0.0001$) but not mutated channels ($F = 0.223$, $P = 0.879$).

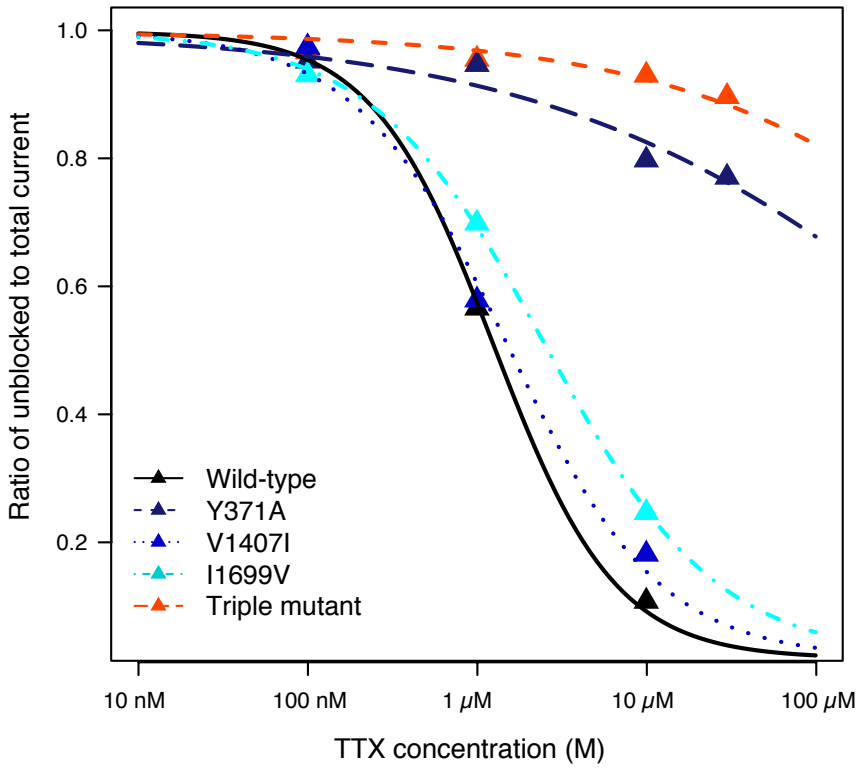


**Figure 2.5: Dose-response curves for each $Na_v1.6$ construct exposed to TTX.**

Data are shown as the mean ratio of unblocked to total current elicited by a 50 ms pulse from -100 to -15 mV at each TTX concentration. Pooled data were fit with a non-linear Hill equation. All three mutations provide increased resistance relative to wild-type mouse $Na_v1.6$. However, the triple mutant shows the highest level of resistance, with a 2,832-fold increase in $IC_{50}$ relative to wild-type channels.

**Table 2.1: Estimated half-maximal inhibitory concentrations ($IC_{50}$) of TTX for each $Na_v1.6$ construct.** $IC_{50}$ values are shown as the concentration (mean ± SEM) of TTX (μM) that blocked half of the channels, estimated from the dose-response curve. The $IC_{50}$ ratio was taken as the fold increase in TTX resistance.

| Construct | n | $IC_{50}$ | $IC_{50}$ Ratio |
|---|---|---|---|
| Mouse $Na_v1.6$ | 21 | 1.25 ± 0.09 | 1 |
| DI (Y371A) | 17 | 763.7 ± 284 | 608.9 |
| DIII (V1407I) | 13 | 2.34 ± 0.23 | 1.2 |
| DIV (I1699V) | 15 | 4.73 ± 0.42 | 2.0 |
| Triple mutant | 20 | 3551 ± 469 | 2832.4 |

## DISCUSSION

Our results show that rough-skinned newts possess numerous amino acid substitutions across the highly-conserved S5-S6 P-loops of all six $Na_v$ channel paralogs. Many of the amino acid replacements that we identified in newts have been found in other TTX-resistant animals, including pufferfishes, garter snakes, softshell clams, and parasitic mites (31, 33, 38, 69, 75, 76). The effects of these mutations in other species range from a 3-fold to 5,000-fold increase in TTX resistance, extending to concentrations of TTX that are unlikely to be encountered in nature. Although mutations in other regions outside of the P-loops may contribute to elevated TTX resistance, computational modeling and site-directed mutagenesis studies have indicated that P-loop mutations have the greatest impact on TTX binding (29, 67, 68). In addition, recent structural studies employing cryo-electron microscopy (cryo-EM) have confirmed these findings by capturing images of TTX bound to P-loop regions of both cockroach and

human $Na_v$ channels (30, 77). Our results provide further support for the role of P-loop mutations in TTX binding, and importantly, demonstrate that mutations in the critical P-loop regions are necessary and sufficient to provide TTX resistance to the $Na_v$ channel.

The high degree of sequence convergence found across the $Na_v$ channels of newts and other TTX-resistant animals suggests that the evolution of resistance involves a highly constrained walk through a narrow adaptive landscape (16). $Na_v$ channels are critical for neural and muscular signaling, and mutations that reduce TTX sensitivity may also affect other channel functions such as conductance, gating kinetics, and/or the rates of activation and inactivation. In vertebrates, SCN gene duplications have generated numerous channels that possess unique physiological properties and expression patterns in different tissues (18), and subtype-specific functional constraints may impact selection on P-loop mutations differently depending on the domain and the channel they occur in. For example, studies of the skeletal muscle isoform $Na_v1.4$ across a variety of TTX-resistant snake species identify numerous convergent substitutions in the P-loop regions of DIII and DIV, but never in DI or DII (34, 35). The $Na_v1.4$ subtype of TTX-resistant newts, including rough-skinned newts, also possess several mutations in DIV and one in DIII, but none in DI or DII (36). Conversely, mutations in the DI Y/F-371 site are often seen in neural subtypes of TTX-resistant pufferfishes, and we found that this mutation is present in three of the four neural subtypes of newts. Whether or not these patterns have arisen by chance or through $Na_v$ subtype-specific constraints on P-loop evolution would be interesting to explore in future studies.

However, another explanation for the convergent pattern of mutations we discovered could be that the mutated amino acid sites are directly involved in TTX binding, and that replacements at other sites would have no impact on resistance. In particular, mutations are rarely present in the DII P-loop, with only one mutation present in newts ($Na_v1.5$ T938S). Is the lack of mutations in the DII P-loop region due to functional constraints and purifying selection, or do mutations in DII would have no effect on TTX resistance? Recent crystal structures of TTX bound to both vertebrate $Na_v1.7$ and invertebrate $Na_v1$ channels show that TTX directly binds to two DII P-loop sites, the Glu-934 (E) of the DEKA selectivity filter motif and the adjacent Glu-937 (underlined in the consensus sequence in **Figure 2.1B**) (30, 77). The positively-charged guanidinium group of TTX is attracted to the electronegative charge of these acidic residues and forms polar bonds that cause TTX to stick to the channel, preventing access of $Na^+$ ions to the selectivity filter. Thus, in the absence of molecular or physiological constraints, selection for TTX resistance should favor replacement of these acidic residues or adjacent sites for neutral or positively-charged amino acids. However, these sites are invariant across newt $Na_v$ channels and most TTX-resistant channels characterized to date; only two $Na_v$ channels, one sequenced from a pufferfish (*Tetradon* Na 1.4b) and one from a softshell clam (*Mya arenaria* $Na_v1$), are known to possess a mutation in DII. The Glu-937 replacement alone in clams provides up to 3,000-fold resistance to TTX (76). Thus, the lack of mutations in DII are more likely due to functional constraints and purifying selection than to lack of TTX binding sites. As techniques in structural biology such as cryoEM continue to advance, we will learn more about the functional roles of individual amino acids in $Na_v$ and other ion channels, and

these data are likely to improve our understanding of sequence variation and evolution as they relate to protein function.

In our research, we found that V1407I and I1699V mutations in DIII and DIV provided 1.2-fold and 2-fold increases in resistance in $Na_v1.6$, respectively. Replacement at these sites thus provides mild resistance. However, when combined with the large effect DI Y371A mutation, which alone provides a nearly 609-fold increase in resistance, the triple-mutant channel was over 2,800-fold more resistant than wild-type mouse $Na_v1.6$. Thus, these mutations combine additively to provide a nearly 4.5-fold increase in resistance relative to the DI mutation alone. Aside from our study, we are aware of only one other study that examines additive effects of mutations in $Na_v$s: (37) found that DIV mutations contributed a mild increase in resistance (2 to 11-fold) to DI Y401N mutations in rat $Na_v1.2$. Many other TTX binding studies have examined mutations in isolation, and future studies should consider the combinatorial effects of different mutations on overall resistance.

Interestingly, both V1407I and I1699V mutations are present in axolotls (*Ambystoma mexicanum*), a TTX-sensitive salamander outside of the newt family (Salamandridae), as well as in Eastern newts (*Notophthalmus viridescens*), which possess TTX and are closely related to Taricha newts (**Figure 2.2**). Considering that these two mutations provide mild TTX resistance, it is possible that they enabled the evolution of TTX toxicity in newts by facilitating interactions with low concentrations of toxin early during the adaptive walk toward TTX resistance. Because these mutations involve structurally and biochemically similar replacements, their negative impacts on $Na_v$ channel function may be minimal. When combined with the later-arising DI

mutations, these replacements would then have significantly increased resistance to millimolar levels, far beyond any TTX concentration found in natural systems. Thus, seemingly benign substitutions that involve biochemically similar changes may impact toxin binding in unpredictable ways. In this particular case, the DIII and DIV replacements may impact the steric orientation of TTX as it enters the outer vestibule and binds the selectivity filter, despite the fact that TTX does not directly interact with these sites (30). We propose that these mutations may have been present in the common ancestor of Salamandridae and Ambystomatidae. Currently, genomic and transcriptomic resources for salamanders are insufficient to allow us to evaluate and reconstruct the ancestral state of these mutations, and future efforts to investigate the evolutionary origins of TTX toxicity and resistance in salamanders should determine when these mutations arose and why some species of newts were the only salamanders to evolve TTX toxicity.

Overall, our work has shown that the molecular and physiological basis of TTX resistance in newts arises from adaptive amino acid replacements in the P-loop regions of their $Na_v$ channels, some of which occur at identical loci across multiple genes. The evolution of chemical defenses such as neurotoxins provide excellent models for investigating adaptive evolution, as these toxins often target evolutionarily-conserved proteins in animal nervous systems (12, 25, 26). In the case of ion channels, exploring the connections between toxin binding and resistance can yield insight into the general principles of protein structure and physiological function, as well as the molecular bases of adaptive evolution in the nervous system.

**ACKNOWLEDGEMENTS**

We thank Dr. Alan Goldin (University of California, Irvine) for providing constructs for the mouse SCN8A α subunit and the rat β1 and β2 subunits for mutagenesis and electrophysiological recording. We thank Drs. Ke Dong and Ashlee Rowe for their generosity in sharing reagents and protocols, as well as for providing feedback on the manuscript. We are indebted to Dr. Abhijna Parigi for her assistance in performing electrophysiological recordings and analyzing data. We also thank Drs. Harold Zakon and Ben Liebeskind (University of Texas) for generating a preliminary transcriptome of the *T. granulosa* nose. SCN gene sequencing was performed with the assistance of undergraduate students Ben Goheen, Alejandra Ferrer-Díaz, and Jennifer Lough. This work was supported by the BEACON Center for the Study of Evolution in Action under US National Science Foundation Cooperative Agreement No. DBI-0939454; a Bauer Fellowship from Harvard University to LAO; National Science Foundation grants IOS-6531354089 and IOS-1655392 to HLE; and an NSF Graduate Research Fellowship to PMV (Fellow ID: 2014165835).

# APPENDIX

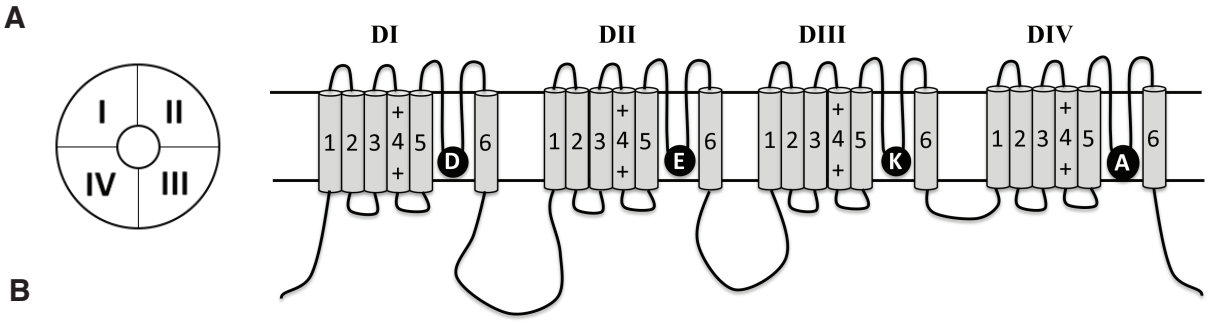


B

```
Consensus:                  FSWAFLSLFRLMTQDYWENLYQLTL FFHSFLIVFRVLCGEWIETMW GAGYLALLQVATFKGWMDIMYA FGNSMICLFQITTSAGWDGLLAP
Homo_sapiens_Nav1.1:        ..............D.......... ..............E...... .F...S.......K........ ..............A........
Mus_musculus_Nav1.1:        ..............D.......... ..............E...... .F...S.......K........ ..............A........
Gallus_gallus_Nav1.1:       ..............D.......... ..............E...... .F...S.......K........ ..............A........
Anolis_carolinensis_Nav1.1: ..............D.......... ..............E...... .F...S.......K........ .........M....A........
Nanorana_parkeri_Nav1.1:    ..............D.......... ..............E...... ..............K........ ..............A........
Xenopus_tropicalis_Nav1.1:  ..............D.......... ..............E...... ..............K........ ..............A........

Homo_sapiens_Nav1.2:        ..............D.......... ..............E...... .L...S.......K........ ..............A........
Mus_musculus_Nav1.2:        ..............D.......... ..............E...... .L...S.......K........ ..............A........
Gallus_gallus_Nav1.2:       ..............D.......... ..............E...... .L...S.......K........ ..............A........
Anolis_carolinensis_Nav1.2: ..............D.......... ..............E...... .L...S.......K........ .....L........A........
Nanorana_parkeri_Nav1.2:    .G............D......MK.. ..............E...... ..............K...P.... ....L....M....A...L....
Xenopus_tropicalis_Nav1.2:  .N............D.......... ..............E...... ..............K...P.... ..............A...L..E.
Taricha_granulosa_Nav1.2:   ..............D.......Q.. ..............E...... A.............K........ ..............G...V..S.

Homo_sapiens_Nav1.3:        ..............D.......... ..............E...... ..............K........ ..............A........
Mus_musculus_Nav1.3:        ..............D.......... ..............E...... ..............K........ ..............A........
Gallus_gallus_Nav1.3:       ..............D.......... ..............E...... ..............K........ ..............A........
Anolis_carolinensis_Nav1.3: ..............D.......... ..............E...... A.............K........ .....L........A........
Nanorana_parkeri_Nav1.3:    ..............D......M... ..............E...... .F...........K........ .........M....A........
Xenopus_tropicalis_Nav1.3:  ..............D.......... ..............E...... .F...........K...E.... ..............A........
Taricha_granulosa_Nav1.3:   ..............D*......... ..............E...*.. .F...........K........ .........M....A........

Homo_sapiens_Nav1.4:        ......A.......D.....F.... ..........I...E...... .L...S.......K........ ....I....E....A......N.
Mus_musculus_Nav.4:         ......A.......D.....F.... ..........I...E...... .L...S.......K........ ....I....E....A......N.
Gallus_gallus_Nav1.4:       ..............D.....F.... ..............E...... .L...S.......K........ ....I.........A......S.
Anolis_carolinensis_Nav1.4: ......A.......D.....F.... ..........I...E...... .L...S.......K........ ....I....M....A......N.
Nanorana_parkeri_Nav1.4:    ......A.......D.....F.... ..........I...E...... .L...S.......K........ .........E....A......N.
Xenopus_tropicalis_Nav1.4:  .N............D.....F.... ..........I...E...... .L...S.......K........ ....I.........A......N.
Taricha_granulosa_Nav1.4:   .N............D.....F.... ..........I...E...... .L...S.......K..*..... ..*.I.....*...A..**..I.

Homo_sapiens_Nav1.5:        .A....A.......D*..R...Q.. ...A...I..I...E...... ..............K........ .A...L........A......S.
Mus_musculus_Nav1.5:        .A....A.......D*..R...Q.. ...A...I..I...E...... ..............K........ .A...L........A......S.
Gallus_gallus_Nav1.5:       .G............D...R...Q.. .......I..I...E...... ..............K........ .A...L........A......N.
Anolis_carolinensis_Nav1.5: .G............D...R...Q.. .......I..I...E...... ..............K...E.... .A...L........A......H.
Xenopus_tropicalis_Nav1.5:  .G............D.......Q.. ..............E...... ..............K........ ..............A.....N.
Taricha_granulosa_Nav1.5:   .G....A.......D*..T...Q.I ..............E...... A.............K........ ..............A......N.

Homo_sapiens_Nav1.6:        ......A.......D......... ..............E..... ..............K....... ..............A......L.
Mus_musculus_Nav1.6:        ......A.......D......... ..............E...... ..............K........ ..............A......L.
Gallus_gallus_Nav1.6:       ......A.......D......... ..............E...... ..............K........ ..............A......L.
Anolis_carolinensis_Nav1.6: ......A.......D......... ..............E...... ..............K........ ..............A......L.
Nanorana_parkeri_Nav1.6:    ......A.......D........S. ..............E...... .........*...K........ ..............A......L.
Xenopus_tropicalis_Nav1.6:  ......A.......D......... ..............E...... ..............K........ ..............A......L.
Taricha_granulosa_Nav1.6:   .G....A.......D*........ ..............E...... .........*...K........ ..........*...A......L.
```

**Figure A2.1: Protein alignment of $Na_vs$ across a range of vertebrate taxa.** (A) The structure of the $Na_v$ alpha subunit, shown from top (left) and side of the channel (right). (B) Amino acid alignments of the S5-S6 linkers across the four domains. Mutations that were tested in this study or have been previously shown to affect TTX resistance are highlighted in red. The DEKA motif is shown in the alignment for reference to the structure in (A).

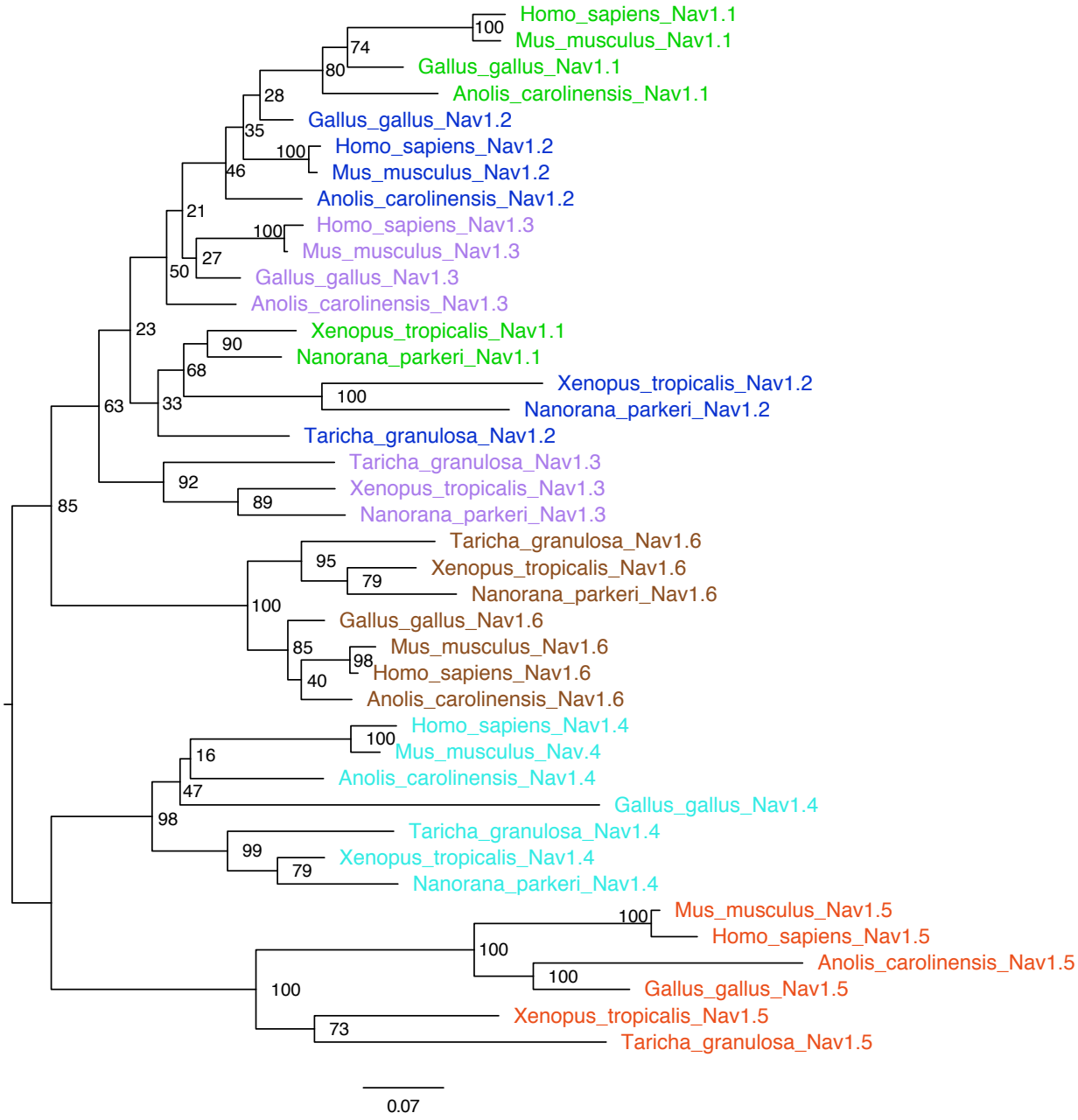


**Figure A2.2: Maximum-likelihood phylogenetic tree of vertebrate $Na_v$ protein sequences.** Major $Na_v$ gene families are color coded, and support values on each node reflect 1000 bootstrap replicates. The tree is rooted to create four main clades reflecting the two rounds of whole genome duplication that created the four ancestral vertebrate SCN genes. In this tree, $Na_v1.1$, $Na_v1.2$, and $Na_v1.3$ do not form monophyletic clades between amphibians and amniotes. Previous work has shown that although these genes maintain synteny across the two groups, the amphibian SCN sequences share more sequence similarity with each other than with the orthologous amniote genes (43). Nevertheless, we found that the *T. granulosa* sequences were each related to the orthologous gene in amphibians.

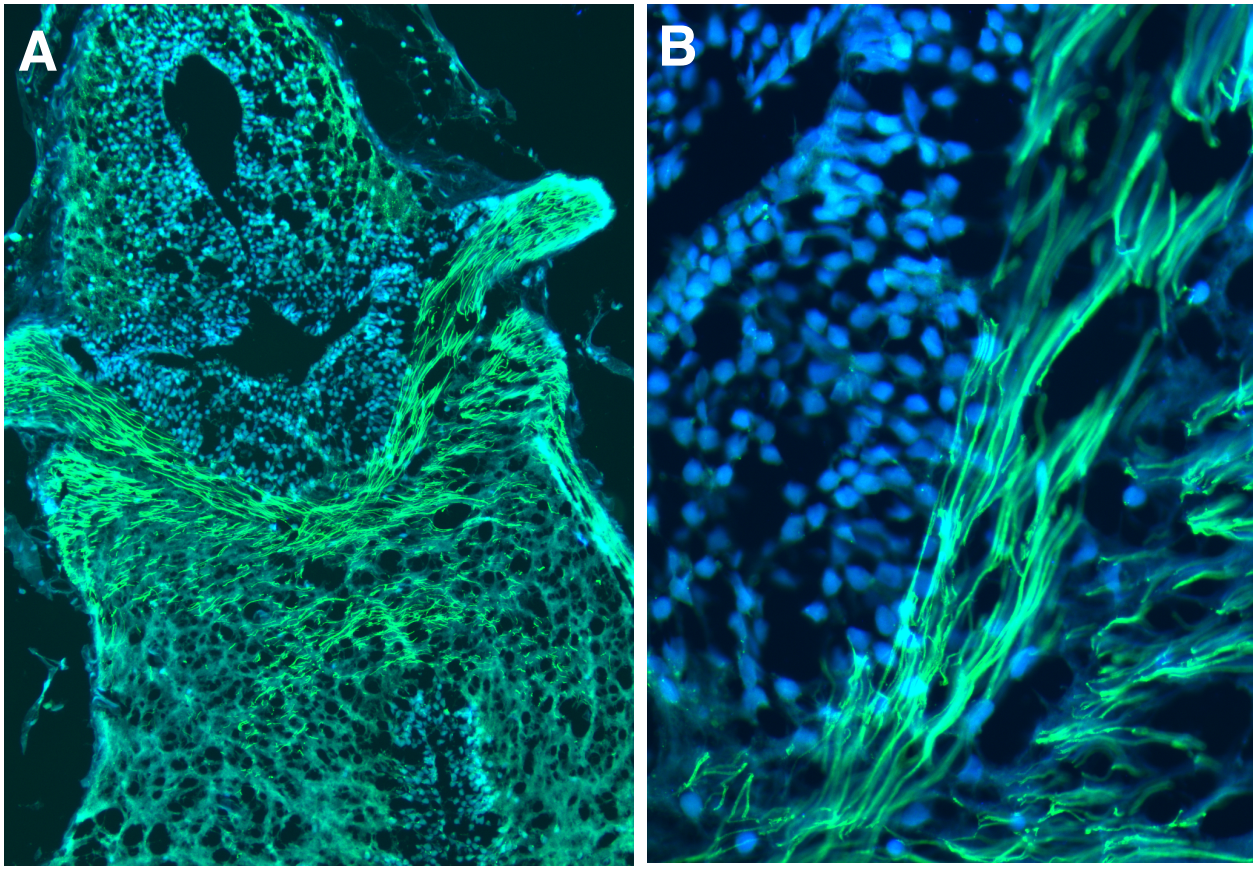


**Figure A2.3: $Na_v1.6$-like immunoreactivity in the mid- and hindbrain of *T. granulosa*.** Immunofluorescence with mouse anti-$Na_v1.6$ is shown in green, and Hoechst 33258 counterstain labeling cell bodies is shown in blue. Anterior is toward the top. (A) Horizontal section through the brain showing $Na_v1.6$ expression in unmyelinated axons descending from the third and lateral ventricles. (B) Higher magnification showing $Na_v1.6$-like expression specifically associated with unmyelinated axons.

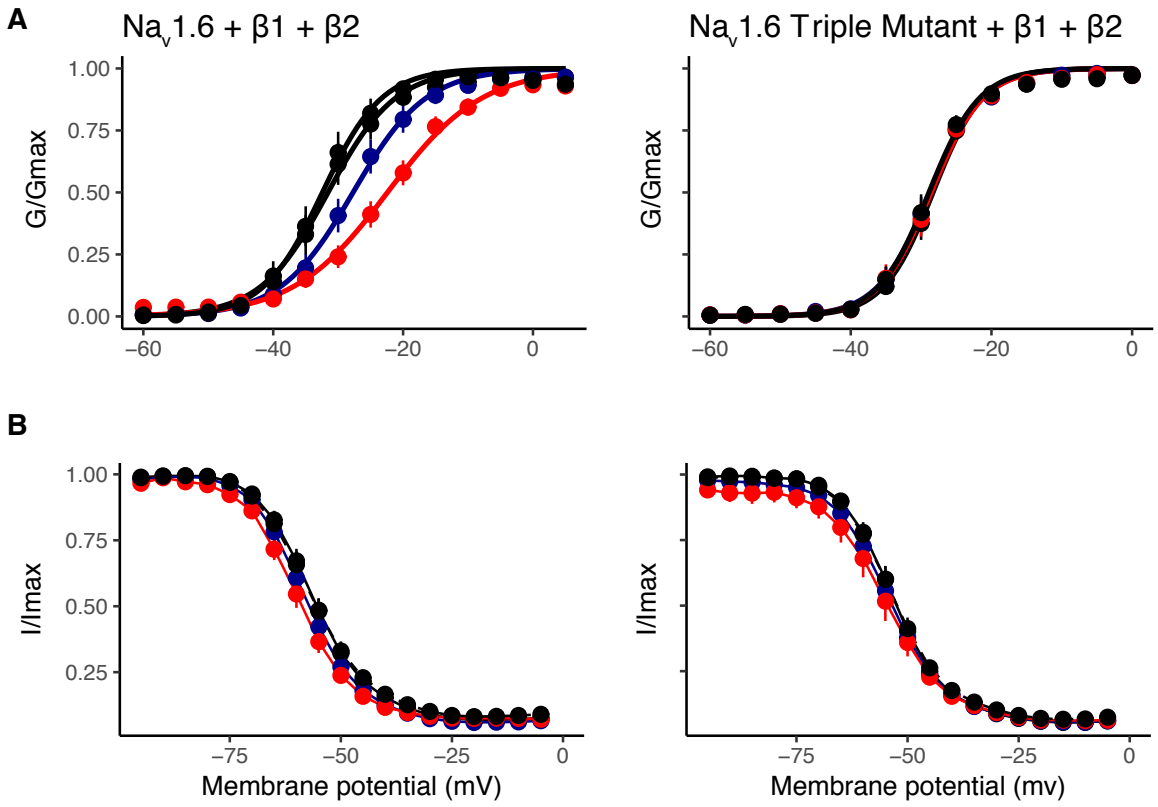


**Figure A2.4: Conductance and fast inactivation curves for wild-type and triple mutant channels.** (A) In wild-type channels, the voltage dependence of half-maximal activation ($V_{50}$) is shifted to more positive membrane potentials in the presence of TTX. However, this effect does not occur in the triple mutant channel. (B) Fast inactivation is not impacted by the presence of TTX for either channel.

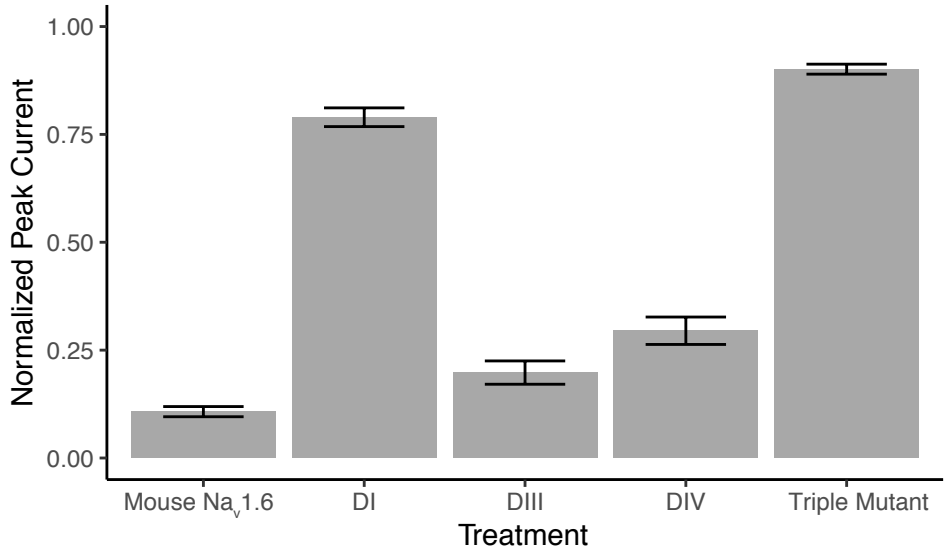


**Figure A2.5: Effect of TTX on peak Na+ current on each channel.** Proportion of $Na^+$ current remaining with a 50 ms pulse from -100 mV to -15 mV in the presence of 10 μM TTX. TTX significantly reduced the current in the wildtype channel as well as in the DIII, and DIV mutants, but currents in the DI and triple mutant constructs were not significantly affected. Nevertheless, the proportion of current remaining in the channels containing the DIII and DIV mutations was significantly greater than in the wildtype channel.

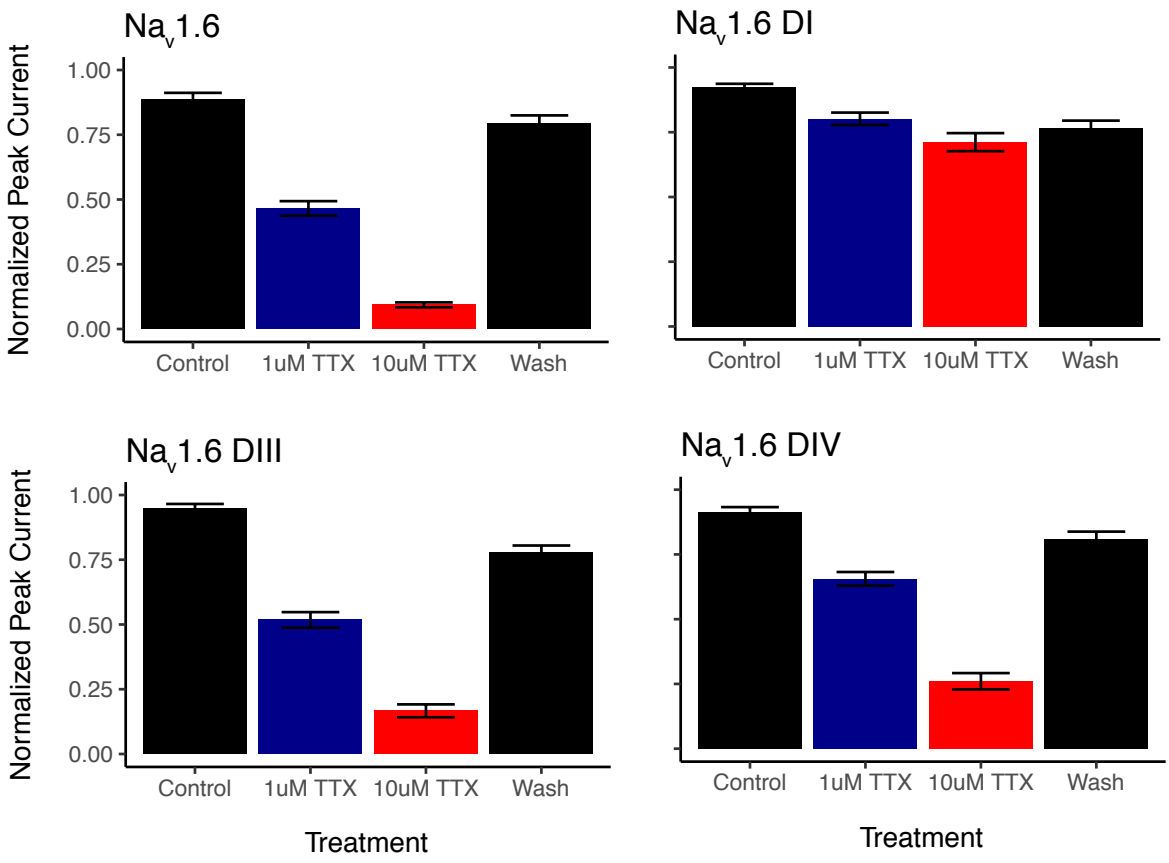


**Figure A2.6: Effect of TTX on peak currents in wild-type and three mutant channels.** Peak currents were elicited by a 50 ms pulse to -15 mV from a holding potential of -100 mV. All channels were significantly blocked by 1 μM TTX, but DI was not (see text for details).

# REFERENCES

## REFERENCES


1. Vermeij GJ (1994) The evolutionary interaction among species: selection, escalation, and coevolution. *Annual Review of Ecology and Systematics*:219–236.

2. Thompson JN (1999) The raw material for coevolution. *Oikos*:5–16.

3. Zaman L, et al. (2014) Coevolution Drives the Emergence of Complex Traits and Promotes Evolvability. *PLoS Biol* 12(12):e1002023.

4. Morran LT, Schmidt OG, Gelarden IA, Parrish RC, Lively CM (2011) Running with the Red Queen: host-parasite coevolution selects for biparental sex. *Science* 333(6039):216–218.

5. Dawkins R, Krebs JR (1979) Arms races between and within species. *Proc R Soc Lond, B, Biol Sci* 205(1161):489–511.

6. Abrams PA (2000) The evolution of predator-prey interactions: theory and evidence. *Annual Review of Ecology and Systematics*:79–105.

7. Brodie ED III, Brodie ED Jr. (1999) Predator-prey arms races. *BioScience* 49(7):557–568.

8. Brodie ED, Ridenhour BJ (2003) Reciprocal selection at the phenotypic interface of coevolution. *Integrative and Comparative Biology* 43(3):408–418.

9. Whittaker RH, Feeny PP (1971) Allelochemics: chemical interactions between species. *Science* 171(3973):757–770.

10. Heidel-Fischer HM, Vogel H (2015) Molecular mechanisms of insect adaptation to plant secondary compounds. *Current Opinion in Insect Science* 8:8–14.

11. Després L, David J-P, Gallet C (2007) The evolutionary ecology of insect resistance to plant chemicals. *Trends in Ecology & Evolution* 22(6):298–307.

12. Tarvin RD, Santos JC, O'Connell LA, Zakon HH, Cannatella DC (2016) Convergent Substitutions in a Sodium Channel Suggest Multiple Origins of Toxin Resistance in Poison Frogs. *Mol Biol Evol* 33(4):1068–1081.

13. Tarvin RD, et al. (2017) Interacting amino acid replacements allow poison frogs to evolve epibatidine resistance. *Science* 357(6357):1261–1266.

14. Catterall WA, et al. (2007) Voltage-gated ion channels and gating modifier toxins. *Toxicon* 49(2):124–141.

15. Smith JM (1978) Optimization Theory in Evolution. *Annual Review of Ecology and Systematics* 9(1):31–56.

16. Smith JM (2004) Natural selection and the concept of a protein space. *Nature* 225(5232):563–564.

17. Carneiro M, Hartl DL (2010) Adaptive landscapes and protein evolution. *Proc Natl Acad Sci USA* 107(suppl_1):1747–1751.

18. Hille B (2001) Ion Channels of Excitable Membranes, Third Edition.

19. Catterall WAW (2000) From Ionic Currents to Molecular Mechanisms - The Structure and Function of Voltage-Gated Sodium Channels. *Neuron* 26(1):13–13.

20. Isom LL, et al. (1992) Primary structure and functional expression of the beta 1 subunit of the rat brain sodium channel. *Science* 256(5058):839–842.

21. Isom LL, De Jongh KS, Catterall WA (1994) Auxiliary subunits of voltage-gated ion channels. *Neuron* 12(6):1183–1194.

22. Isom LL (2001) Sodium channel beta subunits: Anything but auxiliary. *Neuroscientist* 7(1):42–54.

23. Hodgkin AL, Huxley AF (1952) Currents carried by sodium and potassium ions through the membrane of the giant axon of Loligo. *The Journal of Physiology* 116(4):449.

24. Hodgkin AL, Huxley AF (1952) A quantitative description of membrane current and its application to conduction and excitation in nerve. *The Journal of Physiology* 117(4):500.

25. Cestèle S, Catterall WA (2000) Molecular mechanisms of neurotoxin action on voltage-gated sodium channels. *Biochimie* 82(9-10):883–892.

26. de Lera Ruiz M, Kraus RL (2015) Voltage-Gated Sodium Channels: Structure, Function, Pharmacology, and Clinical Indications. *J Med Chem* 58(18):7093–7118.

27. Bane V, Lehane M, Dikshit M, O'Riordan A, Furey A (2014) Tetrodotoxin: Chemistry, toxicity, source, distribution and detection. *Toxins* 6(2):693–755.

28. Narahashi T, Moore JW, Scott WR (1964) Tetrodotoxin blockage of sodium conductance Increase in lobster giant axons. *J Gen Physiol* 47(5):965–974.

29. Fozzard HA, Lipkind GM (2010) The tetrodotoxin binding site Is within the outer vestibule of the sodium channel. *Marine Drugs* 8(2):219–234.

30. Shen H, et al. (2018) Structural basis for the modulation of voltage-gated sodium channels by animal toxins. *Science* 362(6412):1–8.

31. Venkatesh B, et al. (2005) Genetic Basis of Tetrodotoxin Resistance in Pufferfishes. *Current Biology* 15(22):2069–2072.

32. Geffeney S, Brodie ED, Ruben PC (2002) Mechanisms of adaptation in a predator-prey arms race: TTX-resistant sodium channels. *Science* 297(5585):1336–1339.

33. Geffeney SL, Fujimoto E, Brodie ED, Ruben PC (2005) Evolutionary diversification of TTX-resistant sodium channels in a predator-prey interaction. *Nature* 434(7034):759–763.

34. Feldman CR, Brodie ED, Pfrender ME (2009) The evolutionary origins of beneficial alleles during the repeated adaptation of garter snakes to deadly prey. *Proceedings of the National Academy of Sciences* 106(32):13415–13420.

35. Feldman CR, Brodie ED, Pfrender ME (2012) Constraint shapes convergence in tetrodotoxin-resistant sodium channels of snakes. *Proceedings of the National Academy of Sciences of the United States of America* 109(12):4556–4561.

36. Hanifin CT, Gilly WF (2014) Evolutionary history of a complex adaptation: Tetrodotoxin resistance in salamanders. *Evolution* 69(1):232–244.

37. Maruta S, Yamaoka K, Yotsu-Yamashita M (2008) Two critical residues in p-loop regions of puffer fish Na+ channels on TTX sensitivity. *Toxicon* 51(3):381–387.

38. Jost MC, et al. (2008) Toxin-Resistant Sodium Channels: Parallel Adaptive Evolution across a Complete Gene Family. *Molecular Biology and Evolution* 25(6):1016–1024.

39. McGlothlin JW, et al. (2014) Parallel Evolution of Tetrodotoxin Resistance in Three Voltage-Gated Sodium Channel Genes in the Garter Snake Thamnophis sirtalis. *Molecular Biology and Evolution* 31(11):2836–2846.

40. McGlothlin JW, et al. (2016) Historical Contingency in a Multigene Family Facilitates Adaptive Evolution of Toxin Resistance. *Current Biology* 26(12):1616–1621.

41. Hirota K, Kaneko Y, Matsumoto G, Hanyu Y (1999) Cloning and Distribution of a Putative Tetrodotoxin-Resistant Na +Channel in Newt Retina. *Zoological Science* 16(4):587–594.

42. Catterall WA (2003) International Union of Pharmacology. XXXIX. Compendium of Voltage-Gated Ion Channels: Sodium Channels. *Pharmacological Reviews* 55(4):575–578.

43. Zakon HH, Jost MC, Lu Y (2011) Expansion of Voltage-dependent Na+ Channel Gene Family in Early Tetrapods Coincided with the Emergence of Terrestriality and Increased Brain Complexity. *Molecular Biology and Evolution* 28(4):1415–1424.

44. Yu FH, Catterall WA (2003) Overview of the voltage-gated sodium channel family. *Genome Biol* 4(3):207.

45. Catterall WA, Kalume F, Oakley JC (2010) Na V1.1 channels and epilepsy. *The Journal of Physiology* 588(11):1849–1859.

46. Hu W, et al. (2009) Distinct contributions of Na(v)1.6 and Na(v)1.2 in action potential initiation and backpropagation. *Nature Publishing Group* 12(8):996–1002.

47. Nieto FR, et al. (2012) Tetrodotoxin (TTX) as a therapeutic agent for pain. *Marine Drugs* 10(12):281–305.

48. Vornanen M, Hassinen M, Haverinen J (2011) Tetrodotoxin Sensitivity of the Vertebrate Cardiac Na+ Current. *Marine Drugs* 9(12):2409–2422.

49. Caldwell JH, Schaller KL, Lasher RS, Peles E, Levinson SR (2000) Sodium channel Na(v)1.6 is localized at nodes of ranvier, dendrites, and synapses. *Proceedings of the National Academy of Sciences* 97(10):5616–5620.

50. Lorincz A, Nusser Z (2010) Molecular Identity of Dendritic Voltage-Gated Sodium Channels. 328(5980):906–909.

51. Smith MR, Smith RD, Plummer NW, Meisler MH, Goldin AL (1998) Functional analysis of the mouse Scn8a sodium channel. *Journal of Neuroscience* 18(16):6093–6102.

52. Chen Y, et al. (2008) Functional properties and differential neuromodulation of Nav1.6 channels. *Molecular and Cellular Neuroscience* 38(4):607–615.

53. Hill AS, et al. (2008) Ion Channel Clustering at the Axon Initial Segment and Node of Ranvier Evolved Sequentially in Early Chordates. *PLoS Genet* 4(12):e1000317.

54. Osorio N, et al. (2010) Persistent Nav1.6 current at axon initial segments tunes spike timing of cerebellar granule cells. *The Journal of Physiology* 588(4):651–670.

55. Mercer JN, Chan CS, Tkatch T, Held J, Surmeier DJ (2007) Nav1.6 Sodium Channels Are Critical to Pacemaking and Fast Spiking in Globus Pallidus Neurons. *Journal of Neuroscience* 27(49):13552–13566.

56. Wakely JF, Fuhrman GJ, Fuhrman FA, Fischer HG, Mosher HS (1966) The occurrence of tetrodotoxin (tarichatoxin) in amphibia and the distribution of the toxin in the organs of newts ( Taricha). *Toxicon* 3(3):195–203.

57. Yotsu M, Iorizzi M, Yasumoto T (1990) Distribution of tetrodotoxin, 6-epitetrodotoxin, and 11-deoxytetrodotoxin in newts. *Toxicon* 28(2):238–241.

58. Tsuruda K, Arakawa O, Kawatsu K, Hamano Y (2002) Secretory glands of tetrodotoxin in the skin of the Japanese newt Cynops pyrrhogaster. *Toxicon* 40:131–136.

59. Mebs D, Arakawa O, Yotsu-Yamashita M (2010) Tissue distribution of tetrodotoxin in the red-spotted newt Notophthalmus viridescens. *Toxicon* 55(7):1353–1357.

60. Kaneko Y, Matsumoto G, Hanyu Y (1997) TTX resistivity of Na+ channel in newt retinal neuron. *Biochem Biophys Res Commun* 240(3):651–656.

61. Hanifin CT, Yotsu-Yamashita M, Yasumoto T, Brodie ED III, Brodie ED Jr. (1999) Toxicity of dangerous prey: variation of tetrodotoxin levels within and among populations of the newt Taricha granulosa. *J Chem Ecol* 25(9):2161–2175.

62. Song L, Florea L (2015) Rcorrector: efficient and accurate error correction for Illumina RNA-seq reads. *Gigascience* 4(1). doi:10.1186/s13742-015-0089-y.

63. Grabherr MG, et al. (2011) Full-length transcriptome assembly from RNA-Seq data without a reference genome. *Nat Biotechnol* 29(7):644–U130.

64. Li W, Godzik A (2006) Cd-hit: a fast program for clustering and comparing large sets of protein or nucleotide sequences. *Bioinformatics* 22(13):1658–1659.

65. Simao FA, Waterhouse RM, Ioannidis P, Kriventseva EV, Zdobnov EM (2015) BUSCO: assessing genome assembly and annotation completeness with single-copy orthologs. *Bioinformatics* 31(19):3210–3212.

66. Feldman DH, Lossin C (2014) The Nav channel bench series: Plasmid preparation. *MethodsX* 1:6–11.

67. Penzotti JL, Fozzard HA, Lipkind GM, Dudley SC Jr (1998) Differences in Saxitoxin and Tetrodotoxin Binding Revealed by Mutagenesis of the Na+ Channel Outer Vestibule. *Biophysical Journal* 75(6):2647–2657.

68. Satin J, et al. (1992) A mutant of TTX-resistant cardiac sodium channels with TTX-sensitive properties. *Science* 256(5060):1202–1205.

69. Du Y, Nomura Y, Liu Z, Huang ZY, Dong K (2009) Functional expression of an arachnid sodium channel reveals residues responsible for tetrodotoxin resistance

in invertebrate sodium channels. *Journal of Biological Chemistry* 284(49):33869–33875.

70. Yotsu-Yamashita M, et al. (2000) Binding Properties of 3H-PbTx-3 and 3H-Saxitoxin to Brain Membranes and to Skeletal Muscle Membranes of Puffer Fish Fugu pardalis and the Primary Structure of a Voltage-Gated Na+ Channel α-Subunit (fMNa1) from Skeletal Muscle of F. pardalis. *Biochem Biophys Res Commun* 267(1):403–412.

71. Wu M, Ye N, Sengupta B, Zakon HH (2013) A naturally occurring amino acid substitution in the voltage-dependent sodium channel selectivity filter affects channel gating. *Journal of Comparative Physiology A: Sensory, Neural, and Behavioral Physiology* 199(10):829–842.

72. Hanifin CT, Brodie ED (2008) Phenotypic mismatches reveal escape from arms-race coevolution. *PLoS Biol* 6(3):e60.

73. Yotsu-Yamashita M, Mebs D (2003) Occurrence of 11-oxotetrodotoxin in the red-spotted newt, Notophthalmus viridescens, and further studies on the levels of tetrodotoxin and its analogues in the newt's efts. *Toxicon* 41(7):893–897.

74. Kudo Y, Yasumoto T, Konoki K, Cho Y, Yotsu-Yamashita M (2012) Isolation and Structural Determination of the First 8-epi-type Tetrodotoxin Analogs from the Newt, Cynops ensicauda popei, and Comparison of Tetrodotoxin Analogs Profiles of This Newt and the Puffer Fish, Fugu poecilonotus. *Marine Drugs* 10(12):655–667.

75. Soong TW, Venkatesh B (2006) Adaptive evolution of tetrodotoxin resistance in animals. *Trends in Genetics* 22(11):621–626.

76. Bricelj VM, et al. (2005) Sodium channel mutation leading to saxitoxin resistance in clams increases risk of PSP. *Nature* 434(7034):763–767.

77. Shen H, Liu D, Wu K, Lei J, Yan N (2019) Structures of human Nav1.7 channel in complex with auxiliary subunits and animal toxins. *Science* 363(6433):1303–1308.

## CONCLUSIONS

In my dissertation research, I demonstrate that TTX toxicity in the poisonous rough-skinned newt (*Taricha granulosa*) is due to a symbiotic association with TTX-producing bacteria in the newt host's skin. I found that several bacterial genera, including *Pseudomonas, Aeromonas, Shewanella,* and *Sphingopyxis*, isolated from the skin of toxic newts produced TTX in lab cultures. Interestingly, I also found that certain bacterial genera, particularly *Pseudomonas*, are present in significantly higher abundance in the microbiota of a population of toxic newts compared with a population of non-toxic newts. Thus, the differential abundance of TTX-producing bacteria in the newt microbiome may offer a mechanism to explain the observed patterns of geographic variation in TTX toxicity across the Pacific Northwest of the United States. Future studies should explore possible correlations between host toxicity and microbiome structure, and whether predictable differences in the structure or diversity of newt microbiota could underlie adaptive evolutionary responses in the famous coevolutionary arms race between newts and garter snakes.

Coinciding with the evolution of this toxic symbiosis, newts accumulated amino acid substitutions in their $Na_v$ channels. Newts possess six $Na_v$ channels that are differentially expressed across the nervous and muscular systems, and I identified mutations in the TTX binding site of all six channels. I further demonstrated that some of these mutations affect TTX binding in a widely-expressed channel, $Na_v1.6$, by inserting three newt-specific mutations into the orthologous channel from the house mouse (*Mus musculus*). Although the wild-type mouse channel was sensitive to TTX in a dose-dependent manner, the three newt mutations provided a >2,800-fold increase in TTX

resistance relative to the mouse channel, rendering the channel insensitive to concentrations of TTX as high as 100 μM; thus, these mutations provide significant resistance to TTX levels not seen in nature. Nevertheless, the impact of these mutations on other biophysical properties of the channel, such as gating kinetics, ion selectivity, and channel conductance are unknown. Future studies could explore whether TTX resistance mutations negatively impact these other channel properties, which may indicate that evolutionary trade-offs may occur between TTX toxicity and $Na_v$ channel function.

Overall, my dissertation research contributes to the growing understanding that symbiotic microorganisms can directly affect animal physiology and evolution, and that biologists should consider the effects of the microbiome when examining other aspects of their favorite animal's biology. The work presented here provides a direct functional link between a microbiome-derived neurotoxin and adaptive evolutionary responses in the $Na_v$ channels of toxic newts. I believe the rough-skinned newt will be an excellent model for exploring the connections between microbiome and host phenotypes for many years to come.